# Antigen discrimination in primary human T cells


**Johannes Pettmann**

Profs. Omer Dushek & Simon Davis

Sir William Dunn School of Pathology

University of Oxford

This dissertation is submitted for the degree of

*Doctor of Philosophy*

St. Edmund's Hall

Hilary Term 2021

*I would like to dedicate this thesis to my loving parents, my sister, and my partner Athena.*

# Acknowledgements

First of all, I would like to thank my supervisors Omer Dushek and Simon Davis for the great supervision throughout my DPhil. In particular, I value their passion for science, always being ready to discuss any new results, and their support for any challenge I faced during my studies. Furthermore, I highly appreciate all the time they spent helping me to correct my thesis. Their scientific suggestions improved this thesis substantially.

Next, I want to thank everyone in Omer's and Simon's laboratories, and the adjacent laboratories of Anton van der Merwe and Marion Brown. Special thanks go to my supervisors Mafalda Santos and Philipp Krüger and the students I was able to supervise over the years. I would like to specifically thank Enas Abu-Shah, Anna Huhn, Daniel Wilson, Mikhail Kutuzov, and Mafalda for working with me on the review and research article I have authored during my DPhil. Scientifically, Anton and Marion provided very valuable input over the years. I also want to thank the people involved in my thesis committee, transfer of status, and confirmation of status: Michael Dustin, Marco Fritzsche, and Anton. I would also like to thank all collaborators I have been able to work with. Next, I want to thank Graham Ogg and Roger Geiger for agreeing to examine this thesis. I am very much looking forward to hear their thoughts and suggestions at my viva. Furthermore, I appreciate the help I received from the directors

and former directors of my course: Christoph Tang*, Fiona Powrie, Helen McShane, Nicole Zitzmann, and Jan Rehwinkel. I also want to thank the administrators at the Dunn School and the course: Dawn Gibbons, Lucinda Risius, and Louise Samson. Of course, none of this would have been possible without funding from the Wellcome Trust and I was very sad when I heard that the course will not be funded by the Wellcome Trust anymore.

Research is nowadays impossible without all the work that goes on in the background. I therefore want to thank everyone at the Sir William Dunn School of Pathology, and the MRC Weatherall Institute of Molecular Medicine. I have spent most of my time at the Dunn School, but I enjoyed working in both departments because of their vibrant environments and scientific excellence. The Dunn School, its head Matthew Freeman, and the people involved in administration, deserve a special thanks for how well they handled the Coronavirus pandemic. Matthew excelled at keeping us informed, even when there was considerable uncertainty about how things would develop.

Lastly, I want to thank my course mates, and my friends, Angela, Armin, Cornelia, Ester, Felix, Jesús, Jonny, Juli, Lea, Lilli, Ron, Sarah, Stephanie, Violaine, and Vivian for making my time at Oxford special. I am also grateful for my wonderful family, and partner, Athena. None of this would have been possible without their continuous support.

*Who, if he ever reads this, I apologize to, for not knowing that his full first name is not Chris, as I have falsely stated in the acknowledgments of [1].

# Contributions

This thesis includes the work of others. All the SPR experiments were performed by Mikhail Kutuzov, who also performed the initial analysis (e.g. double referencing and extracting the steady-state responses) of the data. I fitted the data to determine the $K_D$s and performed all further analyses. Additionally, he performed the production, purification, and refolding of TCR and the purification of CD58, CD86, and ICAM1 from supernatants produced by me. Lastly, he helped with writing the methods section on SPR and protein production. pMHC refolds were generated by Mikhail Kutuzov, Marcus Bridge, or myself. Daniel Wilson and my supervisor, Omer Dushek, contributed to mathematically deriving the equation for fitting a kinetic proofreading model. T cell isolation, transductions, and maintenance were performed as shared tasks within the laboratory. Lastly, I used engineered CHO cells created by Jesús Siller Farfán and TCR-KO Jurkat cells from Edward Jenkins.

I would like to thank Ron Gejman for providing me with a plasmid for the A6 TCR and Sebastian Springer for his help with expressing empty MHC and providing the plasmids (not included in this thesis). I also want to thank Johannes Huppa for hosting me in his laboratory in Vienna for 2 weeks to perform some experiments (data not included in this thesis) and providing me with reagents. Thanks also go to his laboratory members Rene Platzer and Florian Kellner.

Some data generated by me and presented in chapter 2.2.4 have been previously submitted as part of a DPhil thesis [2] and also as part of a published manuscript [3]. Data presented in chapters 3.2.2, 3.2.3, and 4.2 have been published in [4]*. A previous version of this manuscript contains some additional data on short-circuiting kinetic proofreading and is therefore cited where appropriate [5]. In this thesis, I heavily reference some of the findings in this work, which were not all generated by me. Specifically, additional antigen discrimination data on dendritic cells was generated by Enas Abu-Shah, while Anna Huhn performed a meta-analysis of published literature on the TCR and other receptors.

*In the examined version this was still a pre-print.

# Abstract

Antigen discrimination is the process by which T cells differentiate self from foreign antigens. They do this using their T cell receptors (TCRs) that recognize peptide antigens bound to major histocompatibility complexes (pMHCs) and this TCR/pMHC interaction is augmented by a host of other co-signaling receptors including adhesion receptors. Despite extensive work, the quantitative ability of T cells to discriminate antigen and the molecular mechanisms underlying it remain debated. We developed an improved binding assay that allowed measurement of ultra-low affinity TCR/pMHC interactions, generated >30 different peptide variants for two different human class I-restricted TCRs and accurately measured their affinities. Surprisingly, we found an affinity floor at a $K_D$ of ~2 mM that could not be further lowered even by changing the peptide sequence dramatically. This could represent the self-pMHC affinity at which T cells are selected during positive selection in the thymus. I utilized the $K_D$s generated by our new binding assay to characterize the 'discrimination power', which is a measure of a receptor's ability to discriminate between ligands with different affinities or off-rates. I found that the discrimination power of the TCR was much lower than the 'near-perfect discrimination', previously reported, and that in some settings it was increased by CD2 and LFA-1. Furthermore, these adhesion receptors increased the sensitivity to pMHC, while accelerating pMHC-dependent TCR downregulation, indicating that they likely influence the way the TCR binds pMHC. In the future, this new understanding could be useful for improving the

sensitivity and discrimination power of artificial receptor constructs used in immunotherapy, enhancing their safety and efficacy.

# Contents

# List of Figures

# List of Tables

# Abbreviations

| | |
|---|---|
| $K_D$ | dissociation constant |
| $N$ | mumber of proofreading steps |
| $k_{off}$ | off-rate |
| $k_{on}$ | on-rate |
| $k_p$ | proofreading rate |
| $\tau$ | lifetime |
| ln | natural logarithm |
| log | decimal logarithm |
| **41BB** | also known as CD137 |
| | |
| **ABC-SMC** | approximate Bayesian computation-sequential Monte Carlo |
| **ANOVA** | analysis of variance |
| **AP-1** | activator protein 1 |
| **APC** | antigen-presenting cell |
| **APL** | altered peptide ligand |
| | |
| **BCR** | B cell receptor |
| **BFP** | biomembrane force probe |
| **BRS** | basic-rich sequence |
| **BSA** | bovine serum albumin |
| **BTN** | Butyrophilin 3A1 |
| | |
| **CAR** | chimeric antigen receptor |
| **Cas9** | CRISPR associated protein 9 |

| | |
|---|---|
| **CD** | cluster of differentiation |
| **CD2AP** | CD2-associated protein |
| **CD2BP** | CD2 antigen cytoplasmic tail-binding protein |
| **CDR** | complementary-determining region |
| **CHO cell** | chinese hamster ovary cell |
| **CI** | confidence interval |
| **CIN85** | Cbl-interacting protein of 85 kDa; also known as SH3KBP1 |
| **CRD** | cysteine-rich domain |
| **CRISPR** | clustered regularly interspaced short palindromic repeats |
| **Csk** | C-terminal Src kinase |
| **DAG** | diacylglycerol |
| **DC** | dendritic cell |
| **DMEM** | Dulbecco's modified Eagle medium |
| **EC** | effective concentration |
| **ECD** | extracellular domain |
| **ELISA** | enzyme-linked immunosorbent assay |
| **EM** | electron microscopy |
| **ER** | endoplasmic reticulum |
| **FACS** | fluorescence activated cell sorting |
| **Fc** | fragment crystallizable region |
| **FC** | flow cell |
| **Fc$\gamma$RI** | Fc$\gamma$ receptor 1 |
| **FCS** | fetal calf serum |
| **FRET** | Förster resonance energy transfer |
| **FSC** | forward scatter |
| **Fyn** | Src family tyrosine kinase |
| **Gads** | GRB2-related adaptor downstream of Shc; also known as GRAP2 |
| **geo.** | geometric |
| **gMFI** | geometric mean fluorescence intensity |
| **GPCR** | G protein-coupled receptor |

| | |
|---|---|
| **GPI** | glycosylphosphatidylinositol |
| **Grb2** | growth factor receptor-bound protein 2 |
| **GSEM** | glutamine synthetase expression medium |
| **GYF** | glycine-tyrosine-phenylalanine |
| **HCMV** | human cytomegalovirus |
| **HLA** | human leukocyte antigen |
| **HML** | human mucosal antigen |
| **hMSH2** | MutS homolog 2 |
| **HTLV-1** | human T-lymphotropic virus 1 |
| **ICAM** | intercellular adhesion molecule |
| **Ig** | immunoglobulin |
| **IgG** | immunoglobulin G |
| **IL2** | interleukin-2 |
| **$IP_3$** | inositol triphosphate |
| **ITAM** | immunoreceptor tyrosine-based activation motif |
| **JAM-A** | junctional adhesion molecule A; also called F11R |
| **KO** | knock-out |
| **KP** | kinetic proofreading |
| **LAD** | leukocyte adhesion deficiency |
| **LAT** | linker for activation of T cells |
| **Lck** | lymphocyte-specific protein tyrosine kinase |
| **LDH** | lactate dehydrogenase |
| **LFA** | lymphocyte function-associated antigen |
| **LPAM** | lymphocyte Peyer's patch adhesion molecule |
| **Mg** | magnesium |
| **MHC** | major histocompatibility complex |
| **MICA** | MHC class I polypeptide–related sequence A |
| **MR1** | major histocompatibility complex class I-related gene protein |

**MSX** methionine sulfoximine
**mTOR** mechanistic/mammalian target of rapamycin

**Nck** non-catalytic region of tyrosine kinase adaptor protein 1
**NF$\varkappa$B** nuclear factor kappa-light-chain-enhancer of activated B cells
**NFAT** nuclear factor of activated T cells
**NK** natural killer
**NMR** nuclear magnetic resonance
**norm.** normalized
**NTR** non-catalytic tyrosine-phosphorylated receptors
**NYE** cancer/testis antigen 1; also known as CTAG1B, LAGE2 or NY-ESO-1

**OD** optical density
**OptiMEM** optimized minimal essential medium
**OT** optical trap

**PAGE** polyacrylamide gel electrophoresis
**pAPC** professional APC
**PD-1** programmed cell death protein 1
**PI3K** phosphatidylinositol 3-kinase
**PLC$\gamma$1** phospholipase C$\gamma$ 1
**pMHC** peptide-MHC
**PRR** pattern recognition receptor

**RAG** recombination-activating gene
**RAP1** Ras-related protein 1
**RBC** red blood cell
**ref.** reference
**RPMI** Roswell Park Memorial Institute
**RU** response units

**scFv** single-chain variable fragment
**SD** standard deviation
**SDS** sodium dodecyl sulfate

| | |
|---|---|
| **SEM** | standard error of the mean |
| **SH2** | Src homology 2 domain |
| **SH3** | Src homology 3 domain |
| **SLP-76** | SH2 domain containing leukocyte protein of 76 kDa |
| **SMAC** | supramolecular activation cluster |
| **Sos** | son of sevenless |
| **SPR** | surface plasmon resonance |
| **SSC** | side scatter |
| **Syk** | spleen tyrosine kinase |
| **TC** | tissue culture |
| **TCR** | T cell receptor |
| **TdT** | terminal deoxynucleotidyl transferase |
| **TM** | transmembrane |
| **TNF** | tumor necrosis factor |
| **TNFR** | TNF receptor |
| **transd.** | transduced |
| **UT** | untransduced |
| **VLA** | very late activation antigen |
| **ZAP-70** | zeta-chain-associated protein kinase 70 |

*I have not failed. I've just found 10,000 ways that won't work.*

**Thomas Edison**

*If we knew what it was we were doing, it would not be called research, would it?*

**Albert Einstein**

# Chapter 1

# Introduction

T cells are lymphocytes found in all jawed vertebrates. They mediate important effector functions in the immune system and orchestrate the adaptive immune response in several ways through cell-to-cell interactions and release of cytokines. Furthermore, they form an important part of immunological memory. T cells have increasingly become the focus of therapeutic interventions, such as for the treatment of cancers or autoimmune diseases.

The function of T cells crucially depends on their ability to discriminate between self and non-self antigens. While abundant self is meant to be ignored, T cells readily recognize non-self, such as pathogens or tumor-associated antigens, and start an immune response. They therefore form the core of the adaptive immune system. They also engage directly in effector functions and orchestrate other immune functions, such as the production of antibodies by B cells, which usually depends on T cell help. One unique feature of T cells is that when their TCR (T cell receptor) is created randomly through the process of somatic recombination, they do not know what their cognate ligand is. This applies similarly to B cells, however, their activation usually depends on T cell help and T cell are required for the generation of high affinity antibodies through the process of hypermutation [6]. Immune coverage by the adaptive immune system is achieved through the production of large numbers of naïve T cell clones, many of which will never become activated. Given the physical limit of the number of T cells an individual can harbor, T cells need to be inherently cross-reactive. In the following sections, I will discuss the experimental evidence for antigen discrimination. I will be reviewing how the TCR binds pMHC and the role of the adhesion receptors CD2 and LFA-1 in this process. Lastly, I will explain different models of antigen discrimination and TCR triggering.

## 1.1 T cells must be highly sensitive and discriminatory

Antigen recognition by T cells is functionally characterized by a combination of sensitivity, specificity*, and speed. One of the most striking features of T cells is their ability to respond to <10 cognate antigens, while ignoring the abundant self antigens. High sensitivity is particularly important in the presence of immune evasive mechanisms to reduce the number of antigens presented on the cell surface. Such mechanisms are employed by many viruses [9] and are commonly found in tumors [10]. *In vitro*, $CD4^+$ T cells have been observed to respond to a single pMHC [11, 12]. Similarly, $CD8^+$ T cells were shown to respond to 3 or fewer ligands [13, 14].

Notably, T cells cannot employ long temporal integration to achieve high sensitivity, since on average T cells spend only 1–5 min scanning each antigen-presenting cell (APC) [15–19]. Such rapid scanning is essential given that individual T cell clones can be comprised of very few cells and enables individual dendritic cells (DCs) to interact with thousands of T cells per hour, assuming around 250 T cells can be in contact with an individual DC simultaneously [18]. In fact, the requirement for fast dissociation after scanning is one potential reason for the low affinities of the receptor/ligand pairs involved in conjugation [20]. While priming of naïve T cells may require interactions with APCs over many hours [17, 21, 22], *in vitro* and *in vivo* data suggest that the decision making is much more rapid. For example, when T cells were isolated from mice 5 min after *i.v.* injection of peptide, they showed signs of activation [23]. Furthermore, when T cells were stimulated *in vitro* with antibodies, phosphorylation of downstream molecules such as ZAP-70 or LAT was observed after less than 60 s [24]. Using photoactivatable peptide-MHC (pMHC), Huse *et al.* could measure LAT phosphorylation and

*The term specificity has historically been used in the T cell field to describe different properties. For example in modeling, it is often defined as $truepositive/(truepositive + falsepositive)$ (e.g. in [7]). In T cell biology, it is sometimes used to describe the opposite of promiscuous/cross-reactive (e.g. in [8]). However cross-reactivity does not only depend on specificity, but also sensitivity (see also Discussion). In my analysis I therefore introduce the new term 'discrimination power'.

calcium fluxing after less than 10 s [25]. Consistently, individual contacts between T cells and APCs that constitute the primary unit of antigen recognition similarly were found to last only 10–20 s [19, 26].

Achieving high speed and sensitivity is particularly challenging if a high discrimination power is required. Discriminating between self and non-self antigens is a core function of T cells and a defect in this ability can lead to debilitating autoimmunity or susceptibility to infections and cancer. Despite intensive research, no structural difference has been identified between TCRs binding activating (agonistic) versus non-activating (non-agonistic) peptides [27–29]. Instead, T cells are thought to discriminate antigens based on sampling a continuous biophysical property of the binding event, such as affinity or lifetime. This conclusion is supported by multiple, independent experiments using a similar approach. T cells expressing a defined TCR with a known cognate peptide were stimulated with the cognate peptide or a variant of it. These altered peptide ligands (APLs) were produced by introducing 1–2 amino acid substitutions into the cognate peptide. Strikingly, sometimes even a single amino acid substitution was able to abrogate the T cell response completely [30–32]. To understand the difference in binding between agonists and non-agonists, the authors measured the affinities or lifetimes of the TCR/pMHC interaction by surface plasmon resonance (SPR) using recombinant proteins. Intriguingly, in different murine systems, including class I and class II TCRs, they found that a 3–10-fold decrease in lifetime or affinity is sufficient to render an agonist into a non-agonist [30–36]. This represents a very high level of discrimination and is sometimes referred to as 'absolute discrimination'* [37].

*Absolute discrimination is a theoretical construct, but is used here to refer to extremely good discrimination. Given the ambiguous meaning, I will be using the term 'near-perfect discrimination' throughout this thesis.

## 1.2 T cell development generates self reactive TCRs

T and B cells are unique in their ability to recognize a ligand that they were never previously exposed to. In the case of T cells these are peptides not represented in the body's peptidome. These peptides may be derived from exogenous sources, such as commensals or pathogens, or neoantigens created through genomic mutations. How does one solve such a complex task? T cells have evolved to express a TCR created through the somatic recombination of numerous TCR genes and further introduction of mutations, creating a unique receptor only present on each individual T cell clone.

The human genome has 4 TCR loci: *TRA* and *TRD* located on chromosome 14, and *TRB* and *TRG* on chromosome 7. They encode for the $\alpha$ and $\delta$, and $\beta$ and $\gamma$ chain of the T cell receptor, respectively. While there are 4 possible chains, the functional TCR is a heterodimer. Usually it is composed of either an $\alpha\beta$ or $\gamma\delta$ dimer, however, T cells expressing $\delta/\alpha\beta$ or a hybrid chain containing parts from 2 TCR loci have been described [38, 39]. Conventional MHC-restricted T cells* exclusively express $\alpha\beta$TCR, while unconventional T cells may express either of the aforementioned dimers.

T cell development and TCR recombination occurs in the thymus. Thymocytes start recombining the *TRB* locus and only cells expressing functional $\beta$ chain progress to the recombination of the *TRA* locus [40]. Recombination is dependent on the RAG1/2 protein complex and lack thereof results in severe combined immunodeficiency with lack of T and B cells. The possible diversity varies in each organism and is estimated to be in the order of $10^{18}$ for humans [41, 42]. Notably, this is a purely theoretical diversity. Any given individual will harbor significantly fewer unique T cell clones. For example, a human has fewer than $10^{12}$ T cells with $<10^8$ unique, naïve T cell clones [43, 44]. This number is far from sufficient to cover a theoretical peptidome diversity of $20^9 \approx 10^{11}$ for a 9 amino acid peptide (much more for a class

*In the following, I will be using the generic term 'T cells' to refer to conventional, $\alpha\beta$TCR-expressing T cells.

II peptide), if each TCR binds only 1 specific peptide [45]. Since a naïve T cell does not know its ligand *a priori*, each TCR must recognize many peptides presented on MHC to ensure full coverage of the peptidome. This inherent cross-reactivity is estimated to be in the order of 1 million peptides per given T cell clone [45].

Since recombination results in receptors with novel specificities, there needs to be a mechanism to prevent T cells reacting to ubiquitous self ligands. These mechanisms include processes in the periphery, as well as, a negative selection step during T cell development. In the thymus, T cells binding self-peptide loaded MHCs (self pMHCs) too strongly will be eliminated (negative selection). Furthermore, T cells not binding MHC at all, will die from 'death by neglect' (positive selection) [40]. Since their ligand will always be presented in the context of MHC, any T cell not responding to MHC at all, will be incapable of reacting to any meaningful foreign ligand [46]. Thymic selection results in the generation of MHC-restricted T cells with random TCRs, that do not activate when encountering self-antigen. It therefore sets the stage for antigen discrimination in the periphery.

## 1.3 The structure of the T cell receptor

The T cell receptor is a complex assembly of multiple transmembrane proteins. From the early days of TCR structural analysis, structural information was used to inform the mechanism of TCR triggering and how T cells discriminate antigens. While today there are many unligated or ligated structures of the TCR$\alpha\beta$ available, and most recently a structure of the whole TCR complex [29], this knowledge has not led to a convincing conclusion on the mechanisms of TCR triggering, yet, but helped exclude some models.

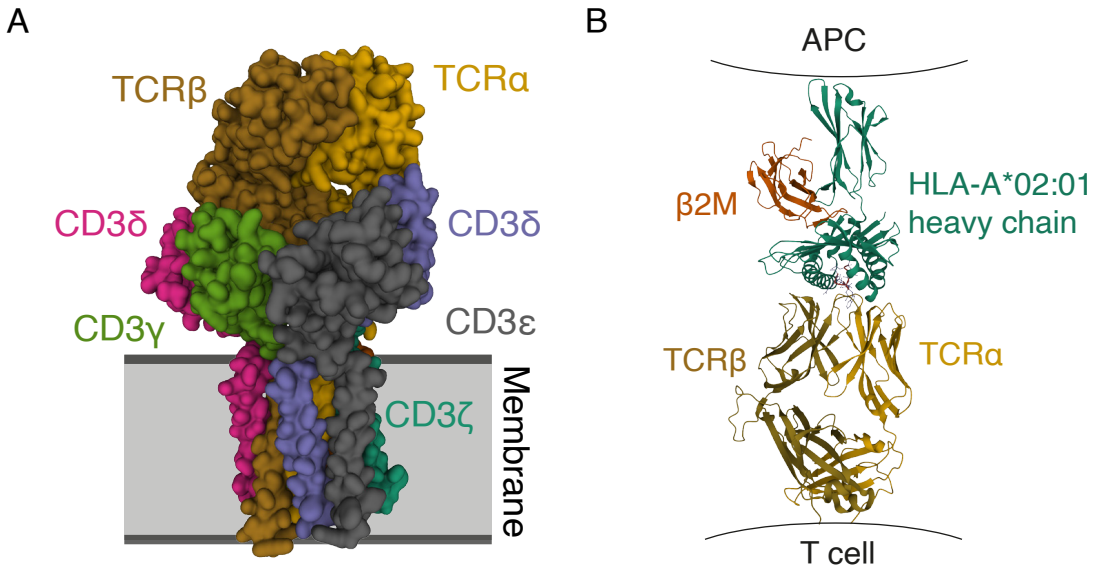


**Figure 1.1: The structure of the T cell receptor.**
**(A)** Structure of a αβTCR complex without resolved by cyro-EM (PDB: 6JXR) [29]. The second CD3ζ is hidden in this view. **(B)** The structure of the class I-restricted 1G4 TCRαβ interacting with MHC (PDB: 2BNQ) [47].

The functional αβTCR* is a complex consisting of four different dimers, namely TCRαβ, CD3ζζ, CD3γε and CD3δε (Figure 1.1A). The TCR is a disulfide-linked dimer with two extracellular immunoglobulin (Ig)-like domains each and a very short cytoplasmic chain. CD3ε, CD3δ, and CD3γ each have one extracellular Ig-like domain and an unstructured intracellular tail with one immunoreceptor tyrosine-based activation motif (ITAM) per chain. ITAMs include two short tyrosine-containing sequences (consensus: YxxL/I), separated by a 6–8 amino acid spacer [48] and generally confer activating signals upon phosphorylation. CD3ζ, in contrast, has a short, extracellular domain, a single transmembrane domain with an embedded intermolecular disulfide bridge, and a long (113 amino acid), unstructured cytoplasmic tail with 3 ITAM sequences. The TCR complex is held together by electrostatic interactions between the transmembrane regions and extracellular domains and is unstable if any component is missing. The TCRαβ dimer contains a total of 2 lysine and 1 arginine residue that form electrostatic interactions with aspartate and glutamate residues in the transmembrane domains

*I will use the term αβTCR to refer to the whole TCR:CD3 complex, and TCRαβ for the αβ heterodimer.

of CD3δε, CD3γε and CD3ζ subunits [49–51]. Furthermore, motifs in the extracellular domains of CD3δε, CD3γε and TCRαβ were thought to be important for assembly of a functional complex [52–54]. Most subunits contain an ER retention signal that prevents expression on the cell surface of not fully assembled TCR complexes [55]. CD3ζζ lacks this signal and can therefore be expressed independently on the plasma membrane [56]. Incomplete TCR/CD3 complexes are quickly removed from the cell surface by degradation or recycling [57–60]. The TCRαβ has been intensively structurally studied with numerous unbound or MHC-conjugated murine and human TCR ectodomain crystal structures available. Recently the structure of a full-length human TCR in association with all CD3 subunits was resolved by cryo-EM [29], confirming a 1:1:1:1 stoichiometry of the complex. Interestingly, when the structures of CD4 and pMHC-ligated TCR were overlaid, they match the cryo-EM structure well, indicating that there are no large conformational changes within the TCRαβ upon binding.

## 1.4 Ligand recognition by T cell receptors

TCRs can bind a variety of different ligands, including peptides presented on major histocompatibility complex (MHC) class I & II, lipids presented on CD1a–d, stress ligands like MICA and hMSH2, or metabolites presented on MR1 or BTN3A1 [46]. Given that the signaling chains are thought to be conserved in different T cells, this has important implications for the mechanism underlying antigen discrimination by T cells. For example, being able to recognize such a diverse array of ligands would be more difficult if the TCR is activated through conformational change, as compared to other mechanisms of TCR triggering.

On conventional T cells, αβTCR binds to peptide presented on MHC I or II (Figure 1.1B). MHC class I molecules are dimers comprised of the invariant β2M (beta-2-microglobulin) with a heavy chain encoded by the *HLA* (human leukocyte antigen) *-A*, *-B* and *-C* genes in humans. Class II molecules are also dimers, formed by an alpha chain and a beta chain encoded on the

*HLA-DR*, *-DQ*, and *-DP* genes in humans. MHC genes are generally considered the most polymorphic genes in the human genome with more than 20,000 known class I and over 7,000 class II alleles (IPD-IMGT v3.41.2). Different MHC variants vary in their binding specificity for peptides, thereby conferring an evolutionary advantage for a large polymorphism in the population. The binding groove of MHC class I is closed on each end and therefore can only hold peptides 8–10 amino acids long [40]. Some larger peptides can bind too, but they result in bulging [61]. The binding site of class II is more size-promiscuous, being able to bind peptides between 13–20 amino acids long [40]. Each MHC dimer can bind a large variety of peptides. Notably, MHC class I is only stable on the cell surface as a trimer of heavy chain, $\beta$2M, and peptide [40].

Binding of TCR to MHC occurs through its 3 complementary-determining regions (CDRs) in each of the TCR$\alpha$ and $\beta$ chain. These regions correspond the most highly variable sequences in the TCR genes. CDR1 and 2 are germline-encoded, while CDR3, being the most variable, is the product of V(D)J-junctional diversity and the addition or removal of random P- and N-nucleotides by a protein complex that includes terminal deoxynucleotidyl transferase (TdT). Most crystal structures of TCR/pMHC complexes show the TCR binding in a diagonal orientation with a 30–45° angle [62]. There are reports of a reversed binding orientation for both class I and class II TCRs [63, 64]. CDR3$\alpha$ and $\beta$ are oriented in the center and in direct contact with the peptide, while CDR1/2 contact predominantly the germline-encoded parts of MHC [61].

### 1.4.1 TCR interactions are weak

Previous research has established that the T cell response is correlated to the binding strength of the TCR/pMHC bond [30, 31, 35, 65]. Interestingly, the affinity of this interaction in solution is lower than for many other receptors in the immune system. Natural TCRs typically have

dissociation constants ($K_D$s) of 1–100 $\mu$M for their cognate antigens [66]. The low TCR/pMHC affinities are the result of relatively slow on-rates and fast off-rates. In comparison, B cell receptors commonly reach $K_D$s of less than 1 nM [67]. Notably, TCR/pMHC affinities are not structurally limited, since *in vitro* engineered TCRs can reach >5 orders of magnitude higher affinities [68], implying that low affinities have a functional relevance. Indeed, engineered, high affinity TCRs do not necessarily lead to an improved function [69]. Alternatively, the affinity may be limited by the recombination process. For example, B cells require hypermutation in presence of the antigen to generate high affinity antibodies [6]. This process does not exist in T cells.

In a comparison of a small sample of TCRs, Cole *et al.* found TCRs binding class I MHC tend to have slightly higher affinities, usually about 2–30 $\mu$M $K_D$ for human class I TCRs, and 20–100 $\mu$M $K_D$ for class II TCRs [70]. Furthermore, they find pathogen-specific TCRs bind stronger than TCRs directed against self-antigens. Interestingly, the decreased affinity of class II TCRs is a result of a smaller on-rate, while the off-rate is relatively consistent between different TCRs. Cole *et al.* hypothesize that this is a result of the flatter topology of the peptide in MHC class II, thereby exposing less surface for binding. Functionally, the decreased affinity could be a necessity to achieve higher cross-reactivity, allowing CD4 cells to cover the much larger class II peptidome (as a consequence of having longer peptides) with a similar number of T cells. Dissociation constants for the interaction of TCRs with self-pMHC are difficult to measure by current technology and consequently the affinity to 'self' is unknown. Notably, these self-interactions are physiologically important and provide T cells with tonic signals, crucial for T cell maintenance *in vivo* [71].

### 1.4.2 TCR interactions at the membrane

Initial work on antigen discrimination has correlated T cell responses with binding parameters measured in 3D, usually by SPR. In these assays, one binding partner is immobilized while the other is in solution. At the T cell interface, however, both interacting molecules are embedded in membranes. Multiple factors can change the binding in such an environment dramatically to what is measured *in vitro* using recombinant proteins. First, the TCR/pMHC binding occurs at areas of close membrane proximity, termed close contacts (see also Figure 1.2) [72], leading to an increased effective on-rate, due to the high local concentrations. Such an effect could be further enhanced if the TCR is enriched in clusters. Microclusters occurring after initial triggering are well established [73, 74]. Furthermore, nanoclusters of TCR on resting T cells have been observed too [75–77]. Given high local concentrations, membrane-proximity, and relatively slow diffusion, rebinding of the TCR to the same pMHC can increase the effective dwell time massively [78]. Serial triggering, a mechanism to explain high sensitivity, where one pMHC goes through a series of binding events with different TCRs [79–82], also depends on high local TCR concentrations. Moreover, binding of the TCR to pMHC also leads to engagement of the CD4 or CD8 co-receptors [55], forming a ternary complex that is not present in SPR. Such a complex may be more stable than a TCR/pMHC dimer. Most importantly, thermal membrane fluctuations, size mismatches between different receptor/ligand pairs (such as TCR/pMHC and LFA-1/ICAM1), active polymerization processes, and electrostatic repulsion of the glycocalyces are expected to exert a force on molecular interactions at the interface [83–86].

Multiple assays have been used to directly investigate binding kinetics at the T cell interface (*in situ*). Johannes Huppa and colleagues at the Davis laboratory found strongly accelerated kinetics when using a Förster resonance energy transfer (FRET)-based assay to measure 2D kinetics of CD4 T cells binding to class II MHC [87]. Their technique measures FRET between

labeled pMHC on a lipid bilayer and labeled TCR on T cells. In comparison to values measured by SPR, association was increased by around 100-fold, while dissociation was accelerated by 4–12-fold. Huang *et al.* also reported accelerated kinetics for a class I TCR using an adhesion-based assay [88]. In this assay, a red blood cell (RBC) coated with pMHC class I is brought into contact with a T cell with a micropipette. Since the T cell is also fixed in place via a micropipette, a retraction of the RBC leads to its deformation and bond rupture can be microscopically observed as a relaxation of the RBC. They found that 2D on-rates varied strongly and correlated with T cell responses. This is in contrast to 3D kinetics, where on-rates usually do not change drastically, but the off-rate correlates with functional responses [78]. Similar results on 2D kinetics were found with CD4 T cells [89]. However, 2D and 3D kinetics were quite well correlated in that study. Further support for accelerated unbinding come from a diffusion-based assay, where the diffusion slowdown of pMHC on a lipid bilayer is observed upon TCR binding [90]. Subsequent conflicting results using this assay, where bond dissociation was observed to be slower than in SPR, rather than faster, likely is an artifact of the imaging conditions chosen [91]. Since they used a much longer exposure time compared to previous studies, they potentially missed short-lived binding events, biasing their results towards longer lifetimes. Together these results highlight that binding in the physiological context of an T cell/APC interaction will likely exert different dynamics than when measured with recombinant proteins *in vitro*. However, 3D kinetics or affinities measured by SPR can still predict antigen discrimination, assuming 2D and 3D values are correlated. As discussed below, active exertion of force on the TCR/pMHC bond may be one mechanism that can cause a bad correlation by changing the off-rates relative to 3D off-rates of some peptide more than of others [92].

## 1.5 TCR signal transduction

Explanations for how the TCR achieves good discrimination generally invoke the TCR proximal signaling chain. The TCR proximal signaling cascade of T cells comprises numerous binding and phosphorylation events, that may serve as kinetic proofreading steps to achieve effective antigen discrimination.

Initially, stimulating TCRs with pMHC leads to a rapid phosphorylation of tyrosines in the ten ITAMs of the CD3/TCR complex by the Src family kinases Lck and Fyn [93, 94]. Lck is lipid-anchored and can non-covalently associate with CD4 and CD8 [95, 96]. One theory is that binding of the co-receptor to TCR-bound pMHC brings Lck in direct proximity of the CD3 ITAM, allowing efficient phosphorylation [97]. The activity of Lck is controlled by multiple tyrosine phosphorylation sites. Phosphorylation of Y505 by Csk leads to inactivation, while pY394 has an activating effect [94]. Interestingly, both sites can be dephosphorylated by the large phosphatase CD45, leading to an unphosphorylated, primed state with low kinase activity [98]. This dual role of CD45 has important implications for signal induction, as discussed below [99].

Phosphorylation of CD3 ITAMs is followed by binding of the Syk kinase ZAP-70 [100, 101], which propagates the signal by phosphorylating the scaffolding protein LAT, where signal amplification and divergence occurs [102–104]. Interestingly, Lck and ZAP-70 both have highly, but oppositely charged active centers, leading to distinct substrate specificities with little overlap [105, 106]. ZAP-70 itself can also be phosphorylated at 3 activating and 1 inhibitory tyrosine residues.

Upon phosphorylation LAT forms microclusters that are enriched with TCR and other signaling molecules [73, 76]. *In vitro* reconstitution showed these clusters form by cross-linking of LAT through Grb2, Sos, Gads, SLP76 and Nck [107]. Loss of LAT or SLP-76 results in a severe

TCR signaling defect, similar to lack of Syk and Zap-70, or Lck and Fyn [94]. LAT phosphorylation leads to propagation of the main signaling pathways through the production of the soluble second messengers diacylglycerol (DAG) and the lipid inositol triphosphate ($IP_3$) by phospholipase C$\gamma$ 1 [94]. Ultimately, they lead to the activation of 3 key transcription factors, that control the effector functions: NF$\chi$B, AP-1 and NFAT [94]. The actual effector functions induced depend on the state of the T cell and contextual signals received. Full T cell activation requires signaling through multiple pathways. For example, NFAT activity without AP-1 activation leads to T cell anergy, rather than activation [108].

CD3 ITAM phosphorylation is the earliest detectable biochemical correlate of TCR triggering and has been intensively investigated. CD3$\varepsilon$ and CD3$\zeta$ were found to interact with the plasma membrane through basic-rich sequences (BRSs) in their unstructured tails [109–111]. This is possible since the inner leaflet of the plasma membrane is negatively charged as a result of an asymmetric distribution of phospholipids between the layers. *In vitro* work with reconstituted bicells revealed the unphosphorylated ITAM tyrosine residues buried into the hydrophobic core of the membrane, when observed by NMR [110, 112]. Phosphorylation of the ITAMs by Lck negates some of the charges in the tail, leading to dissociation from the membrane. Xu *et al.* proposed this serves as a safety mechanism to prevent unwanted phosphorylation in resting cells, thereby opening a potential mechanism for conformation- or force-based TCR triggering models. However, it is not clear if dissociation from the membrane is truly a cause or just a consequence of phosphorylation. Furthermore, rather than an on/off-model, the tails likely will be in a thermodynamic equilibrium between membrane-bound and free states. Interestingly, CD3$\delta$ and CD3$\gamma$ do not have BR sequences. While they therefore are not subjected to the same protective mechanism, they are intrinsically less likely to be phosphorylated, since the BR sequence is important for the binding of Lck [105, 106]. This offers a possible explanation why CD3$\varepsilon$ and CD3$\zeta$ with mutated BRS, unable to bind membrane, are being less phosphorylated inside the cell [111, 113]. Notably, the release of calcium during activation

may help negate negative membrane charge [114]. Since calcium is a downstream messenger of TCR signaling, this could serve as feed-forward loop, amplifying activation, rather than causing it. Consistent with this, inhibition of calcium in T cells decreases phosphorylation of CD3$\varepsilon$ and CD3$\zeta$ [114].

### 1.5.1 Co-receptors

Binding of TCR to MHC is accompanied by the binding of the co-receptors CD4 or CD8 for MHC class II- and class-I-restricted T cells, respectively. Co-receptors are thought to play a role in the kinetic proofreading chain that may power the T cell's ability to discriminate between antigens [115, 116]. Furthermore, they are important for the sensitivity to antigen, particularly to low-avidity TCRs [117]. Lastly, co-receptors are involved in controlling cross-reactivity.

Both co-receptors contain extracellular domains with Ig-like domains and intracellular tails capable of associating with the kinase Lck. T cell activation can occur in the absence of co-receptors, but sensitivity to antigen is severely decreased [11, 14, 118]. Structurally, CD4 and CD8 are quite distinct. CD4 is a monomer with 4 Ig-like domains and a 40 amino acid long intracellular tail. CD8 is expressed as either a CD8$\alpha\alpha$ homodimer or CD8$\alpha\beta$ heterodimer and only has 1 extracellular Ig-like domain, plus a long and rigid stalk region. On conventional $\alpha\beta$ T cells, CD8 is expressed as a heterodimer. In contrast, on $\gamma\delta$ T cells, NK cells and certain dendritic cells, it is expressed as a homodimer of the $\alpha$ chain. The affinities for co-receptors to MHC are generally low. The dissociation constant for human CD4 to MHC in solution is estimated to be in the mM range, while the 2D affinity is also very low with a $K_D$ of about 5,000 molecules/$\mu m^2$ [119]. CD8 binds human MHCs with a $K_D$ of about 150 $\mu$M, while murine CD8 binds significantly more tightly with about 50 $\mu$M $K_D$ [120]. CD8 is implicated in controlling the cross-reactivity of T cells, for example by changing to the less active $\alpha\alpha$ isoform [121],

downregulation through internalization or transcriptional inhibition [122, 123], or changing the activity through CD8 glycosylation [124–126]. Consequently, mice need a higher affinity binding to achieve higher cross-reactivity, yielding the same antigen coverage with a smaller T cell repertoire. Consistently, murine TCR affinities were also found to be higher than for human TCRs [70, 120].

## 1.6 Accessory receptors impact TCR signal transduction

The interaction of T cells with antigen presenting cells (i.e. target cells or professional APC) is complex in nature and not only dependent on the TCR/pMHC interaction, but many more counter-receptors. This includes co-stimulatory, co-inhibitory, and adhesion molecules. Structurally, most of these proteins are comprised of Ig-like domains (e.g. CD2 or CD28) or cysteine-rich domains (CRD; TNF receptor superfamily). In combination with cytokines, accessory receptors provide the context for T cell activation. Accessory receptors may act through intracellular signaling, but can also influence of TCR/pMHC binding by creating membrane proximity. CD2 and LFA-1 play an important role in antigen sensitivity and (as shown in this thesis) contribute to antigen discrimination, as well.

### 1.6.1 CD2 and its ligands

CD2 (also known as LFA-2) is a heavily glycosylated protein from the immunoglobulin (Ig) superfamily, involved in co-stimulation and adhesion. It is primarily expressed on the surface of T cells, NK cells, thymocytes, thymic B cells and to a lesser extent DCs [127] and is enriched on memory T cells [128]. CD2 is involved in thymic selection and antigen recognition by T cells, and the activation of NK cells and has received increased attention in the last years as a potential target to treat autoimmune disease. In humans, CD2 binds to the struc-

turally similar Ig-like protein CD58 with which it shares limited sequence homology [129]. CD58 exists in a second isoform in humans with a transmembrane domain and cytoplasmic tail, instead of a GPI-anchor. CD58 is broadly expressed in hematopoietic cells and also many non-hematopoietic cells, including endothelial cells, erythrocytes and keratinocytes [127].

### Structure and interactions of CD2

Binding of CD2 to its ligand is mediated through electrostatic interactions, with little surface complementarity [129, 130]. The affinity of CD2 is relatively low with a 3D affinity of 9–22 $\mu$M, a consequence of a fast off-rate [131]. This low affinity has been implicated in allowing transient T cell interactions [20]. Furthermore, the affinity might be limited by the force required to extract the lipid-anchored isoform of CD58 [132, 133]. CD2 is expressed at a density of about 100 molecules/μm$^2$ on peripheral T cells [134] and half-maximal binding was determined to occur at about 5–7 molecules/μm$^2$ [134, 135]. Therefore, significant binding is expected to occur despite its low affinity. Furthermore, activation of T cells has been shown to increase CD2's avidity moderately through a combined mechanism of a 1.5-fold increased expression and a 2.5-fold increase in 2D affinity [136, 137]. This is also accompanied by a temporary, but stark increase in immobile fraction of CD2. Notably, the adhesion mediated by CD2 might be limited by diffusion, as adhesion was more efficient with the much more mobile GPI-anchored than the TM isoform of CD58 [138].

While homologs of CD58 are found in other mammals such as pigs and sheep, and even some lower vertebrates such as zebrafish, it is absent in rodents [139, 140]. Instead CD2 binds a structurally related protein called CD48 in mice [141] and other rodents. Interestingly, throughout evolution from fish to mammals the intracellular tail of CD58 became shorter [140], while CD48 only exists as a GPI-anchored form. Moreover, unlike CD58, the expression of CD48 is mostly restricted to the hematopoietic compartment. Human CD2 binds CD58 with a ~5-fold

higher 3D affinity than does rat CD2 to CD48, and this difference is elevated to ~40-fold [142] for the 2D dissociation constants.

CD2 co-precipitates with TCR/CD3 [143, 144] and PI3K [145], but no direct interaction has been shown. CD2 has a 166 amino acid long unstructured cytoplasmic tail that lacks classical ITAM sequences and any other tyrosine residues but contains a highly conserved proline-rich region. This region hosts 5 putative SH3-binding sequences, each containing 3–5 prolines [146, 147], and mediates a number of interactions, such as with CIN85 [148, 149] and its alternative splicing variant CD2BP3 [150], the kinases Fyn and Lck [151–153], CD2BP1 [154] and CD2AP [152]. Motif 1 and 2 can furthermore act as binding site for glycine-tyrosine-phenylalanine (GYF) domains [153, 155], such as in the GYF prototypic CD2BP2 [146]. The tail terminates in an asparagine residue, which was shown to be involved in avidity regulation [156, 157], but was dispensable for CD2-mediated signaling.

## Function of CD2

CD2 shares some traits with CD28 and might fulfill a similar co-stimulatory role in specific contexts. For example, co-stimulation of CD2 was shown to be the primary pathway of activation in CD28-negative T cells [158]. Mice lacking both CD2 and CD28 do not show a strong *in vivo* phenotype, but a severe defect when T cells are stimulated *ex vivo* [159]. While CD28 integrates more distally of the TCR signaling cascade and leads to potent activation of NF-$\varkappa$B, stimulation through CD2 converges more proximal and preferentially leads to mTOR signaling via phosphorylation of S6 ribosomal protein [160–162].

In humans, CD2 and CD28 have a similar affinity for their ligands [163]. However, CD28 does not mediate adhesion efficiently, due to a combination of low mobility and low expression [164], potentially resulting in inefficient nucleation of adhesive contacts. Unlike CD2, CD28 engagement does not increase TCR downregulation [165]. When bound to their ligands, both

receptor/ligand pairs are expected to span a similar intermembrane distance based on their similarity in dimensions. Consequently, CD2 and CD28 both accumulate together with the TCR at the center of the immunological synapse [164, 166]. The positioning of CD2 depends on its cytoplasmic tail, which allows binding of the adapter molecule CD2AP [152]. At high expression levels, CD2 also accumulates in a ring between peripheral and distal SMAC in the immunological synapse, termed the 'CD2 corolla', with other molecules such as CD28, LAT and activated Src-family kinases [167, 168].

CD2 is thought to facilitate TCR/pMHC binding by creating close contacts (see also Figure 1.2). Consistent with its function, elongating CD48 in a rodent system decreased binding and inhibited T cell activation [169]. Despite its important proposed function, early studies in mice where CD2 was either genetically removed through a knock-out or inhibited with antibodies did not show an overt phenotype during T cell development or activation [170–172]. However, subsequent studies showed a subtle defect of CD2-null cells in response to antigen and in thymic selection [173–176]. Two groups have quantitatively assessed the effect of CD2 on T cell activation and found CD2 engagement reduced the dose required to stimulate proliferation or cytokine secretion of murine CD4 and CD8 T cells 3–100-fold [165, 175, 176]. Interestingly, the shift in the dose response increased for lower affinity ligands, implying that CD2 could influence antigen discrimination. This was accompanied by increased downregulation of the TCR, consistent with the idea that CD2 increases TCR/pMHC binding. Why there is a clear phenotype when T cells are tested *in vitro*, but no apparent systemic defects, is a matter of speculation. It is possible that adaptation *in vivo* masks strong effects or that there are compensatory receptor/ligand interactions. Notably, the importance of CD2 in humans is likely to be higher than in rodents, since the ligands in mice and humans differ in tissue-restriction and affinity. We have recently shown that CD2 has a similar effect in humans using an affinity-enhanced TCR [3]. In this thesis, I show a similar effect when using a natural TCR and human T cells.

Additional data highlight the importance of the CD2/CD58 axis in humans. First, viral antagonism by a human cytomegalovirus (HCMV) protein has been reported and results in decreased killing by $CD8^+$ T cells and NK cells [177, 178]. In a CRISPR screen in cancer cells, loss of CD58 was highly associated with evasion of T cell killing [179]. Interestingly, the CD2/CD58 axis was also shown to be important for activation of CAR T cells [180]. Mutations in CD58 or loss of expression on tumor cells has been implicated in therapeutic resistance to CAR T cells [181]. Loss of CD58 has also been observed outside of CAR T cell therapy in Hodgkin's and diffuse large B cell lymphoma and results in decreased NK cell and T cell mediated cytotoxicity [182, 183]. Moreover, a specific mutation in CD58, which resulted in increased expression, was associated with protection in multiple sclerosis patients [184]. They suggest this allele confers protection by increasing CD58 expression, which when engaged by regulatory T cells enhances their function. Polymorphisms in CD58 are also associated with neuromyelitis optica [185] and rheumatoid arthritis [186]. In a mouse model, variations in the CD2 gene were associated with susceptibility to type 1 diabetes [187]. Therapeutically, CD2 is actively targeted by alefacept, a CD58-Fc fusion protein, licensed for treatment of psoriasis and investigated as type 1 diabetes treatment [188, 189]. Siplizumab is a humanized antibody currently under investigation for psoriasis, solid and stem cell transplantations, graft-versus-host disease and CD2-positive malignancies [190–195]. Furthermore, peptides mimicking the CD58 binding site have been investigated to treat collagen-induced arthritis in a mouse model [196, 197].

### 1.6.2 LFA-1 and its ligands

Integrins are a family of heterodimeric adhesion receptors expressed on leukocytes, platelets, and non-hematopoietic cells. There are 18 $\alpha$ and 8 $\beta$ subunits known, forming 24 unique $\alpha\beta$ dimers. Integrins play an important role in leukocyte trafficking, adhesion to the extracellular matrix, APC conjugation and cell activation [198]. Defects in the integrin pathways, known as leukocyte adhesion deficiency (LAD), cause severe immunodeficiency in humans

[199]. Leukocytes express at least 10 different integrins, including members of the $\beta 2$ and $\beta 7$ family that are exclusive to leukocytes [200]. For example, T cells express LFA-1 (CD11a/CD18), VLA-4, LPAM-1, VLA-5, and VLA-6, with some subsets also expressing HML-1, VLA-1, and VLA-2 [200]. LFA-1 is the most intensively studied integrin expressed on T cells and is involved in T cell/APC contacts and extravasation. In addition to collagen, it binds ICAM-1–5 and JAM-A, which are all members of the immunoglobulin superfamily with 2–9 Ig-like domains. In the context of T cell interacting with APCs, ICAM-1 is considered the most important ligand and has been suggested to form homodimers on the cell surface [201, 202]. Expression of ICAM-2, ICAM-3 and JAM-A can also be detected on professional APCs, such as DCs and monocytes. T cells express ICAM-2 and some ICAM-1, ICAM-3, and JAM-A according to mRNA analysis [203].

LFA-1 is thought to exist in an equilibrium of 3 allosteric states with vastly different ligand affinities: closed bent, open bent, and an open extended conformation with low, intermediate, and high ligand affinity, respectively, with high-affinity binding depending on the presence of $Mg^{2+}$ [204]. LFA-1 binds ICAM1 more strongly than ICAM2 or ICAM3 [205] with a $K_D$ of ~0.2 $\mu$M, ~5 $\mu$M, and >1 mM for the high, intermediate and low affinity state, respectively [205–207]. Dimerization of ICAM1 increases this further to ~5 nM [202, 206]. Importantly, signals through other pathways can change the conformation of LFA-1 (inside-out signaling), but LFA-1 can also transmit binding signals via its cytoplasmic tails (outside-in signaling). Signals received through the TCR, chemokine receptors, or selectin can induce a shift towards an intermediate affinity, open conformation [208, 209]. However, to reach the highest affinity conformation, stabilization by ligand binding and the application of perpendicular force are required. LFA-1 binding to ICAM1 shows a remarkable strengthening under force, producing what is called a catch bond, that helps with its function during leukocyte trafficking [210]. Force application requires immobilized ICAM1 and immobilization on DCs upon maturation has been shown to be important for T cell activation and adhesion [211]. Bi-directional

signaling through LFA-1 is mediated by the interactions of its intracellular tail with proteins such as RAP1 (a small GTPase) or Kindlin3 [208]. During outside-in signaling, LFA-1 interacts with the kinases ZAP-70 and Lck and activation of the former is required to shift into the high affinity state [212]. LFA-1 forms microclusters upon T cell activation that migrate centripetally to form a ring around the central immunological synapse [213, 214]. Segregation of LFA-1 from the TCR is consistent with its larger size compared to the TCR or other molecules such as CD2 or CD28 (see also Figure 1.2) [99, 215]. Recent work indicates that LFA-1 forms small, transient rings around TCR microclusters and these structures depend on the actin cytoskeleton [216]. Comparison with other data suggests that these rings present the periphery of a membrane protrusion, with the TCR localized in the center [1, 216, 217].

Lack of the $\beta$2 chain that forms part of LFA-1 and other integrins or loss of Kindlin3 cause LAD. Knockout of the LFA-1-specific $\alpha$L chain results in a more subtle immune defect with a normal response to viruses including lymphocyte choriomeningitis virus and vesicular stomatitis virus, but impaired proliferation and activation of T cells *in vitro* [218]. Furthermore, ICAM1 on APCs is important for T cell memory formation, but lack of it can be compensated by other activating factors, such as through an increase in antigen dose or co-stimulation [219]. Interestingly, T cells lacking ICAM-1 do not form aggregates, but unlike LFA-1 deficient cells, they proliferate normally in response to stimulation [220]. Quantitative analysis of T cells lacking LFA-1, showed a similar phenotype to CD2-deficient cells, with a 10- to 100-fold higher required dose of antigen, and decreased TCR downregulation [221–223]. Notably, the effects of a CD2 and LFA-1 knock-out are additive and can result in a 100-fold shift in the dose response curve [165]. A similar effect was observed for B cells lacking LFA-1 [224]. Lack of LFA-1 also results in a defect in regulatory T cell function and development [225, 226]. While stimulation of LFA-1 can increase production of Th1 cytokines dramatically, in the absence of CD28 engagement it leads to T cell anergy [227, 228].

## 1.7 TCR triggering

The mechanism by which the TCR transduces ligand-binding into an intracellular event leading to the activation of Lck has been the focus of intense research, yet there is still considerable dissensus and the co-existence of mutually exclusive models. Unlike any other receptor, the TCR does not know its ligand and is confronted with an abundance of chemically similar self-ligands. Faced with these challenges, T cells evolved a highly complex receptor and signaling machinery. Some TCR triggering models, such as the conformational change model, explain both how the TCR is triggered and how antigen discrimination occurs. Other models, such as kinetic segregation, only concern the triggering process and require mechanisms like kinetic proofreading to explain antigen discrimination.

### 1.7.1 Conformation change models

Conformational change models were among the first models to be investigated for the TCR. Many other receptors, such as the large family of G protein-coupled receptors (GPCRs) [229], work by this principle. Ligand binding to these receptors may work by allostery, i.e. binding stabilizes a rare equilibrium state, rather than inducing a different conformation directly. Conformational change models offer an attractive alternative since they are able to explain the exquisite specificity and sensitivity. In contrast to other receptors, however, the TCR needs to recognize structurally diverse ligands and TCRs are inherently unable to co-evolve with their peptide ligands. Furthermore, comparison of TCRs with or without ligand showed only substantial conformational changes in the variable regions of the TCR, but no consistent structural changes in the constant domains [27–29]. The lack of conformational change observed in crystal structures of TCR is unlikely a consequence of missing molecular context such as glycosylation, association of CD3 subunits and presence of transmembrane domains, since an

unligated cryo-EM structured of the whole TCR complex overlapped strikingly with a crystal structure of the same TCR in a complex with a cognate pMHC [29]. In their work, they also did not find any overt signs of multiple allosteric states whose equilibrium could be influenced by ligand-binding. Molecular dynamics simulations have further strengthened the case against conformational changes [230].

### 1.7.2 Mechanosensing

More recently, conformational change models have regained traction due to the finding that T cells can exert forces on the TCR/pMHC bond [231]. In such a model, T cells may apply force to test the bond, causing a force-induced conformational change [232]. Since these changes are only appearing upon application of force, one would not expect to find them in crystal or cryo-EM structures of TCR/pMHC complexes, where binding happens in solution. Force may also directly change the kinetics of the TCR/pMHC interaction.

Work done by the Reinherz group found direct evidence for structural differences between the TCR binding to agonistic versus non-agonistic pMHCs [233]. They investigated the lifetime as a function of forces, using a single-molecule optical trap (OT) either in a purely *in vitro* system with recombinant proteins or by probing TCRs on a T cell. This technique works by exerting force on a bead when it is displaced from a laser beam (referred to as trap). They found a catch bond (i.e. a bond strengthening under force) with agonistic pMHC with a peak at 15 pN, but not irrelevant pMHC, using either experiments with recombinant proteins or a cellular approach [233]. Binding was accompanied by a structural change of the TCR from a compact to an extended state, observed as a small displacement of the OT bead, without bond rupture. They found larger displacements with activating versus non-activating pMHC. Further research has suggested the occurrence of this structural change in the pre-TCR of thymocytes [234]. In this model, the force-induced conformational change is transduced into the CD3

units, where it leads to dissociation of the ITAM-containing cytoplasmic tails [235]. Such a release is proposed to lead to spontaneous phosphorylation and subsequent downstream activation.

Interestingly, the elongation observed in the TCR$\alpha\beta$ using recombinant proteins was up to 150 Å, twice the size of the whole TCR, and even more when using cells, therefore raising concerns how physiological these structural changes are. Differences between tested pMHC were smaller ($\sim$40 Å) and more consistent with a TCR that is not completely unfolded. They determined this structural change to be dependent on the FG loop in the constant region of the TCR$\beta$ chain [236]. It is intriguing that the FG loop is only present in mammalian $\alpha\beta$TCR, but not $\gamma\delta$TCRs [237], raising questions if this mechanism would be applicable to $\gamma\delta$ T cells.

### 1.7.3 Kinetic segregation

Another class of models is based on segregation of the TCR and other molecules on the membrane upon ligand binding by the TCR. Kinetic segregation of the TCR, integrins and the large phosphatase CD45 was first observed in the immunological synapse [238–241] and is predicted by the differences in size [215]. CD45 is highly expressed on T cells and other hematopoietic cells and efficiently catalyses the dephosphorylation of a broad spectrum of targets [98]. Under resting conditions, the negative effect of CD45 is expected to outweigh spontaneous phosphorylation of TCR ITAMs by Lck by a factor of 100 [242]. Binding of TCR to pMHC leads to a segregation of TCRs and CD45 (Figure 1.2). In contrast, the kinase Lck is intracellular and therefore not affected by kinetic segregation. Consequently, the ratio of dephosphorylation to phosphorylation of the CD3 ITAMs by CD45 and Lck, respectively changes in favor of phosphorylation, ultimately leading to TCR triggering [99, 243].

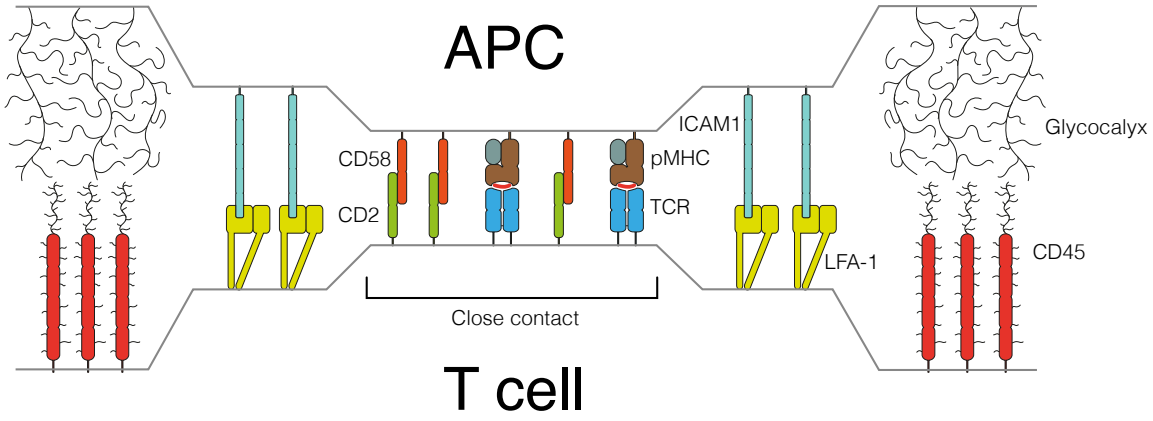


**Figure 1.2: Kinetic segregation of molecules at the surface of T cells.**
On the surface of T cells, molecules can segregate based on their molecular heights. Such a segregation has been described on a micro-meter scale in the immunological synapse, and occurs on a smaller scale on the initial close contacts. TCR bound to pMHC is relatively small and therefore binding is not energetically favored. Adhesion molecules like CD2 can create close-contacts where TCR can bind to pMHC. Such contacts are surrounded by LFA-1 bound to ICAM1 and more distally, large glycoproteins such as the phosphatase CD45.

Interestingly, kinetic segregation is not directly ligand dependent. Indeed, evidence for ligand independent triggering of TCRs in close contacts supports this view [72, 244]. How does the T cell differentiate agonists and non-agonists in this model? Fernandes *et al.* give a possible explanation based on experimental data and mathematical simulations. In their model, close contacts cause phosphorylation of any TCR passing them [245]. However, due to fast diffusion, TCRs not bound to a ligand do not acquire sufficient phosphate modifications to induce downstream signaling. Ligand binding slows diffusion drastically, thereby allowing full phosphorylation and T cell activation. Since binding needs to reach a certain time, this model effectively implements kinetic proofreading on a binding model. Notably, this model is highly sensitive to changes in close contact radius. Extending the radius quickly results in ligand independent triggering and therefore poses the question of how the T cell might regulate this tightly. Since close contacts likely are the results of microvilli (membrane protrusions of T cells) tips pressing against the target cells [1], it is possible that these structures are limiting the size that such contacts could grow to. Another attractive idea comes from the work

of Razvag *et al.* They find that large segregation (>200 nm) of CD45 from TCR correlates negative with phosphorylation [244]. In their data, CD45 needed to be at an optimal distance of about 40 nm. This is consistent with the dual role of CD45, facilitating TCR activation by dephosphorylating an inhibitory phospho-tyrosine of Lck, while at the same time preventing it by direct dephosphorylation of TCR ITAMs [98]. While T cells may form large close contacts, the size of the zone where productive phosphorylation can occur is intrinsically limited by a minimal distance of CD45, allowing the diffusion of unphosphorylated Lck into the contact. Interestingly, kinetic segregation is not restricted to the TCR. Many important immune receptors, such as the BCR, Fc-receptors, and multiple types of NK receptors, belong to the class of non-catalytic tyrosine-phosphorylated receptors (NTRs) [246]. These receptors do not possess any intrinsic kinase activity, but they contain tyrosine residues that can be phosphorylated by independent kinases such as Lck. All of them are relatively small and therefore fit the kinetic segregation model. Direct evidence has been found, for example, for the Fc-receptor mediated phagocytosis of macrophages [247].

In addition to observing segregation in functional cells, extensive work has focused on shining light on the biophysical sources of segregation. One challenge has been measuring the height of CD45 reliably. While the TCR/pMHC bond has been determined to span about 13 nm, determining the effective height of CD45 has proven to be more complicated. Its ectodomain is rigid and stretches about 15 nm [72], but is further extended by heavy O-glycosylation in a mucin-like region, resulting in a total hydrodynamic length of about 22 nm [248]. Segregation is a result of entropic effects and direct electrostatic repulsion [83, 249]. Furthermore, the membrane elasticity determines the energetic penalty imposed on proteins with mismatched sizes [86]. Notably, CD45 exists in multiple isoforms and the longer isoform was found to be more efficiently excluded in a reconstituted membrane system [250]. Differences in height of as little as 5 nm can drive efficient exclusion, however even in absence of height difference segregation can occur due to crowding effects [251]. Binding of a receptor can lead to local

enrichment (e.g. a microcluster) in a membrane domain. Unbound receptors, or unrelated receptors will segregate out, even if there is no difference in size. Kinetic segregation was proposed over 20 years ago, yet due to the technical challenges of imaging the dynamic events driving segregation, initially faced a slow adoption in the field. New technology has helped uncover some the details of this mechanism and may support confirming kinetic proofreading in the TCR field and beyond.

## 1.8 Mechanisms of antigen discrimination

While T cells are one of the most studied cells in the human body, how they become activated on a molecular level and how they discriminate antigens still remain largely unsolved. T cells may discriminate antigens in different ways through sampling of: (1) Qualitative properties, such as the ability to induce a conformational change. (2) Quantitative properties, such as the TCR/pMHC lifetime or affinity. In models based on conformational change, the mechanism of triggering is also responsible for antigen discrimination. In contrast, in kinetic segregation an intracellular signaling machinery is required to discriminate between signals produced from binding agonistic versus non-agonistic ligands. The predominant model in the field is kinetic proofreading [252].

### 1.8.1 Kinetic proofreading models

Kinetic proofreading (KP) is a model of an intracellular signaling pathway that can achieve improved antigen discrimination. It predicts T cell responses to correlate with the off-rate of the TCR/pMHC interaction. Experimental evidence, where the off-rate (or its inverse, the lifetime) measured by SPR at least partially predicts the potency of a ligand, supports this 'lifetime dogma' [30, 31, 35, 65]. Notably, $K_D$s and off-rates of APLs for a given TCR are often closely

correlated and may explain why other studies found that affinities are also a good predictor of potency [78]. Kinetic proofreading can be evaluated in contrast to the occupancy model. In this model, activation depends only on receptor occupancy, which in turn is a function of the affinity and the dose of the ligand [253]. This model can be considered the null hypothesis, since it represents the simplest receptor/ligand model. In this model, the discrimination is limited to the fold difference in affinity or lifetime (for the latter assuming a constant on-rate; $K_D = k_{off}/k_{on}$). For example, a 10-fold difference in affinity between an agonist and non-agonist would produce the same receptor occupancy and therefore signal, if the non-agonist's concentration was 10-fold higher. Since non-agonistic self-peptide is ubiquitously present in our bodies, this model is not compatible with the physiological requirements of antigen discrimination.

### Classical kinetic proofreading

Based on these shortcoming to explain the T cell discrimination observed experimentally, kinetic proofreading was proposed [252]. Initially it was evaluated as a mechanism to achieve high fidelity during DNA replication or protein translation [254, 255]. Importantly, kinetic proofreading is a model of the receptor proximal signaling pathway and therefore compatible with many TCR triggering models, such as the kinetic segregation model [99]. Unlike the occupancy model, kinetic proofreading operates out of equilibrium under energy consumption to achieve a higher specificity. Specifically, upon binding its ligand, the receptor/ligand complex ($C_0$) must undergo one or multiple independent irreversible modifications ($C_i$) until it reaches a signaling-competent state ($C_N$; Figure 1.3A). Since each step requires the ligand to be bound for a certain time ($\tau_p = 1/k_p$) to allow modification to occur, the quantity of signaling-competent complex ($C_N$) strongly depends on the off-rate of the ligand (Figure 1.3B). T cells likely integrate signals received from multiple TCRs. Furthermore, since acti-

vation on a single cell level was shown to be digital [12], T cells need to implement a threshold that defines at what level of $C_N$ they get activated (Figure 1.3).

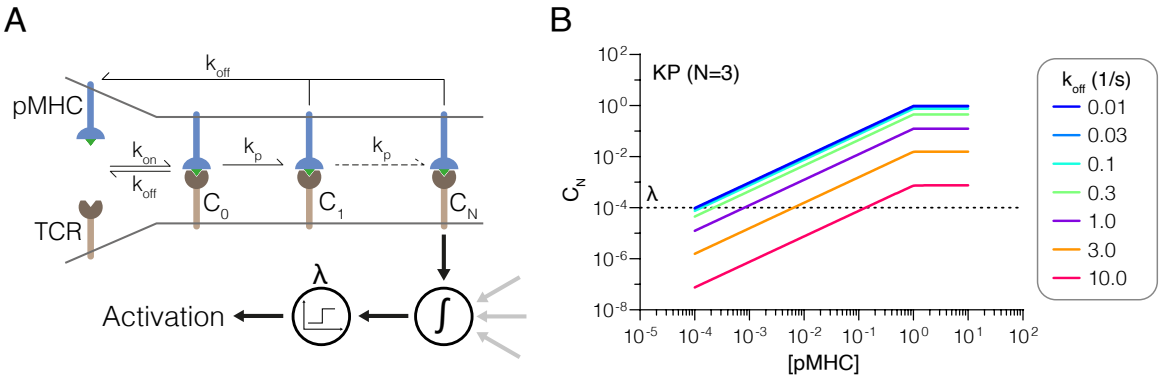


**Figure 1.3: Kinetic proofreading is sensitive to changes in off-rate.**
**(A)** In kinetic proofreading, the ligand/receptor-complex (C) needs to undergo a series of modifications before it starts to transduce produce a signal ($C_N$). Signals from multiple receptors are integrated and subjected to a threshold. **(B)** The number of signaling-competent complexes ($C_N$) depends strongly on the off-rate. Shown is an arbitrarily chosen threshold λ that defines whether a cell becomes activated. See Materials & methods for details on simulations.

In kinetic proofreading, the potency of the ligand is dependent on its off-rate (Figure 1.4A–B). When a population of T cell is stimulated, population heterogeneity results in a typical sigmoidal dose response (Figure 1.4A). However, at low off-rates there is saturation, which depends on the T cell intrinsic threshold (λ). Kinetic proofreading can approximate the idealized model of perfect discrimination. In perfect discrimination, every single molecule of ligand with an off-rate smaller than a cutoff will activate. However, no increase in dose, can ever convert a non-agonist (right) to an agonist (left; Figure 1.4C). In kinetic proofreading, increasing the number of steps leads to better discrimination (Figure 1.4D), however this come at the cost of speed, sensitivity (omitted in Figure 1.4D) and/or energy consumption [7, 256]. Different proximal signaling events, such as CD4/CD8 binding, Lck binding, phosphorylation of the ten different TCR:CD3 ITAMs, ZAP-70 binding and phosphorylation, and LAT phosphorylation [116, 257], have been implicated as the biological implementation of the proofreading chain (Figure 1.5). While kinetic proofreading is consistent with the 'lifetime dogma', it cannot explain the combination of exquisite sensitivity, specificity, and speed observed experimen-

tally. To achieve 'near-perfect' discrimination*, a simple kinetic proofreading model would require long engagement and a large number of agonistic ligands. Based on these apparent shortcomings, more complex models based on kinetic proofreading were developed.

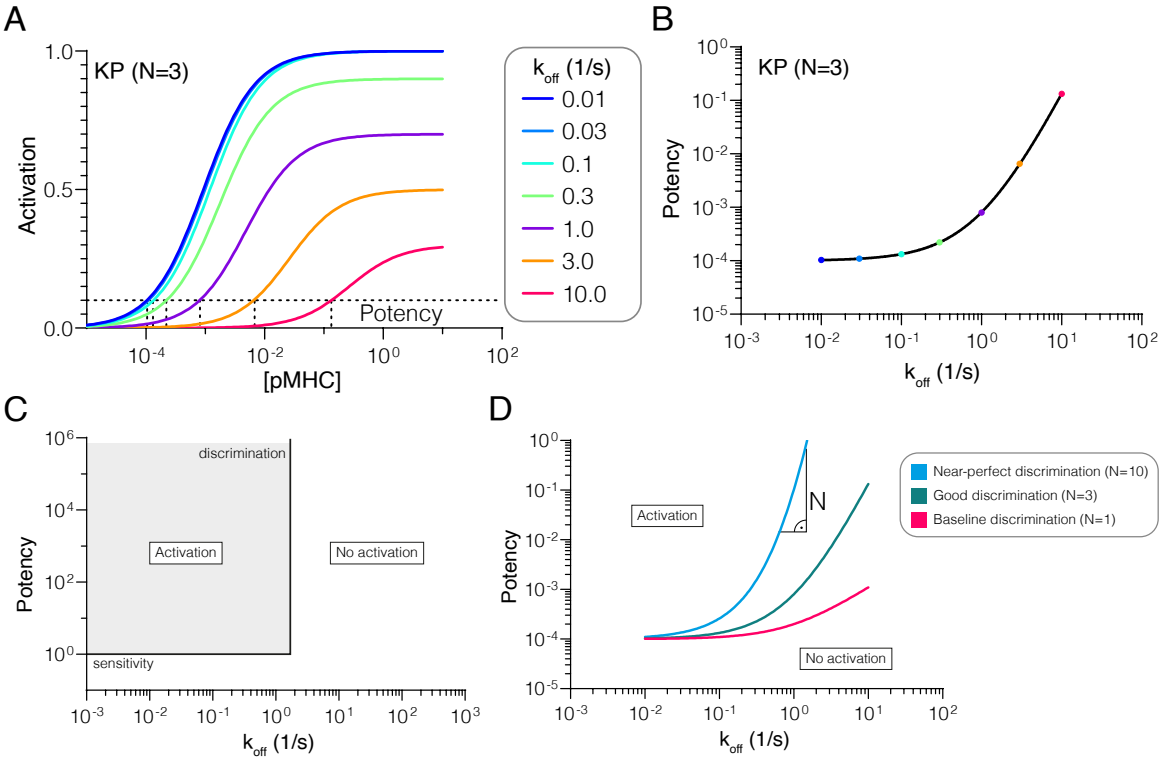


**Figure 1.4: Antigen discrimination in kinetic proofreading.**
**(A)** Simulated dose responses of T cells for antigens with different off-rates/lifetimes. Shown are the results of a kinetic proofreading model with 3 steps. The sigmoidal shape may arise as a result of population heterogeneity. I define potency here as the dose required to reach 10 % activation. **(B)** This potency depends on the off-rate. For small off-rates, the response saturates. **(C)** Perfect antigen discrimination is characterized by perfect sensitivity (i.e. responding to a single molecule of pMHC) and perfect discrimination (i.e. a sharp threshold in off-rate between agonists and non-agonists). **(D)** Kinetic proofreading models with identical sensitivity, but different discrimination powers. Baseline discrimination is the level predicted by an occupancy model (assuming $k_{off} \propto K_D$) or a kinetic proofreading model with one step. See Materials & methods for details on simulations.

*As I will argue in this thesis, the assumption of 'near-perfect' discrimination does not hold true. Once this stringent requirement is dropped, kinetic proofreading becomes compatible with the high sensitivity and speed found in T cells [4].

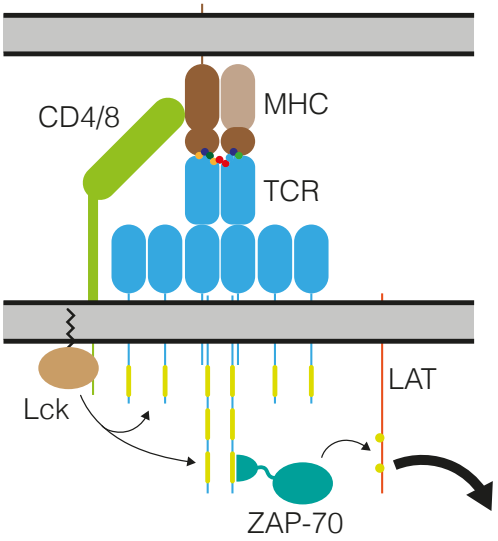


**Figure 1.5: Potential kinetic proofreading steps in the proximal TCR signaling network.** TCR/pMHC binding is followed by co-receptor binding. Next, co-receptor-bound or free Lck phosphorylates the tyrosines of the ten TCR-associated ITAMs. These ITAMs serve as a binding site for the kinase ZAP-70, which can additionally be directly phosphorylated by Lck to increase its activity. ZAP-70 leads to LAT phosphorylation, which serves as an adapter for many more signaling molecules. Each of these steps shown here have been implicated in kinetic proofreading [116, 257]. Yellow squares indicate ITAM sequences. Dots show single phosphorylation sites.

### Kinetic proofreading models with feedback

In classical kinetic proofreading models, signal integration occurs downstream of the proofreading chain. Integration and thresholding of the signal can explain the digital activation profile observed when T cells are stimulated at the single cell level [12]. To achieve better discrimination, T cells may additionally sense antigen dose by measuring receptor occupancy of many TCRs in a model called adoptive sorting [258, 259]. Adoptive sorting implements this adaptation to the dose using a feed-forward loop (Figure 1.6A), however a very similar effect can be achieve using negative feedback instead (Figure 1.6B). In either case, occupancy is integrated from multiple TCRs to cancel any influence of the antigen dose, while retaining sensitivity to the bond lifetime. Unlike simple kinetic proofreading chains operating in a physiological parameter regime, in such a model, even an extremely high dose cannot turn a non-agonist into an agonistic ligand. Antagonism emerges as an unavoidable consequence of this model [260]. Here adding a non-agonist can reduce the sensitivity for an agonist dramatically. While there is some evidence for antagonism in T cell recognition [261–263], other studies did not identify such effects [264, 265]. Antagonism could potentially be very danger-

ous for the immune system, since it would allow immune evasion by expression of antagonistic peptides. Furthermore, adoptive sorting may not be very robust. If realistic (i.e. finite) parameters are tested for the speed that proofreading modifications are removed, the time to reach activation in this model increases dramatically [256] and becomes incompatible with the physiological requirements of antigen discrimination. For example, ZAP-70 binding was shown to have a longer lifetime than normal pMHC ligands and could therefore represent a not easily reversible step [266–268].

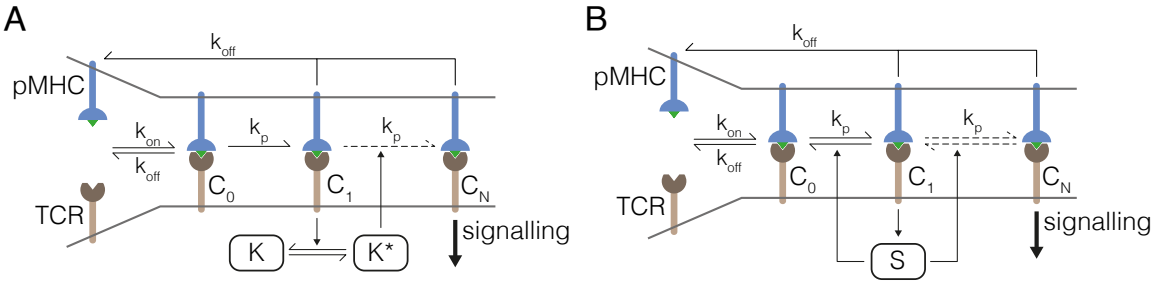


**Figure 1.6: Feedback can improve the discrimination power of kinetic proofreading.** **(A)** The adoptive sorting model includes a feed-forward loop. This loop is shared between TCRs, and is thought to achieve a higher discrimination with the same number of proofreading steps. **(B)** Kinetic proofreading with negative feedback. This results in a very similar effect as in (A).

## 1.8.2 The effect of force on antigen discrimination

The notion that forces are exerted by T cells during scanning and might also be applied to TCR/pMHC bonds [231], fueled research into the contribution of force to antigen discrimination. Some of the most exciting results about forces on the TCR were generated using an assay termed biomembrane force probe (BFP) [269]. In this assay, using a micropipette, a red blood cell (RBC) coupled with a bead that is coated with pMHC class I is brought into contact with a T cell. Since the T cell is also fixed in place via a micropipette, a retraction of the RBC leads to its deformation and bond rupture can be microscopically observed as a relaxation of the RBC. This technique can be used to apply a defined force at a single TCR bond. Liu *et al.* used the BFP assay to apply forces up to 30 pN and observe how the bond lifetime changed at different

forces. When comparing multiple pMHC ligands, they made the interesting observation that agonistic pMHC binding strengthens under force (termed catch bond), while non-agonistic binding weakens under force (slip bond) [269]. Under a force of about 10 pN, they found the differences in lifetime between agonists and non-agonists to be the largest. This led to the idea that T cells might be capable of applying very well-defined forces on the TCR bond to increase the spread in lifetimes, compared to zero-force conditions, thereby improving discriminating between antigens (Figure 1.7).

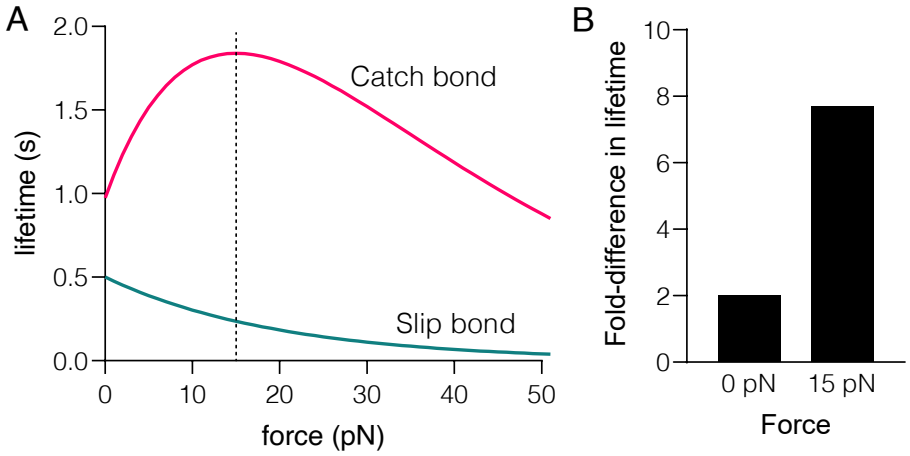


**Figure 1.7: Molecular bonds may strengthen or weaken under force.**
**(A)** The lifetime of catch bonds increases under force, while the lifetime of slip bonds decreases. At high enough forces all catch bonds turn into slip bonds. **(B)** Force may improve the difference in lifetime between antigen and thereby support discrimination by kinetic proofreading. Shown is the fold difference in lifetime between the two antigens displayed in (A). Conversely to what is simulated here, force could also decrease antigen discrimination, if agonists tend to be slip bonds and non-agonists catch bonds.

Sibener *et al.* applied the same methodology to explain why some TCR/pMHC combinations do not confer activation [92]. They isolated different T cell clones, all binding the same pMHC, by tetramer staining. While all of them were able to bind tetramer, some of them did not activate upon stimulation with pMHC. Importantly, they could not explain this difference in activation by either 3D affinity or 2D dwell time. Interestingly, they found that activation was connected to catch bond formation. While $K_D$ and off-rate generally correlated well for a given TCR tested with multiple peptide ligands [78], this is not always true when comparing

different TCRs. In their study they argue that two TCRs binding the same peptide showed different activation. However, inspection of their SPR data indicates that there likely is a significant different in off-rate that may explain the functional differences. Furthermore, one of the main limitations of adhesion-based assays to measure the response to force is the possibility of changes in adhesion frequency during sequential testing [270]. One possible explanation for such 'memory' is restructuring of the T cell surface after activation by the first few binding events. Unfortunately, repetitive testing of the same T cell, rather than using a fresh cell for each repeat, is often a necessity due to the effort involved in changing cells. Indeed, a recent study investigating catch bond behavior with recombinant proteins, could not identify any catch bond for agonistic peptide [271].

A major question arising from these studies is the potential structural mechanism of catch bond formation. An interesting idea was proposed by Wu *et al.* using steered molecular dynamics simulations [234]. In their simulations, a conformational change in MHC upon application of force made all the difference between catch and slip bond. They use high forces since they are a necessity to achieve manageable simulation times. Yet, it is not clear if the drastic conformational changes they observe at hundreds of pNs are plausible, considering some proteins can be extracted from a membrane with as little as ~10 pN force [132]. Notably, previous work on force using the BFP utilized MHC mutants to block co-receptor binding. Hong *et al.* directly investigated the importance of CD8 in thymic selection using thymocytes from OT-I mice [272]. Interestingly they did not find intrinsic catch bonds between the TCR and any self-ligand in the absence of CD8 binding. When they added CD8, the same ligand showed a catch bond, while a positively selecting ligand remained a slip bond.

An alternative explanation for how force may improve specificity without implying catch bonds or structural changes in the TCR was proposed by Klotzsch and Schütz in a theoretical analysis [273]. While the probability function of the lifetime of a bond under no load can be described as an exponential decay, this changes drastically if the bond is set under stress. A

constant velocity applied on the bond (e.g. pulling apart the binding partners) results in a linearly increasing force on the bond in the pN range. Naturally, such a force on the bond is expected to accelerate unbinding, consistent with accelerated unbinding observed in a cellular system, compared to binding of recombinant proteins. Interestingly, applying an increasing force 'tightens' the probability distributions of different ligands and therefore aids discrimination. It is worth highlighting that this effect is only present when a force gradient is applied; a constant force will not result in such a change.

## 1.9 Putting it all together

T cells fulfill a unique role in the immune system. They are able to differentiate with remarkable precision between self and non-self, while maintaining high speed and sensitivity. This ability has profound implications for solving the enigma of TCR triggering. Despite decades of research, it is still not clear if the TCR is activated through conformational change, force, in a ligand-independent ways such as predicted by kinetic segregation, or in a way we have not even thought about yet. Kinetic proofreading is an attractive model of the proximal signaling chain to explain antigen discrimination and compatible with TCR triggering models such as the kinetic segregation model. However, kinetic proofreading struggles to explain the extreme requirements of specificity found in early studies of antigen discrimination while maintaining physiological levels of sensitivity and speed. Surprisingly, as I will discuss, I could not replicate these early findings. When stimulating primary human $CD8^+$ T cells with different peptides, I found antigen discrimination to be good, but not near-perfect. This discrepancy may result from inaccurate SPR measurements used to determine the kinetic and affinities in these early studies. To solve this problem, we developed a new SPR method that allowed better measurements of the binding properties of TCR/pMHC interactions.

# Chapter 2

---

# Effect of CD2 and LFA-1 on T cell activation

## 2.1 Introduction

T cells are a key element of the adaptive immune system. They continously interact with immune and non-immune cells to fulfill their functions. Many of these interactions are supported by the adhesion receptors CD2 and LFA-1 expressed on human T cells. Previous work has established their role in increasing antigen sensitivity in murine systems [165, 175, 176, 221–223]. However, less is known about their role in humans. Studies in humans are particularly important for CD2, because its ligand in humans, CD58, is not present in rodents, where CD2 binds a structurally related protein called CD48. Interestingly, in humans, CD58 binds CD2 with ~5-fold higher affinity than the CD2/CD48 interactions in rodents and this difference is increased to about 40-fold when the affinity is measured in 2D [163]. Furthermore, unlike CD58, which is ubiquitously expressed, CD48 is mostly restricted to the hematopoietic system [141]. Recently, the importance of CD58 for immune evasion in cancer or during viral infections has been recognized [178, 179]. Taken together, although only a subtle role for CD2 has been identified in rodents [274], emerging data suggests that it is likely to have a more prominent role in humans.

Unlike CD2, LFA-1 can bind to multiple ligands, most prominently the family of ICAMs. Of those ligands, the interactions between ICAM1 and the LFA-1 integrin receptor has been studied the most. This interaction has both a role in T cells adhering to APCs as well as in extravasation [275]. Interestingly, in mice, ligation of LFA-1 by ICAM1 causes an increase in sensitivity, similar to the effect of CD2/CD48 engagement [221–223]. This shared functional phenotype on antigen sensitivity is observed despite the fact that CD2 and LFA-1 are part of different protein families exhibiting different ligand affinities, receptor/ligand dimensions, and receptor signaling mechanisms. CD2 is a 2 Ig-like domain protein binding another 2 Ig-like domain protein (CD48 or CD58), yielding a very similar height to the TCR bound to pMHC [133]. In contrast, LFA-1 is a hetero-dimer belonging to the integrin family and its ligand ICAM1 con-

sists of 5 Ig-like domains resulting in a substantially increased height versus CD2 and its ligand. Consequently, they occupy different spaces in the immunological synapse [166, 168, 213, 214]. The affinity of LFA-1 to ICAM1 depends on the activation state of LFA-1. In the high affinity state LFA-1 exhibits significantly higher affinity [205–207] than CD2 to its ligand CD58 [131].

While CD2 and LFA-1 have been studied a lot separately, little is known about how they differ in function of promoting T cell/APC adhesion. Furthermore, most research on CD2 has been done in the context of the CD2/CD48 rodent system. Here, I employ a functional approach to study the effect of CD58 and ICAM1 in primary human $CD8^+$ T cells. In a reductionistic system with immobilized ligands, I find a similar phenotype to what has previously been described in murine models, where ligation of CD2 or LFA-1 by their respective ligands led to a increase in sensitivity to pMHC and the maximum amount of cytokines secreted. When investigating this effect in a co-culture system, I find a qualitatively similar phenotype. Unexpectedly, ligation of CD2 continued to impact antigen sensitivity even when using an affinity-matured TCR that bound the antigen with 1000-fold higher affinity. This work underlines the importance of human CD2 and LFA-1 in increasing the T cell sensitivity to antigen and highlights the utility of reductionist systems in quantifying the impact of co-signaling receptors in antigen recognition.

## 2.2 Results

### 2.2.1 Producing a solid phase stimulation surface

I chose to study the effect of ligation of CD2 or LFA-1 by their respective ligands CD58 and ICAM1 in a reductionistic system where recombinant accessory ligands and pMHC are immobilized on a plate. In contrast to antigen recognition on APCs that express various ligands, this

reductionist system allowed me to generate well-defined surfaces expressing different concentration of both pMHC and CD58 or ICAM-1. To allow potential imaging applications in the future, I chose microscopy-grade glass bottom plates as my substrate. The plates were functionalized by coating them with biotinylated BSA, followed by addition of saturating amounts of streptavidin to allow binding of biotinylated pMHC and CD58 or ICAM1 (Figure 2.1A). This results in a clean, relative homogeneous coating with a linear relationship between ligand added and ligand bound (see Figure 2.1B–C). The resulting slope of slightly over 1, is probably a result of underestimating binding at very low doses. Notably, results depend on the batch of glass plates used and saturation is usually seen around 100–200 ng pMHC binding (~2–4 pmol).

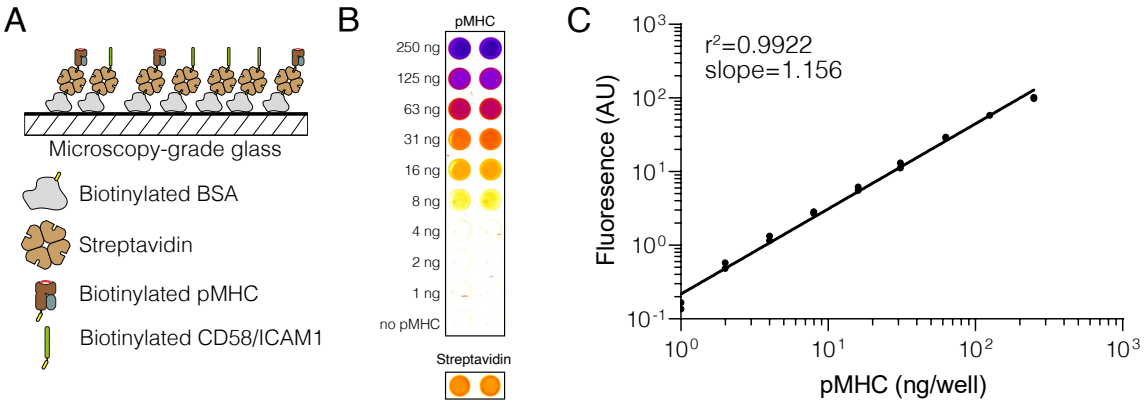


**Figure 2.1: Coating of glass plates allows for linear ligand binding.**
**(A)** Microscopy-grade glass plates are functionalized with biotinylated BSA, followed by binding of streptavidin. Biotinylated recombinant pMHC, followed by CD58 or ICAM1 are then bound in a final step. **(B)** Coating protocol results in even coating when tested either by anti-MHC staining (W6/32 Ab) or when the underlying biotinylated-BSA layer is tested using fluorescent streptavidin. pMHC fluorescence is shown log-transformed. **(C)** Binding of pMHC ligand on plates is linear with respect to the amount of ligand added.

### 2.2.2 Effect of CD58 & ICAM1 in a reductionist system

For stimulation, we isolated primary human $CD8^+$ T cells, bulk-transduced them with the 1G4 TCR, and expanded them (Figure 2.2A). They showed a high purity directly after isolation (Figure 2.2B–C) and expression of the 1G4 TCR after expansion was routinely analyzed using tetramers (Figure 2.2D). The 1G4 TCR binds a cognate peptide called 9C from the NY-ESO testis/tumor antigen presented on HLA*02:01 [276]. For my studies, I used the heteroclitic 9V variant (hereafter called NYE 9V) with improved stability on the MHC [47]. As expected, when the cells were incubated on these plates for 4 h, they responded in a pMHC dose-dependent way by expression of the early activation marker CD69 and the secretion of IL2 (Figure 2.3). Adding either CD58 or ICAM1 caused a dramatic improvement in sensitivity and additionally increased the total amount of cytokine secreted.

To summarize the effect of CD58 and ICAM1 in T cells isolated from multiple donors, I chose to characterize these dose response curves by their maximum ($E_{max}$) and potency. Both measures are derived from fitting the data with a sigmoidal model to smooth out small data errors. Notably, some dose response curves show a decreased response at very high pMHC doses (i.e. a bell-shape). We have previously described this adaptation effect as a result of fast TCR downregulation [277].

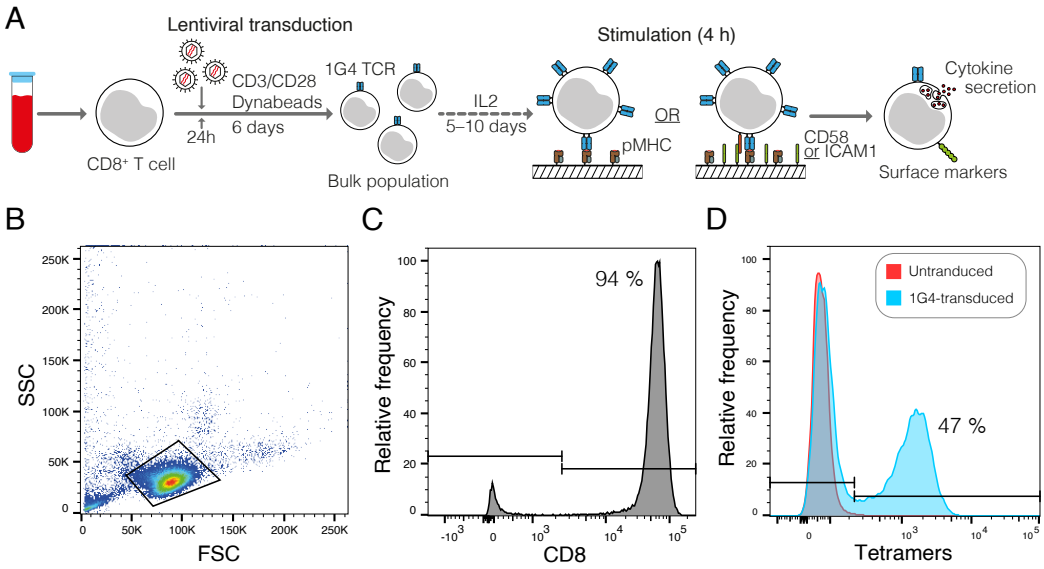


**Figure 2.2: T cell isolation and transduction protocol.**
**(A)** $CD8^+$ T cells were isolated from the blood of healthy donors, stimulated, and transduced with lentivirus encoding the 1G4 TCR. After 11–16 days of expansion, the bulk population was incubated for 4 h on immobilized recombinant pMHC in the presence or absence of CD58 or ICAM1. Activation was measured by flow cytometry (activation markers) and ELISA (cytokine secretion). **(B)** Flow cytometric analysis of T cells after isolation. **(C)** The protocol yields $CD8^+$ T cells with a purity of >90 %. **(D)** Staining with tetramers after transduction and expansion. Transduction efficiency varies between 30–80 %.

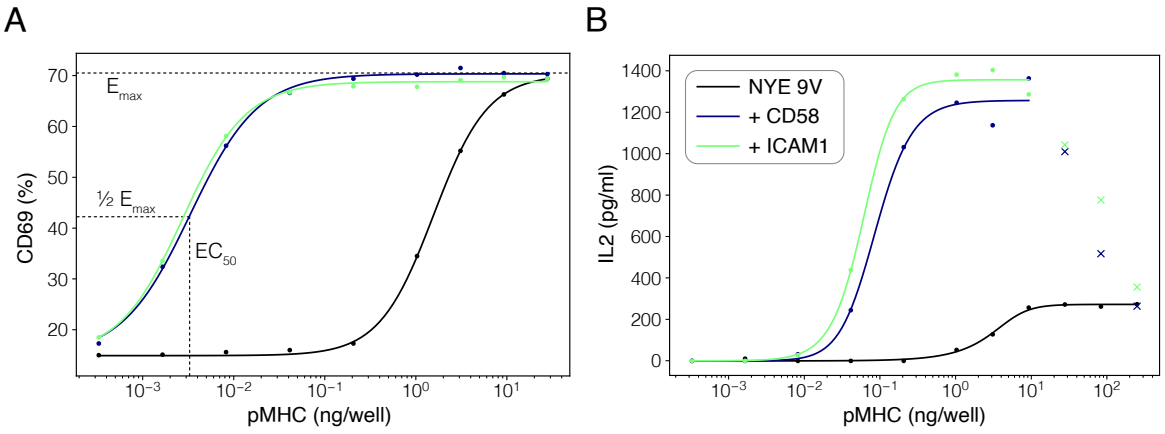


**Figure 2.3: Primary human $CD8^+$ T cells transduced with the 1G4-TCR respond in a dose-dependent way to pMHC.**
**(A)** Example of T cells responding in a pMHC-dependent way by upregulation of CD69 (per cent positive cells). Data was fitted using a sigmoidal model. Adding ICAM1 or CD58 decrease the pMHC dose required for activation. Shown is the $EC_{50}$ (the concentration to reach half-maximal activation) for the CD58 condition. **(B)** T cells also secrete IL2 in the supernatant. Data was fitted using a sigmoidal model. Crosses refer to datapoints that were automatically removed before fitting (bell-shape).

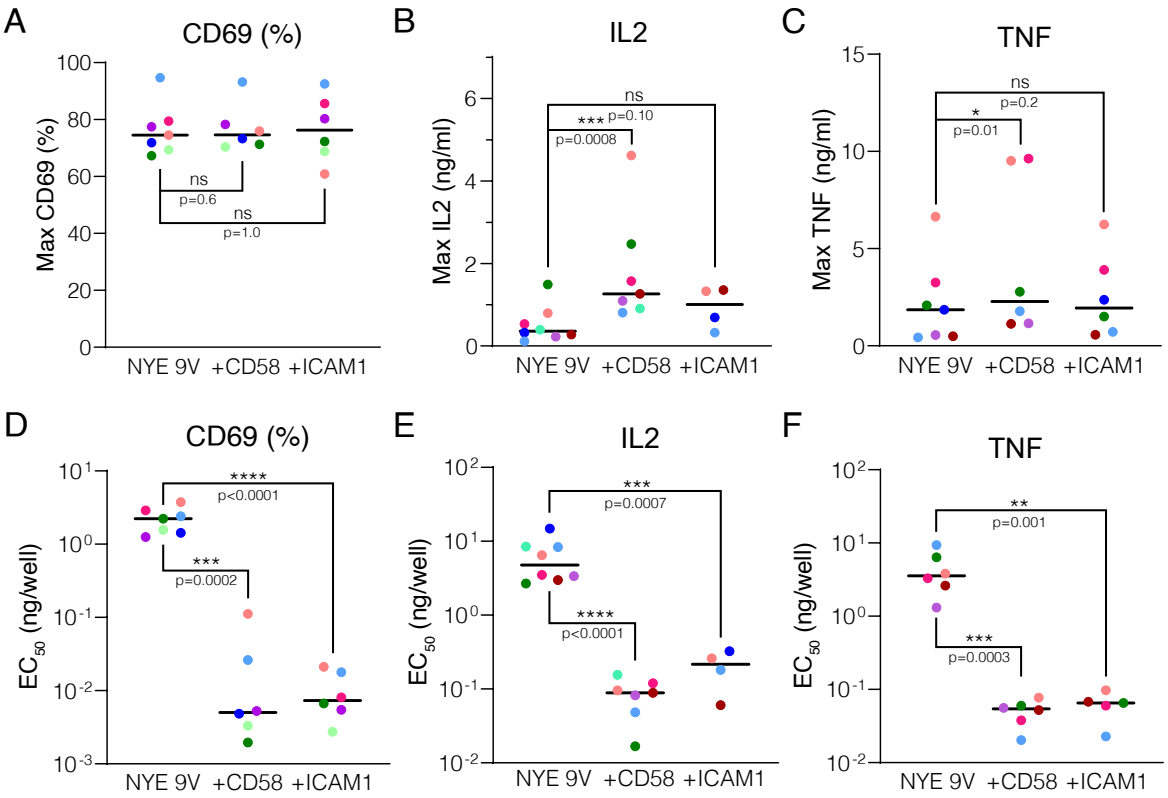


**Figure 2.4: CD58 and ICAM1 increase the sensitivity to pMHC dramatically**
**(A)** Presence of CD58 or ICAM1 does not change the maximum fraction of CD69-positive cells. However, addition of CD58 or ICAM1 results in a small to modest increase of maximum cumulative secretion of IL2 **(B)** or TNF **(C)**. Maximum secretion is defined as the value of a sigmoidal fit at the top pMHC concentration. **(C)** Potency for CD69 (per cent positive cells). Fold difference in geo. mean: 220x for CD58; 270x for ICAM1. Potency for the cumulative secretion of IL2 **(D)** and TNF **(E)**. Fold difference in geo. mean: 64x for CD58; 40x for ICAM1 (IL2) and 79x, 80x (TNF), respectively. Colors indicate data derived from the same blood donor. Statistics in (A)–(F) from Dunnett's multiple comparison test on log-transformed data.

When analyzing data from multiple donors, I find that addition of CD58 or ICAM1 does not change the maximum percentage of CD69 positive cells (Figure 2.4A). As expected, CD69 varies somehow between donors and this likely results from differences in transduction efficacy. The absolute amount of IL2 and TNF detected in the supernatant varies considerably between donors/experiments, but adding CD58 or ICAM1 consistently increased IL2, but TNF less so (Figure 2.4B–C). In contrast, the potency was more conserved between donors. Presence of CD58 or ICAM1 decrease the $EC_{50}$ by more than 100-fold (Figure 2.4D), and this phenotype

is conserved for cytokine secretion (Figure 2.4E–F). As previously described [277, 278], TCR is downregulated from the cell surface in a pMHC-dependent way (Figure 2.5A). Since some of the tetramer dose response curve did not have a well defined minimum, I chose to use the pMHC dose required to cause 40 % downregulation, rather than an $EC_{50}$, to quantify TCR downregulation. Consistent with their adhesion role in promoting TCR/pMHC interactions, the presence of CD58 or ICAM1 increased the pMHC-dependent downregulation of TCR, as measured by 1G4-specific tetramers (Figure 2.5).

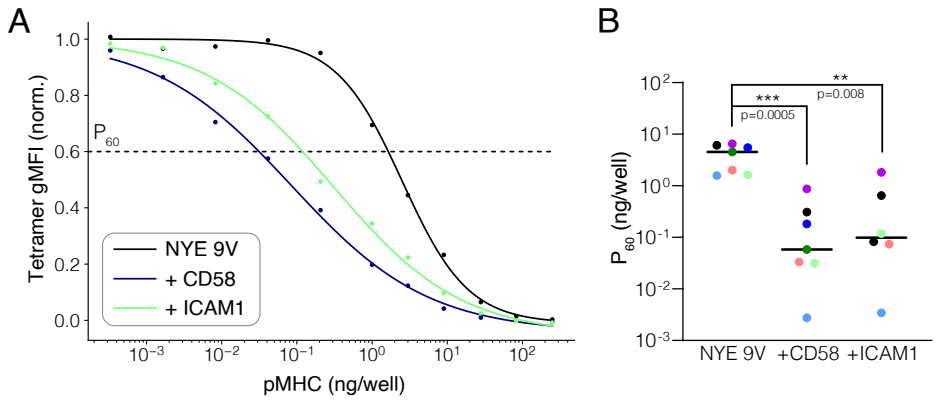


**Figure 2.5: Engagement of CD58 and ICAM1 leads to increased TCR downregulation.**
**(A)** pMHC-dependent downregulation of the 1G4 TCR from the surface (as measured by NYE 9V tetramer staining) is increased upon addition of CD58 or ICAM1. Potency threshold used for (B) is indicated as dotted line. **(B)** TCR downregulation is reproducibly higher with addition of CD58 or ICAM1 than with pMHC alone. Fold difference in geo. mean: 49x for CD58 and 27x for ICAM1. Colors indicate data derived from the same independent experiment/blood donor. Statistics from Dunnett's multiple comparison test on log-transformed data.

## 2.2.3 Effect of CD58 and ICAM1 in a cellular system

I next sought to investigate the phenotype in a more physiological system using a co-culture system of pulsed cells and the same 1G4-transduced $CD8^+$ T cells (Figure 2.6). I chose the human glioblastoma cell line U87, since these cells naturally express HLA-A*02, they are adherent and therefore easy to wash after peptide pulsing, and non-hematologic in origin. Importantly, these cells do not express CD80 or CD86 (Figure 2.7A), excluding a potential compen-

sation as has been described previously between CD2 and CD28 [158]. They naturally express CD58 and ICAM1 and I therefore created cell lines deficient in either or both accessory ligands using CRISPR, followed by sorting of the bulk population (Figure 2.7B), to be able to study the contributions of the molecules to T cell activation.

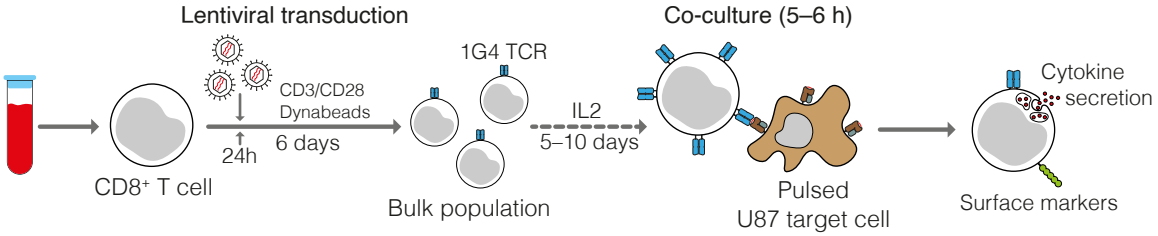


**Figure 2.6: T cell/U87 co-culture system.**
Primary human CD8⁺ T cells were isolated from the blood of healthy donors, stimulated, transduced with the 1G4 TCR, and further expanded. For stimulations, T cells were co-cultured with U87 cells (a glioblastoma cell line expression HLA*02:01) and pulsed with NYE 9V peptide.

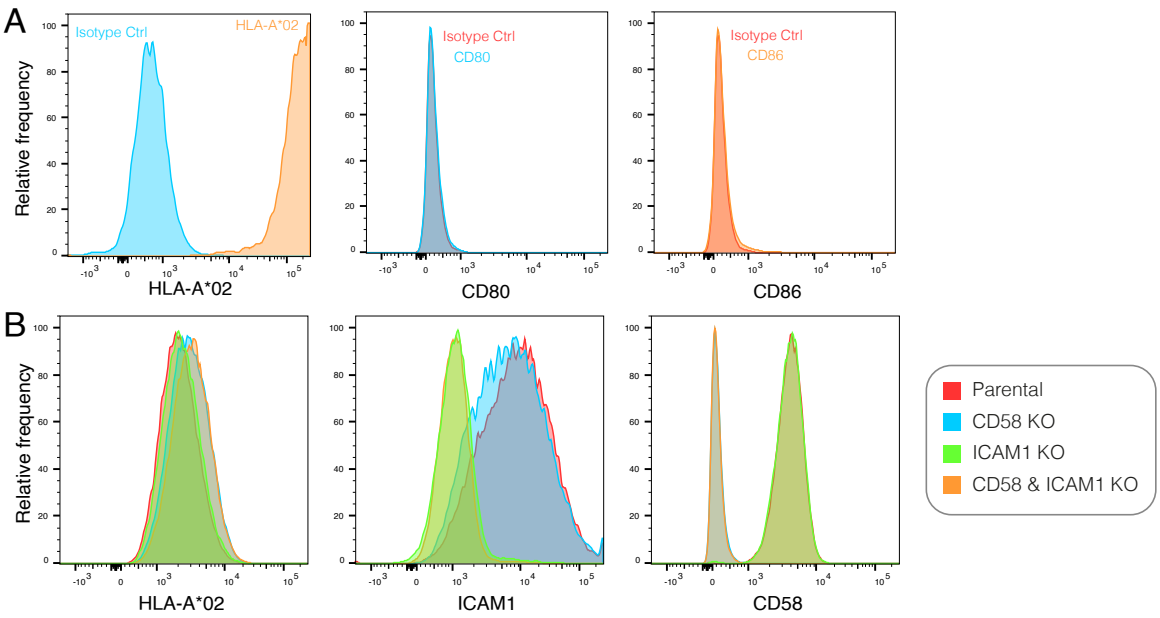


**Figure 2.7: Generation of CD58, ICAM1 & double KOs of the HLA-A2⁺ U87 cell line.**
**(A)** The parental U87 cell line expresses HLA-A2, but not CD80 or CD86. **(B)** CRISPR KO of U87 cells are deficient in CD58, ICAM1 or both, but they have similar HLA-A2 expression.

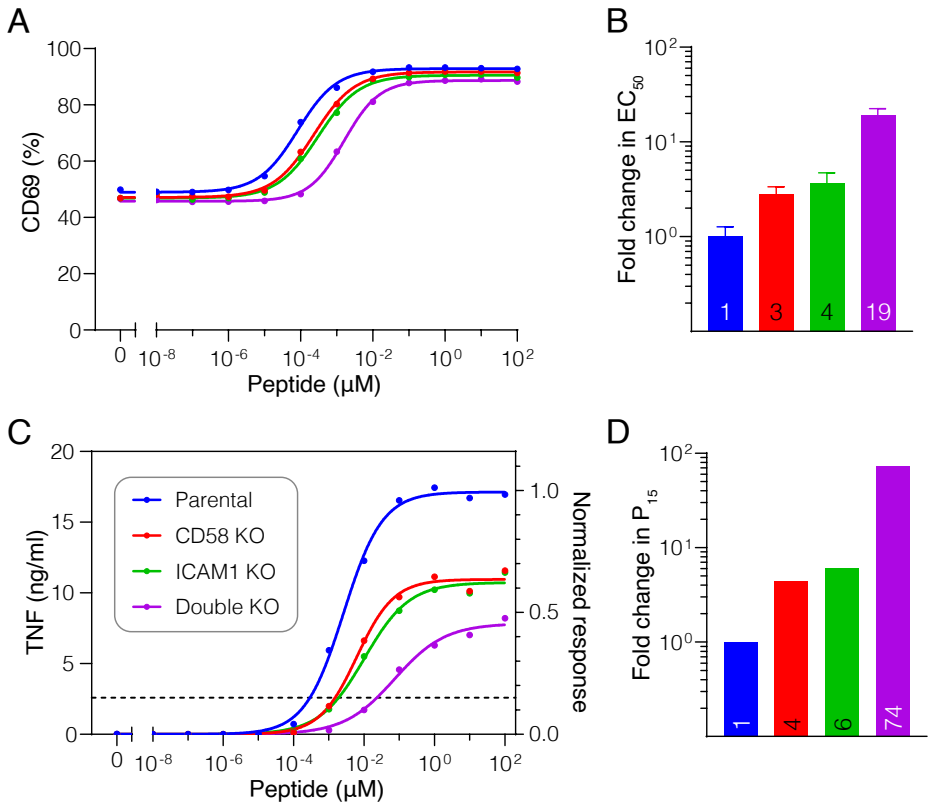


**Figure 2.8: T cells are less sensitive to target cells lacking CD58 or ICAM1.**
**(A)** Effect of CD58, ICAM1 or double knockout on U87 target cells on the upregulation of CD69. **(B)** $EC_{50}$ from fitting the data in (A) with a sigmoidal model. Error bars indicate 95 % CI from fitting. **(C)** Effect of CD58, ICAM1 or double knockout on U87 target cells on TNF secretion. **(D)** Potency as shown in (C) as dotted line from sigmoidal fit.

Knockout of either CD58 or ICAM1 led to a small decrease in sensitivity and maximal cytokine secretion (Figure 2.8). For some of my data the dose response did not have a well defined maximum. Consequently, I chose to define a potency measure that is independent of the $E_{max}$. Based on a control condition (parental) I selected an activation threshold (15 %) and calculated the pMHC concentration required to reach that level of activation for each condition (Figure 2.8C). This method avoids extrapolation, such as when calculating an $EC_{50}$ for a curve with badly defined $E_{max}$. Interestingly, the double KO revealed an additive effect of both molecules. However, the shift (~20-fold) remained smaller than in the plate system, where addition of CD58 or ICAM1 causes a >100-fold increase in pMHC sensitivity. Notably, for cytokines the shift was about ~40–70-fold and therefore similar to what I observed on

plates (~40–80-fold). To independently verify this phenotype, I repeated this experiment using blocking antibodies against CD58, ICAM1, or a combination. The results closely matched those of the KO cell lines (Figure 2.9). For both experiments, inhibition of CD58 or ICAM1 is accompanied by a small decrease in cognate TCR downregulation from the surface (Figure 2.10A–B). Blocking CD58 via antibodies increased the levels of CD2 expression on the T cells (Figure 2.10C–D). Notably, this effect is pMHC-independent. In KO cells, this phenotype is less clear, possibly since interactions of CD2 with CD58 on other T cells are not inhibited in this system.

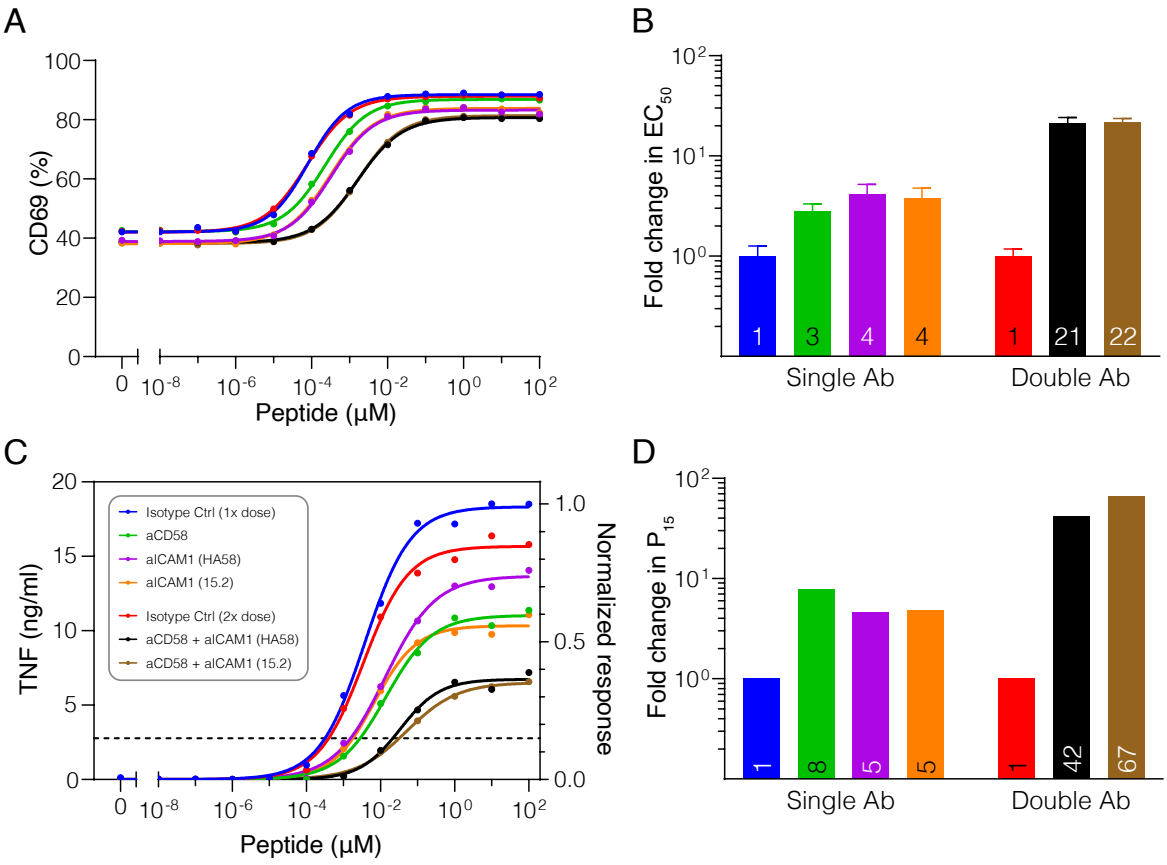


**Figure 2.9: Inhibiting CD58 or ICAM1 binding with antibodies decreases sensitivity to peptide.** **(A)** Effect of adding blocking antibodies to CD58, ICAM1 (2 different clones) or both on upregulation of CD69. **(B)** $EC_{50}$ from fitting the data in (A) with a sigmoidal model. Error bars indicate 95 % CI from fitting. **(C)** Effect of antibody blockage on U87 target cells on TNF secretion. **(D)** Potency as shown in (C) as dotted line from sigmoidal fit. T cells were pre-incubated with antibodies and they remained present during co-culture. Isotype (2x dose) is an additional control to account for the increased antibody dose in the double blocking condition.

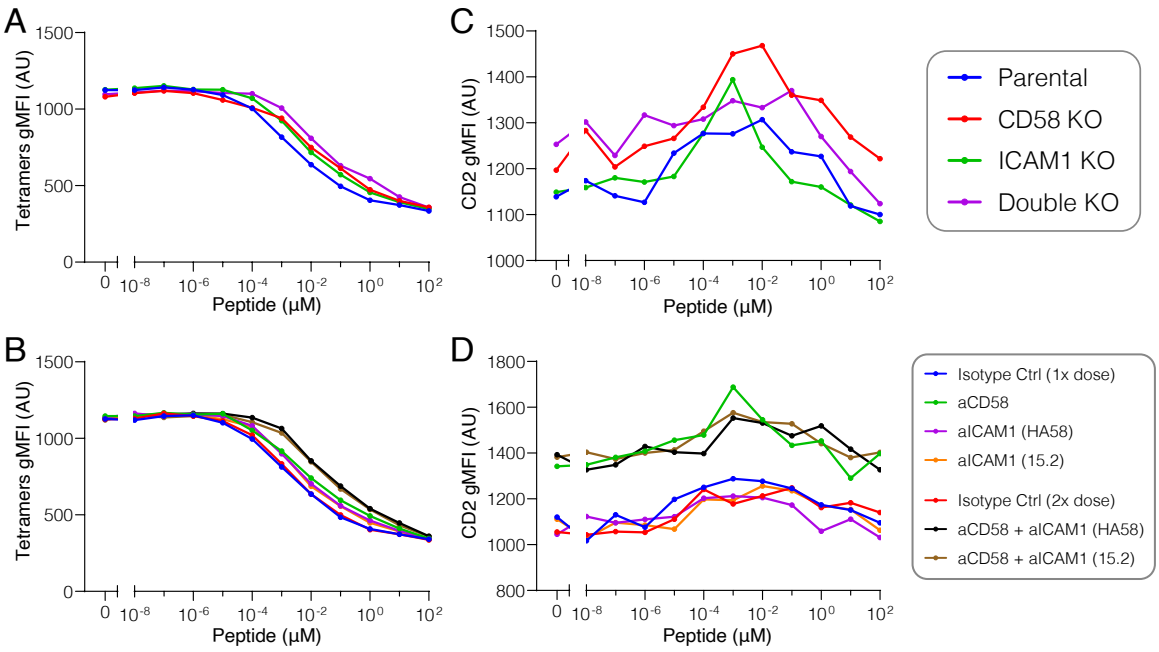


**Figure 2.10: Effect of inhibiting CD58 or ICAM1 on TCR and CD2 downregulation.**
Effect of genetic KO **(A)** or antibody blocking **(B)** of CD58, ICAM1, or both on downregulation of the 1G4 TCR from the T cell surface, measured by tetramer staining. Effect of genetic KO **(C)** or antibody blocking **(D)** of CD58, ICAM1, or both on downregulation of CD2 from the T cell surface.

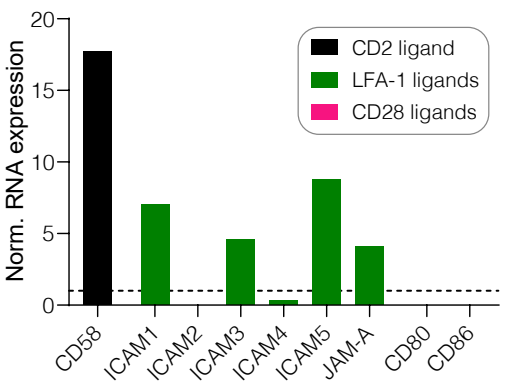


**Figure 2.11: Expression of accessory ligands in U87 cells.**
RNA expression of CD2, LFA-1, and CD28 ligands in the U87 cell line. A value of 1 (dotted line) is defined as the threshold required for protein detection. Data from the Human Protein Atlas [203].

Since the shift in sensitivity seen with U87 cells, when measured by CD69 upregulation, is much smaller than on plates, I sought to investigate if compensatory interactions could play a role. T cells interact with other cells via numerous receptor/ligand pairs and some of these could potentially mask the effect of a CD58 or ICAM1 KO. For example, U87 cells express the LFA-1 ligands ICAM3, ICAM5, and JAM-A in addition to ICAM1, when measured on RNA level

(Figure 2.11). I therefore employed a xenogeneic CHO system previously developed in the laboratory. Due to the cricetine (hamster) origin of these cells, most ligands are not expected to interact with human receptors found on the T cells. Similar to the plate system, this allows for an additive approach, where human ligands to be studied can be introduced. They have been transduced with human HLA-A*02:01 single chain dimer to allow TCR/MHC interactions, as previously described [279]. When examining T cell activation and killing in response to a titration of antigen on CHO cells transduced with human CD58 or not, I only found a modest increase in antigen sensitivity by CD58 (Figure 2.12). Since the shift is not larger than what I observed in U87 cells, this argues for mechanisms other than compensation to explain the difference observed between plate and co-culture systems.

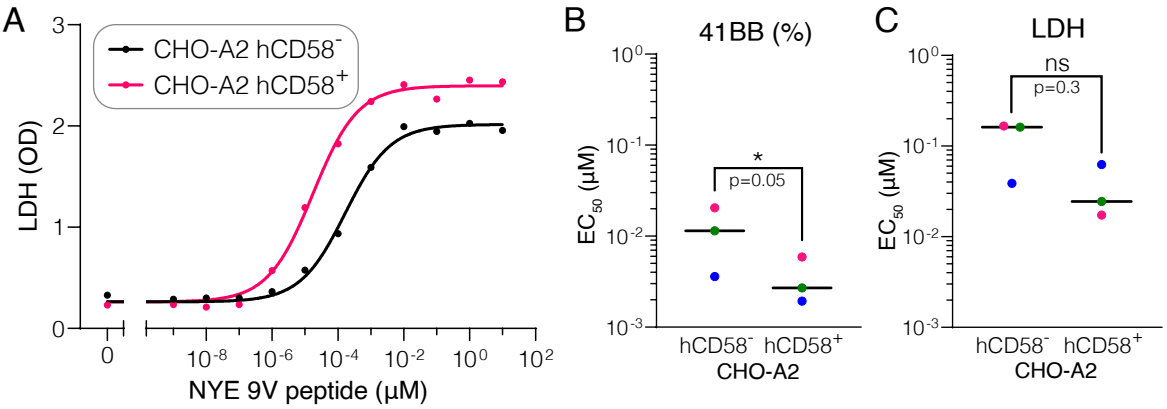


**Figure 2.12: Addition of CD58 increases sensitivity to peptide.**
Pulsed HLA-A*02$^+$ CHO cells were co-cultured for 21–24 h with 1G4-transduced CD8$^+$ T cells. To test the effect of CD58, CHO cells were additionally transduced with a human CD58 transgene. **(A)** Example of CHO cell killing with sigmoidal fit in absence or presence of CD58 on CHO cells. Optical density (OD) of LDH release was measured by ELISA. **(B)** Potency measured by $EC_{50}$ of 41BB upregulation (a T cell activation marker) on T cells. Comparison using paired t-test on log-transformed data. **(C)** Potency measured by $EC_{50}$ of CHO cell killing (as measured by LDH release). Comparison using paired t-test on log-transformed data. LDH: Lactate dehydrogenase.

### 2.2.4 Effect of CD58 in a high-affinity therapeutic TCR*

CD58 loss is a potential mechanism of T cell evasion by cancer cells and infected cells [177, 179, 181]. To study the effect of different doses of CD58, I used a detailed titration. Furthermore, T cell therapies often employ high affinity TCRs or CARs. I therefore sought to investigate the impact of CD58 on antigen sensitivity with an engineered variant of the 1G4 called c58c61 (hereafter referred to as 1G4$^{hi}$) that has been affinity-matured for a ~100,000-fold increase in affinity [68, 82]. For consistency with previously generated data in the laboratory, I used NYE 4A immobilized on commercial streptavidin-coated plates. The 1G4$^{hi}$ binds to NYE 4A with a super-physiological affinity of ~1 nM. Importantly, by using the NYE 4A8K variant, I could stimulate 1G4$^{hi}$-transduced T cells with a physiological affinity, similar to the one of the natural 1G4 binding its cognate peptide NYE 9V (Figure 2.13A).

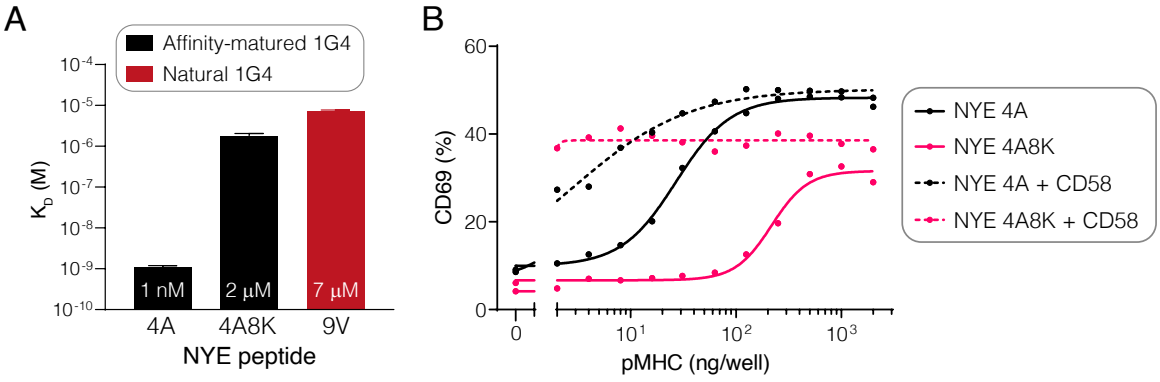


**Figure 2.13: Super-physiological antigen affinity for the 1G4$^{hi}$ TCR results in increased sensitivity in the absence of CD58.**
**(A)** The affinity-matured c58c61 1G4 TCR (1G4$^{hi}$ TCR) binds the NYE 4A peptide with super-physiological affinity, but binds 4A8K with an affinity comparable to the natural 1G4 TCR binding its cognate peptide 9V. Data from [78, 82]. **(B)** Dose response of T cells transduced with 1G4$^{hi}$ TCR and stimulated with immobilized pMHC ± CD58. While the higher-affinity peptide is more potent in absence of CD58, this is reversed in presence of CD58.

*The data in this chapter is published in [3] and is part of another thesis [2].

Stimulating 1G4$^{hi}$-transduced CD8$^{+}$ T cells for 8 h with immobilized pMHC resulted in a typical dose response curve (see Figure 2.13B). The higher affinity peptide NYE 4A produced a dose response shifted to lower doses, compared to 4A8K (Figure 2.13B). As above, CD58 increased the sensitivity to pMHC dramatically for a physiological affinity antigen. Notably, this effect is smaller for 4A, resulting in a reversal of the potency between 4A and 4A8K in presence of CD58 (Figure 2.13B). A detailed titration of CD58 revealed that a small increase in CD58 dose can change sensitivity dramatically (Figure 2.14). Furthermore, the effect of CD58 saturates at high doses. The maximum amount of cytokines secreted is similar for both peptides when CD58 is engaged (Figure 2.15). Notably, the effect on potency saturates around 125 ng CD58, whereas the effect on cytokine $E_{max}$ continues to increase until ~500 ng CD58, indicating that these phenotypes could be mediated by different mechanisms. As expected, CD58 leads to an increased downregulation of the TCR from the cell surface (Figure 2.16A–B). CD2 itself is also downregulated in a CD58-dependent manner, but independent of the pMHC dose (Figure 2.16C–D).

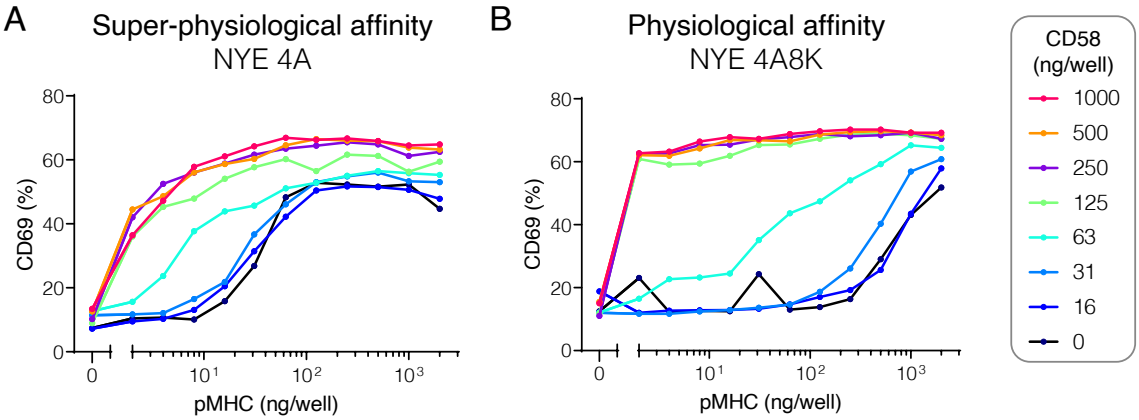


**Figure 2.14: Engagement of CD2 increases the sensitivity of pMHC.**
Effect of titration of CD58 (colors) and pMHC (x-axis) for high affinity NYE 4A **(A)** and physiological affinity NYE 4A8K **(B)** antigens on CD69 upregulation. Notably, due to the different substrate, more pMHC is needed to get the T cells activated than when using the glass plates described above.

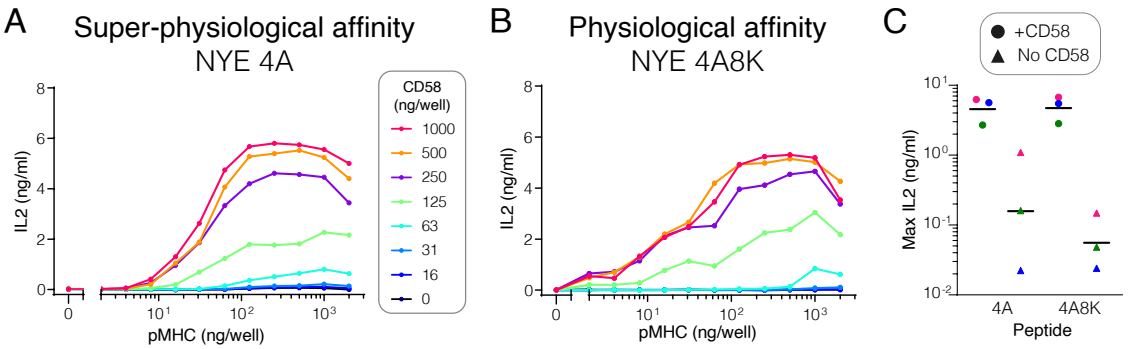


**Figure 2.15: Engagement of CD2 increases the sensitivity of pMHC.**
Effect of titration of CD58 (colors) and pMHC (x-axis) for very high affinity NYE 4A **(A)** and physiological affinity NYE 4A8K **(B)** antigens on IL2 secretion. **(C)** Addition of CD58 consistently increases cytokine secretion for both peptides. Colors indicate data generated from the same blood donor.

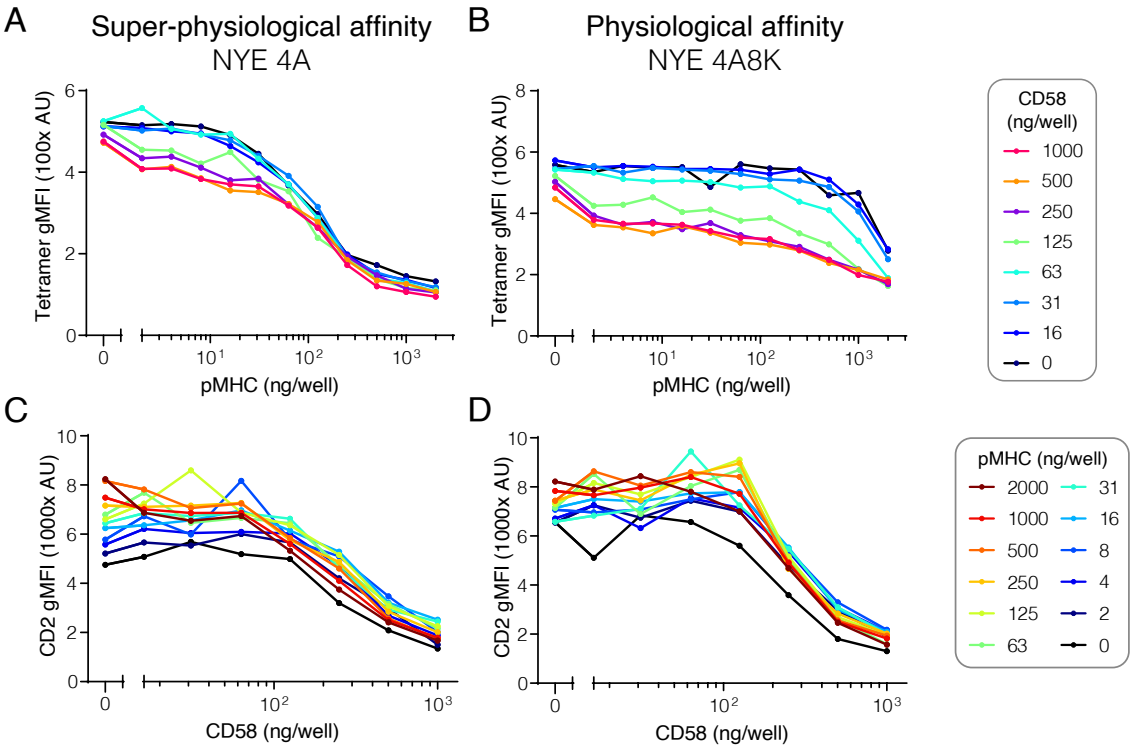


**Figure 2.16: Ligand-dependent downregulation of CD2 and the TCR.**
pMHC-dependent downregulation of surface TCR for NYE 4A **(A)** and 4A8K **(B)** measured by tetramer staining. CD58-dependent downregulation of surface CD2 for NYE 4A **(C)** and 4A8K **(D)**.

To test how sensitive T cells in this system are to changes to CD58 dosage, I fitted all the potency and $E_{max}$ data derived from fitting the dose responses (as described in Figure 2.3) with an additional sigmoidal function. One parameter of these fits is the Hill number, which is close to 1 for a linear relationship. Values greater than 1 are an indication of a system with positive cooperativity that is very sensitive to changes in CD58 dose (ultra-sensitivity). I find that the increase in cytokine secretion is quite sensitive to the CD58 dose used with a Hill slope of 2.1–2.9 (Figure 2.17A–B). To measure the potency, I define a threshold of 10 % of the 1000 ng CD58 condition ($P_{10}$; Figure 2.17C). Interestingly, the potency for NYE 4A and 4A8K is also very sensitive to changes in CD58 (Hill slope: 1.7–18; Figure 2.17D–E). Both $E_{max}$ and potency show Hill slopes significantly larger than 1, indicate some level of ultra-sensitivity (Figure 2.17F).

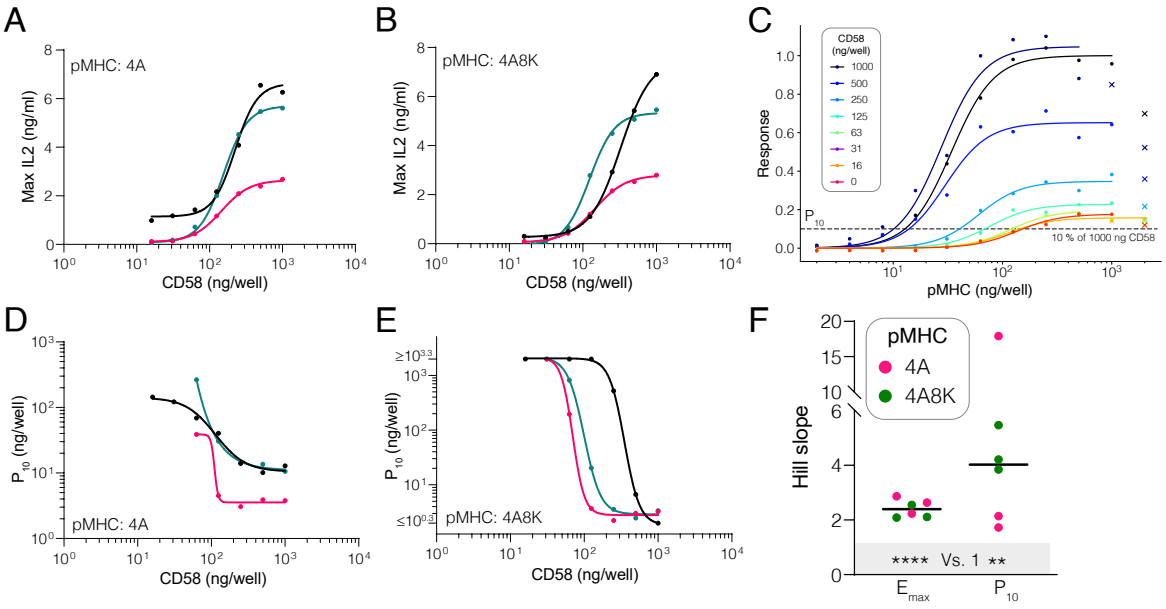


**Figure 2.17: Effect of CD2 on potency and $E_{max}$ is ultra-sensitive.**
Effect of CD58 titration on IL2 $E_{max}$ when responding to NYE 4A **(A)** or 4A8K **(B)**. **(C)** Example of sigmoidal fit of IL2 and the $P_{10}$ threshold used to calculate potency. Data points that were automatically removed due to their contribution to a bell-shape are indicated as crosses. Effect of CD58 titration on IL2 potency to NYE 4A **(D)** and 4A8K **(E)**. **(F)** Summary of hill slopes of sigmoidal fits as shown in (A), (B), (D), and (E). Log transformed data was compared to log 1 (=0) with independent 1-sample t-tests. p<0.0001 for NYE 4A and p=0.008 for 4A8K. Colors in (A), (B), (D), and (E) indicate different blood donors.

## 2.3 Discussion

Here I showed how CD58 and ICAM1 affect the response of primary human $CD8^+$ T cells by employing multiple, complementary experimental systems. I found that CD58 or ICAM1 share a similar phenotype, where addition of either increases the sensitivity >100-fold to immobilized pMHC. Interestingly, while this effect is qualitatively conserved in a cellular system, the magnitude was smaller with cells. Lastly, I showed that even for a TCR with 1000-fold higher affinity, CD58 still plays a pivotal role in increasing sensitivity.

In a plate based system, the effect of CD58 and ICAM1 on sensitivity is dramatic, qualitatively consistent with what has been found in other studies in murine systems for LFA1/ICAM1 and CD2/CD48 (the rodent counterpart of CD58) [165, 175, 176, 221–223]. In both cellular and plate systems, a shift in functional sensitivity is accompanied by an increase in TCR downregulation. Notably, in a comparative study that includes data presented here, we found that the accessory ligands CD86 (ligand to CD28) and CD70 (ligand to CD27) did not, or only moderately increased the sensitivity to pMHC [3]. Of the ligands tested (ICAM1 was not included), CD58 showed the strongest effect on cytokine $E_{max}$ and $EC_{50}$.

I found that CD58 and ICAM1 show very similar phenotypes, consistent with a broadly similar function in enabling cell adhesion. While the dimension of CD2/CD58 matches the TCR/pMHC size well and therefore conceptually can easily facilitate TCR binding in close contacts, LFA-1/ICAM1 is significantly larger. Consistent with their size, CD2/CD58 can localize with TCR/pMHC [166], while LFA-1/ICAM1 is segregated (see also Figure 1.2) [213, 214]. It is therefore thought to be more important for 'macroscopic' adhesion. However, bringing the adjacent membranes to a distance larger than the TCR/pMHC may still be highly beneficial for TCR binding and thereby could explain the very similar phenotype to CD2/CD58 in my work. Interestingly, when titrating CD58, I found T cells to be highly sensitive to changes in the CD58 dose, shown by a hill slope >1. This indicates there might be cooperativity between CD58 molecules. For

example, critical concentration of CD2/CD58 bonds could be required to create sufficiently large domains of membrane proximity to allow TCR/pMHC binding.

Interestingly, the potency shift is >100-fold for a physiological antigen, but this effect is less pronounced for the higher affinity antigen 4A, arguing that this interaction might be less reliant on CD2/CD58 due to its intrinsically higher affinity. Yet, increasing the affinity >1000-fold cannot compensate for the loss of CD58 and therefore affinity-matured TCRs might still be prone to immune-evasion by loss of CD58. Interestingly, when CD58 is present, the lower affinity antigen seems to be more potent than the higher affinity antigen. Potentially, this is a consequence of inhibition of serial triggering for pMHCs that bind too strongly (i.e. too long) to the TCR, as previously observed [79–82].

I found the effect of either CD58 or ICAM1 on pMHC sensitivity to be more pronounced on plates than in co-culture with human cells. One potential explanation could be the presence of other adhesive ligands on these cells. For example, based on public RNA data, U87 cells express the LFA-1 ligands ICAM3, ICAM5 & JAM-A (Human Protein Atlas). Liu *et al.* found ICAM2, but not ICAM3, to be important in sensitizing a pancreatic cancer cell line to killing by $\gamma\delta$ T cells [280], while others reported that ICAM3 on Langerhans cells is important for stimulation of $CD4^+$ T cells [281]. In theory, many potential interactions should be greatly reduced in the CHO system. The similar phenotype in these cells when compared to the U87 system indicates that this may not be due to compensatory interactions. However, I have not ruled out the possibility that CD2 or LFA-1 can bind ligands on hamster cells. Other possible reasons are the mobility of the ligands on a cell compared to the immobile plate system, the presence of a glycocalyx, or the softness of the substrate. For example, previous work found the adhesion of E-cadherin to benefit from less mobility to allow for a more efficient nucleation process [282]. Conversely, a theoretical analysis of integrin binding predicts much higher binding when both receptor and ligand are mobile [283]. Furthermore, they find that bonds formed in a mobile experimental system are more resistant to force. Consistent with these results on

integrin binding, there is similar data for CD2, showing that mobile CD58 is better at binding CD2 [138]. It should be noted that Smith *et al.* worked with reconstituted membrane where no signaling could occur. Immobility of ICAM1 may be important to allow for force-induced activation of LFA-1 and lack of ICAM1 mobility on DCs was shown to impair T cell priming and adhesion [211]. Future experiments with supported lipid bilayers could yield insight into whether mobility is an important factor. Similar to the plates used here, lipid bilayers offer good dose control, but the ligands can move laterally.

Interestingly, the effect of CD2 on increasing cytokine production and enhancing sensitivity might be mediated through separate mechanisms [2]. While the former is likely due to signaling through CD2's long cytoplasmic tail, the increase in sensitivity may be a direct consequence of its adhesion function. CD2 also plays a role for CAR T cell activation [180, 181], even though CARs are generally larger and therefore their size will not match with CD2/CD58. Mutations or loss of CD58 are strongly associated with evasion of T cell killing *in vitro*, as well as in cancer patients [179, 182, 183]. In the future, more subtle approaches to inhibit or enhance the CD2 axis may be required to harness the full therapeutic potential of this molecule. For adoptive CAR T cell therapy, it will be interesting if one can remove CD2 from the equation and therefore make these cells resistant to the loss of CD58 found in some tumors [182, 183].

Here I have shown the effect of CD58 and ICAM1 on T cell activation, cytokine secretion, and TCR downregulation. Surprisingly, ligation of CD2 by CD58 or binding of the much larger LFA-1/ICAM1 pair leads to highly similar phenotypes. Even affinity-matured TCRs rely on CD58 engagement to increase the sensitivity of pMHC. A higher affinity is not beneficial anymore in the presence of CD58, but results in a decreased potency. Interestingly, the phenotype in a co-culture system was less pronounced, even when using CHO cells to eliminate potential compensatory interactions. Experiments on supported lipid bilayers could bridge that gap and help understand the factors contributing to the action of CD58 and ICAM1. Furthermore, comparing ligand densities directly could establish if any difference is due to a lower

number of ligands on cells, compared to what I used on plates for my experiments. In the future, understanding this axis better might help improve therapeutic success in patients with CD58 alterations and to utilize the power of LFA-1 and CD2 in CAR T cell therapy.

# Chapter 3

---

# Measuring ultra-low affinity TCR/pMHC interactions by SPR

## 3.1 Introduction

Surface plasmon resonance (SPR) is the gold standard for measuring interactions between binding partners, such as proteins, small molecules, nucleic acids, or even viruses [284]. It allows one to measure binding kinetics (off- and on-rates) and affinities using slightly different experimental regimes. For monomeric interactions, affinities can also be calculated from measured kinetics ($K_D = \frac{k_{off}}{k_{on}}$). Unlike many other methods, SPR does not require labeling of the binding partners, but rather measures any association onto the surface-proximal volume of the SPR chip. To measure specific binding, one of the binding partners is immobilized on the chip surface or a surface-bound matrix (e.g. dextran) and a potential binding partner is injected over the surface (termed analyte; Figure 3.1A). With the appropriate controls, any binding can then be attributed to a specific interaction between these molecules. However, since the measurement is not specific to one species, SPR is prone to errors by contamination of the analyte with other potential binding partners, differences in buffer composition causing apparent signals, and aggregation of the analyte [284, 285]. The latter is common for proteins at a higher concentration and therefore needs to be strictly excluded to receive meaningful results. Fortunately, some of these artifacts can easily be spotted when inspecting the sensogram (time versus response of an SPR experiment), and improved protein production workflows have made it significantly easier to generate clean products for SPR experiments.

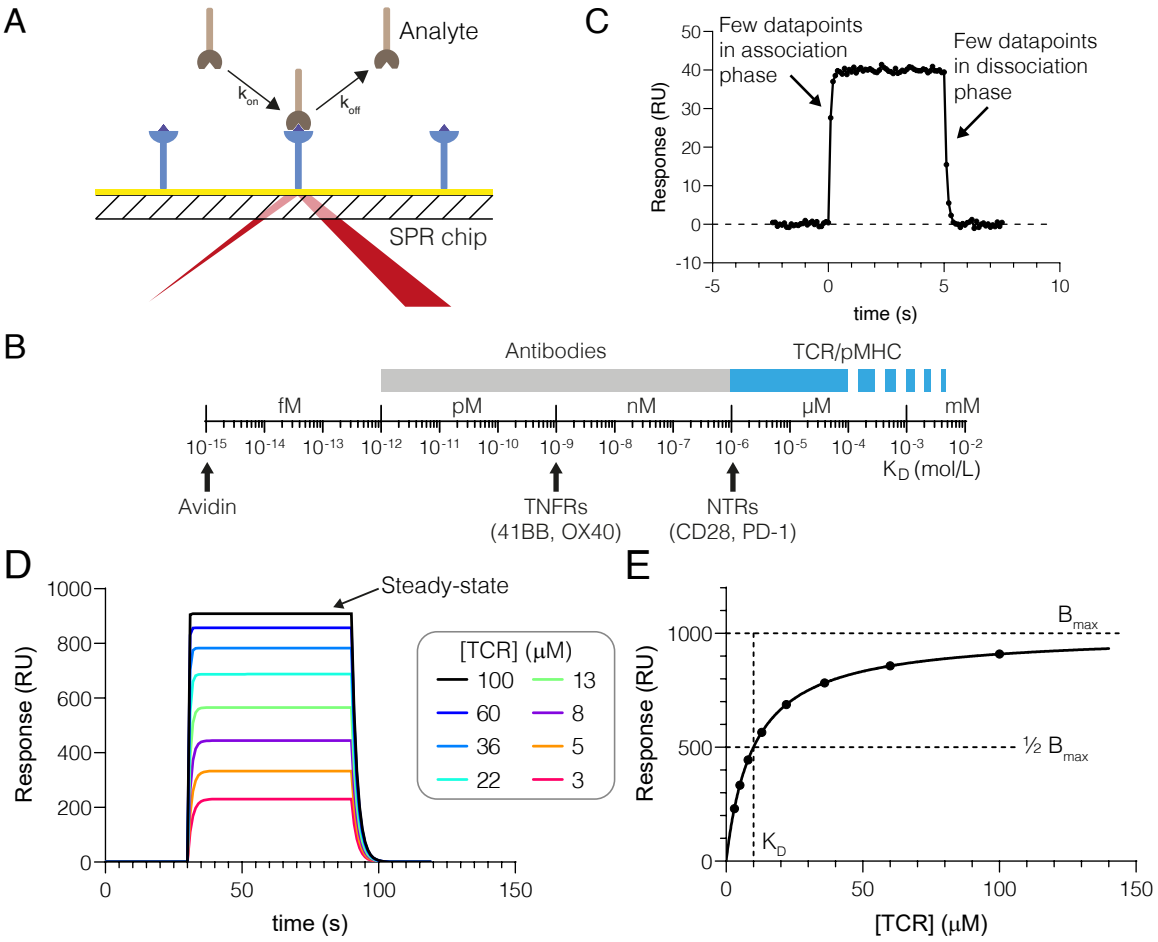


**Figure 3.1: SPR to measure TCR/pMHC interactions.**
**(A)** Principle of surface plasmon resonance (SPR). In our experiments, the pMHC is immobilized on the chip, while a soluble version of the TCR serves as an analyte. **(B)** TCR/pMHC affinities are low compared to other interactions in the immune system. Affinities for cognate TCR/pMHC pairs are usually within a range of 1–100 $\mu$M, but $K_D$s for self-peptide or altered peptide ligands are expected to be substantially higher. **(C)** Simulated SPR experiment of a TCR binding a low affinity pMHC. The fast association and dissociation prevent good kinetic fitting. Simulation parameters: $k_{on} = 50,000\ M^{-1}s^{-1}$; $k_{off} = 10\ s^{-1}$; $[TCR] = 50\ \mu M$. **(D)** Simulated sensogram of a TCR binding immobilized pMHC with an $K_D$ of 10 $\mu$M. **(E)** Steady-state values from (D) over TCR concentration. Indicated are the $B_{max}$ (saturation) and the $K_D$. TNFR: TNF receptor. NTR: non-catalytic tyrosine-phosphorylated receptors.

Measuring the interaction of TCRs with pMHC via SPR has been instrumental in driving our understanding on how T cells recognize their ligands. Interestingly, TCR/pMHC bonds are among the weakest in the immune system (Figure 3.1B). For instance, B cell receptors are similarly structured with variable immunoglobulin-family domains that bind their target and also signal through ITAMs when expressed on the surface of B cells. Yet, they generally ex-

hibit significantly higher affinities than TCRs with $K_D$s ranging from about 1 $\mu$M to picomolar values (Figure 3.1B) [67]. In contrast, typical TCR affinities for cognate peptides are in the range of 2–30 $\mu$M for human class I TCRs, and 20–100 $\mu$M for class II TCRs [70]. Their low affinity results from a combination of a relatively slow on-rate ($\sim 10^3$–$10^5$ $M^{-1}s^{-1}$) and a fast off-rate ($\sim$0.1–1 $s^{-1}$) [66]. Notably, this not an inherent structural limit of the TCR, as *in vitro* affinity-matured TCRs can bind pMHC with antibody-like affinities (e.g. $\sim$50 pM for the high affinity 1G4 variant used in chapter 2).

The affinities and kinetics of a number of class I and some class II TCRs when interacting with their cognate antigen have been determined by SPR. However, $K_D$s and off-rates for peptide variants used in discrimination studies (such as here), cross-reactive peptides, or self-peptides can be significantly higher than 100 $\mu$M and 5/s, respectively. With current technology affinities and off-rates beyond these values have been very difficult to measure and consequently, the affinity of TCRs to self-pMHC is a matter of speculation. Notably, measuring low affinity TCR/pMHC interactions is not an issue of signal-to-noise. Modern SPR technology (such as the Biacore T200 used in this work) are extremely sensitive (<1 RU), and therefore are able to detect even the little binding produced by a low affinity interaction (see Figure 3.1C for an example with a $K_D$ of 200 $\mu$M). For kinetics, the limiting factor is the time resolution of the SPR machine. With a typical frequency of 10 Hz, the maximum achievable off-rates that can be measured are in the order 10 $s^{-1}$ (see Figure 3.1C for example). SPR also allows one to determine the affinity directly through measuring the response at steady-state at different concentrations of analyte (Figure 3.1D; often called equilibrium analysis). At high concentrations (top $[TCR] \gg K_D$), almost all of the active pMHC on the surface will be TCR-bound. The $K_D$ is defined as the analyte concentration required to achieve half-maximal binding, where maximal binding ($B_{max}$) refers to the level of binding when each pMHC on the chip is bound (Figure 3.1E). Therefore, accurate determination of a $K_D$ requires a good estimate of the $B_{max}$. Generally, to reach sufficient binding to calculate the $B_{max}$ by extrapolation, the top TCR con-

centration should be higher than the $K_D$ to be measured (typically somewhere >2–10-fold the $K_D$, depending on the technical error/noise). Although this is feasible for higher-affinity interactions, it can be difficult to achieve for lower affinity interactions because increasing the concentration of the TCR is not practical without introducing aggregates.

Here we aim to overcome this practical limitation on the lower limit of TCR/pMHC affinities that can be measured by SPR. We show that using a new SPR protocol where the $B_{max}$ is independently determined allows reproducible affinity measurements for >1 mM $K_D$s for two different human TCRs. This method is useful for generating peptide panels to study antigen discrimination (see chapter 4), to measure the minimal affinity between TCRs and pMHC, and to investigate the interactions between TCRs and self-pMHC.

## 3.2 Results

### 3.2.1 Steady-state fitting of low affinity pMHC leads to large errors

Here we aimed to develop a SPR-based protocol to measure TCR/pMHC $K_D$s >100 $\mu$M. Since determining the affinity through kinetics is technically limited by the sampling rate of the machine, we decided to use steady-state fitting instead. First, I sought to estimate which $K_D$s can still be reliably measured and which ones cannot. Since this depends on the error, I first investigated TCR/pMHC data in the lab to understand how much it deviates from an ideal binding curve (such as in Figure 3.3C). For simplicity, I ignored other sources of noise, such as from drifts. To test the maximum $K_D$ that can reliably be measured, given this experimental error and a top TCR concentration of 100 $\mu$M, I used Monte Carlo simulations, where I simulated SPR experiments repeatedly with random errors and then fitted the data and extracted the $K_D$. As expected, I find that the variance increases substantially when trying to measure $K_D$s over the top TCR concentration (simulated in Figure 3.2A). This includes many extreme

outliers such that $K_D$s >5,000 $\mu$M or $K_D$s <200 $\mu$M represent over 50 % of the results for a true $K_D$ of 1,000 $\mu$M (Figure 3.2B). Lastly, even when averaging many experiments the geometric mean of the $K_D$ (and even more so the arithmetic mean) will include a substantial bias (Figure 3.2C). For example, at a true $K_D$ of 1000 $\mu$M the geo. mean is >50-fold off the true value, resulting in an apparent $K_D$ geo. mean of ~50,000 $\mu$M. If outliers with very high $K_D$s are excluded, this trend reverses and the $K_D$ is underestimated (visible on Figure 3.2A). Given that it is difficult to achieve TCR concentrations that are significantly larger than 100 $\mu$M, while avoiding aggregation, this limits practically measurable $K_D$s for TCR/pMHC interactions to around 50–200 $\mu$M.

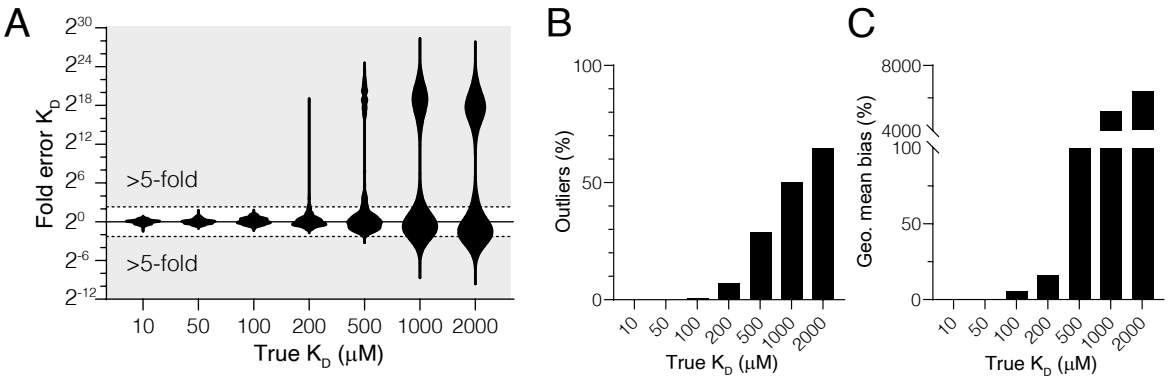


**Figure 3.2: Trying to measure low affinity pMHC can lead to large errors in $K_D$.**
**(A)** Measuring increasingly low affinities with the same top TCR concentrations leads to the introduction of significant variance between experiments. **(B)** The number of experiments with more than >5-fold error (grey area) shows a stark increase at high $K_D$s. **(C)** At higher $K_D$s the geometric mean of multiple experiments does not reflect the true $K_D$ anymore, but rather significantly over estimates the $K_D$. Data generated by Monte Carlo stimulations (n=250 per condition) of steady-state binding with a titration of 8 TCR concentrations, a top concentration of 100 $\mu$M, and a SD of 0.09/RU (estimated from our own experimental data).

### 3.2.2 SPR method to measure low affinity TCR/pMHC interactions*

As shown above, to get an accurate and reproducible estimate of the $K_D$, it is required to use analyte (here the TCR) concentrations that are close to saturating binding ($B_{max}$). For our typical TCR concentration of 50–100 $\mu$M, this would limit the $K_D$s we are able to measure to <100 $\mu$M. We therefore decided to independently determine the $B_{max}$ for SPR experiments using a high-affinity antibody. Since the W6/32 antibody binds all human class I MHCs in a peptide-independent, but conformation-dependent way, we can measure the amount of active pMHC on the chip surface (i.e. the $B_{max}$) independently of reaching saturating TCR concentrations (Figure 3.3A). As expected, the TCR response can vary dramatically between pMHCs, while the antibody response remained similar (Figure 3.3B). If the batch and antibody concentration are kept constant (as in our experiments), antibody binding will only depend on the amount of pMHC immobilized and the active fraction of pMHC. For all our experiments, I first fitted the data directly ($B_{max}$ fitted), where the $B_{max}$ is estimated based on TCR binding (i.e. the traditional way to perform steady-state fitting). Using the same data, I applied a second model, where the $B_{max}$ was constrained to the value that was calculated based on antibody binding ($B_{max}$ constrained). For high affinity pMHC the $B_{max}$ and therefore $K_D$ when using either method is similar, whereas for low affinity pMHC it may vary greatly, based on the lack of data to determine the $B_{max}$ from the TCR binding alone (Figure 3.3C).

*The results in this chapter are published in [4].

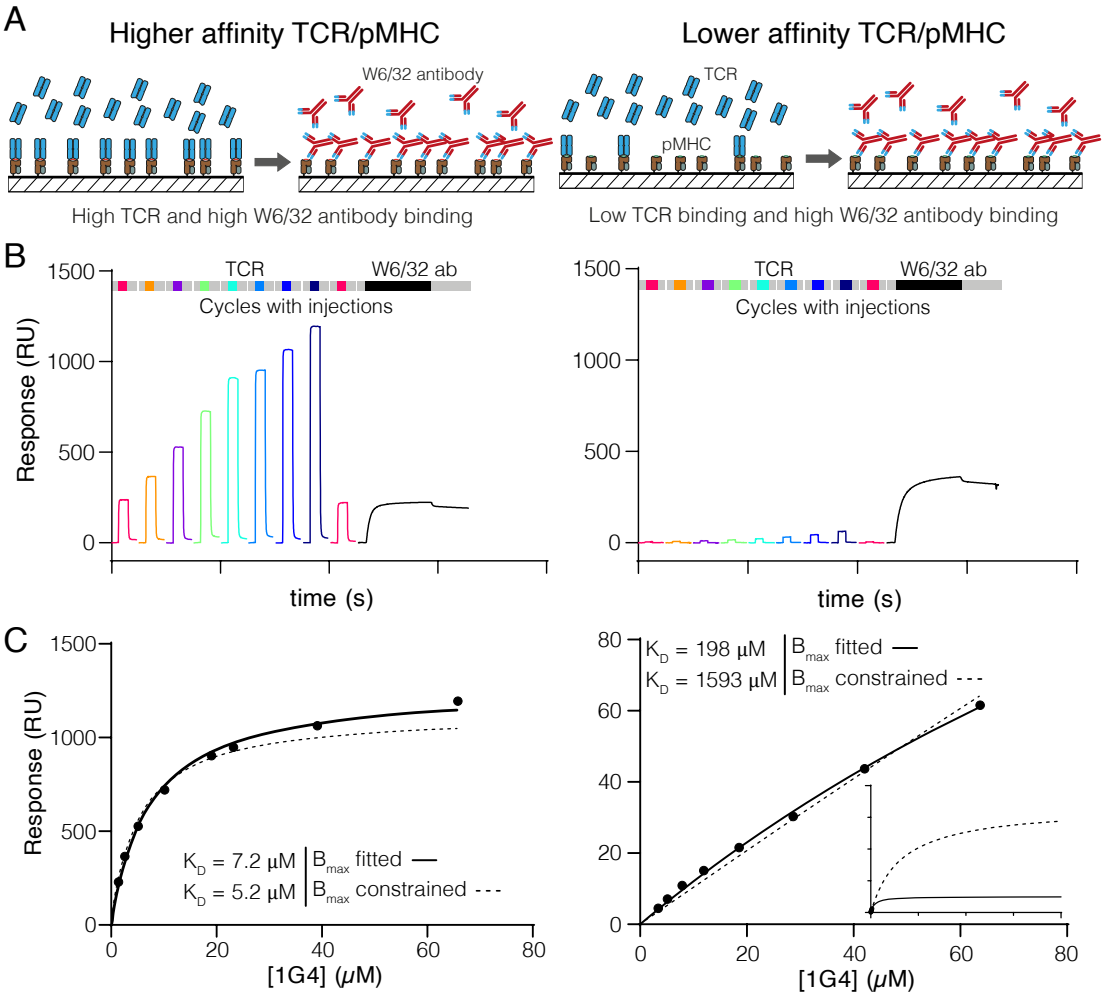


**Figure 3.3: Methodology ultra-low affinity SPR.**
**(A)** The conformation-specific, peptide-independent pan-class I MHC antibody W6/32 allows to measure the $B_{max}$ independently of TCR binding. **(B)** While the TCR response depends on the peptide, the W6/32 shows strong binding even to a low affinity pMHC. Antibody binding is a function of the antibody concentration used, the amount of pMHC immobilized, the active fraction, and the antibody's affinity to MHC. Since we keep the concentration constant between experiments and this antibody binds independently of the peptide, the binding will be a good reflection of the amount of active pMHC on the surface (i.e. the $B_{max}$). **(C)** For a high-affinity TCR/pMHC interaction, using the $B_{max}$ determined by TCR ($B_{max}$ fitted), or the $B_{max}$ determined using the W6/32 antibody ($B_{max}$ constrained) does not change the fit significantly. However, for a low affinity pMHC, where saturation is not achieved, using the antibody $B_{max}$ results in a dramatic change in $K_D$. For the low affinity pMHC, an extrapolated response with a x-axis limit of 10,000 $\mu$M and a y-axis limit of 2,000 RU is shown as an inset. Only on this larger scale, the differences in the fits become obvious. Peptide variants shown: NYE 3A (left) and NYE 5F (right).

We generated an empirical standard curve from high affinity TCR/pMHC experiments (where top [TCR] > 2.5x $K_D$) for two different natural human TCRs. Both the A6 and 1G4 TCR fall on the same curve and the antibody is insensitive to the specific peptide used (Figure 3.4A). Importantly, using the constrained $B_{max}$ method does not introduce additional error when compared to the $B_{max}$ fitted method for high-affinity pMHCs. For lower affinity pMHCs, the variance increased significantly when using the $B_{max}$ fitted method, while it did not increase when using the antibody-determined $B_{max}$ (Figure 3.4B). The $K_D$ measured with $B_{max}$ fitted correlated well at lower $K_D$s, but stoped doing so at higher $K_D$s (Figure 3.4C). Reminiscent of the theoretical analysis above, $K_D$s tend to be underestimated for $K_D$s >20 $\mu$M, with a second peak appearing for pMHC with $K_D$s >1,000 $\mu$M. This second peak represents starkly overestimated values and was clipped to 10,000 $\mu$M in my analysis for brevity.

For our SPR experiments we use CD58 as an inert protein in the reference flow cell and match the immobilization levels. This is necessary since a mismatch in immobilization between the sample and the reference flow cell can hide small signals (volume exclusion effect; Figure 3.5). Furthermore, small drifts within a flow cell can be a cause of errors. For example, the buildup of small air bubbles can cause drifts and high temperatures (i.e. 37°C) promote their formation. Subtracting the reference flow cell signal (single referencing) corrects for larger changes in response, such as bulk effects caused by differences in buffer composition, but it does not account for small differences between the flow cells. To avoid these, we implemented double referencing [285] for all our data analysis, where the buffer injections from the same flow cell are used to correct for small drifts over time (Figure 3.6).

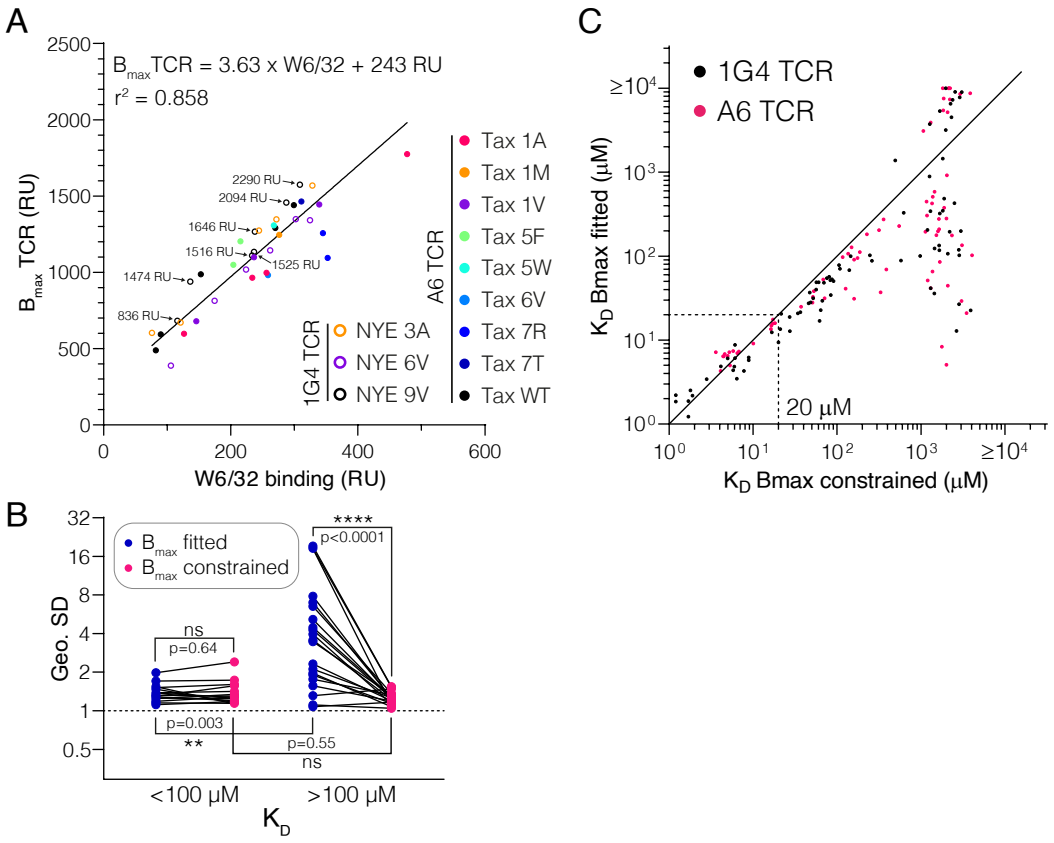


**Figure 3.4: New SPR method allows to measure ultra-low affinity pMHC reproducibly.**
**(A)** Standard curve to correlate W6/32 antibody binding with saturated TCR binding. Immobilization levels of NYE 9V are indicated. As expected, the TCR $B_{max}$ and W6/32 binding depend on how much pMHC is immobilized. However, measuring immobilization does not differentiate between active (i.e. able to bind the TCR) and inactive pMHC. In contrast, W6/32 binding is conformation-specific and therefore offers a better correlate for TCR binding. **(B)** Geometric standard deviation factor (fold change; 1.0 equals no variance) for higher (<100 $\mu$M $K_D$) and lower affinity (>100 $\mu$M $K_D$) pMHCs. Paired testing by two independent Wilcoxon rank tests. Unpaired testing by Kruskal-Wallis test with Dunn's multiple comparison. **(C)** Correlation of $K_D$s obtained with antibody-derived $B_{max}$ ($B_{max}$ constrained) or with traditional fitting ($B_{max}$ fitted). Shown is a loglog line with a slope of 1. An error to underestimate the $K_D$ using the traditional method seems to appear around a $K_D$ of 20 $\mu$M. Note: some of the $K_D$s fitted with the traditional method are significantly larger than 10,000 $\mu$M, but are shown here as 10,000 $\mu$M for better visualization.

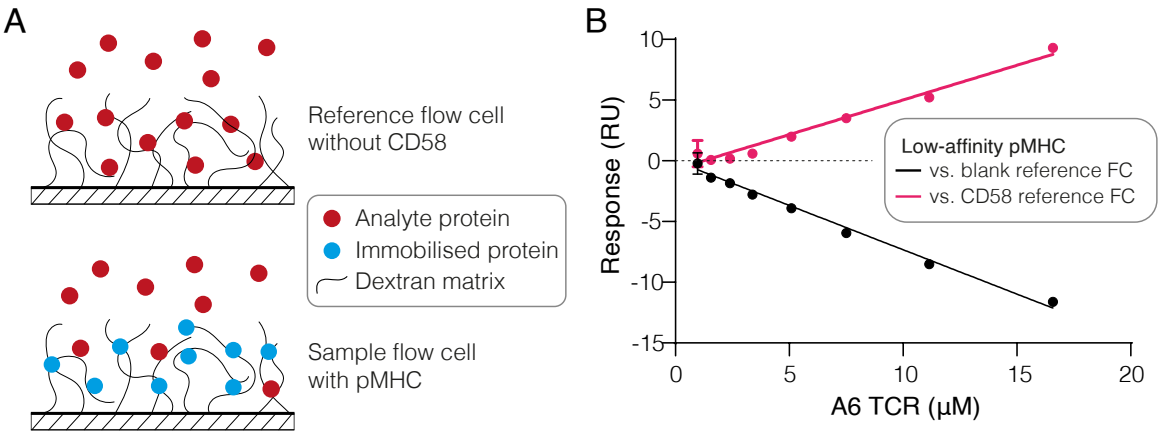


**Figure 3.5: Matching immobilization levels between reference and sample flow cell is important to avoid masking low responses.**
**(A)** Without using CD58 as a control protein, analyte can come closer to the chip surface and cause a signal, without any specific binding required. If this reference signal is now subtracted from the sample flow with immobilized pMHC, it can result in an apparent negative binding. **(B)** The response of a low affinity pMHC referenced to either a blank flow cell or one that had CD58 immobilized. The negative response observed when referencing to a blank flow cell (~10 RU) would be hidden for a high affinity pMHC, where the specific signal is stronger (>100 RU).

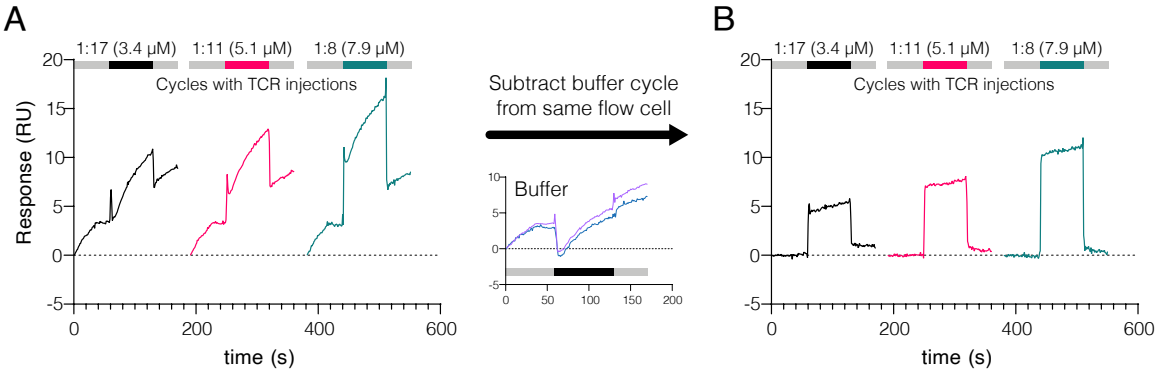


**Figure 3.6: Double referencing allows to adjust for small differences between flow cells.**
A sensogram from a single flow cell with three low TCR concentration injection cycles before **(A)** and after **(B)** double referencing. While the data in (A) is already referenced by the control flow cell, it clearly shows a drift in response over time. To adjust for this, buffer injections from the same flow cell as the sample are used as an additional reference.

### 3.2.3 APL screening*

With the ability to measure ultra-low affinity pMHCs (>1 mM $K_D$), we next sought to screen many different altered peptide ligands to find a panel suitable for functional experiments. Both the 1G4 and A6 TCR are natural human class I TCRs binding peptides presented on HLA-A*02:01. The 1G4 TCR recognizes a peptide from the testis/tumor antigen NY-ESO (NYE) and we use 11 previously described peptides [78, 82]. Many of these have only been studied in the context of an affinity-matured TCR and therefore we did not have a reference $K_D$. As the index peptide and base for all further substitutions, we used the NYE 9V peptide, which contains a C9V mutation to improve stability on MHC [47]. We utilized 6 previously described APLs for the A6 TCR [27, 286], but I also designed 17 additional variants with a focus on substituting position 5 and 7, based on the crystal structure of the A6/HLA-A*02:01 complex [27, 62]. The index peptide for the A6 TCR is derived from the viral Tax protein from human T-lymphotropic virus 1 (HTLV-1). Additionally, our panel includes a yeast peptide (Tel1p) and a peptide derived from a human self peptide (HuD2L9V) that were previously described to bind the A6 TCR [287, 288]. To avoid large differences in stability on MHC, we did not alter the anchor residues 2L9V for any of our 1G4 or A6 APLs.

*The results in this chapter are published in [4].

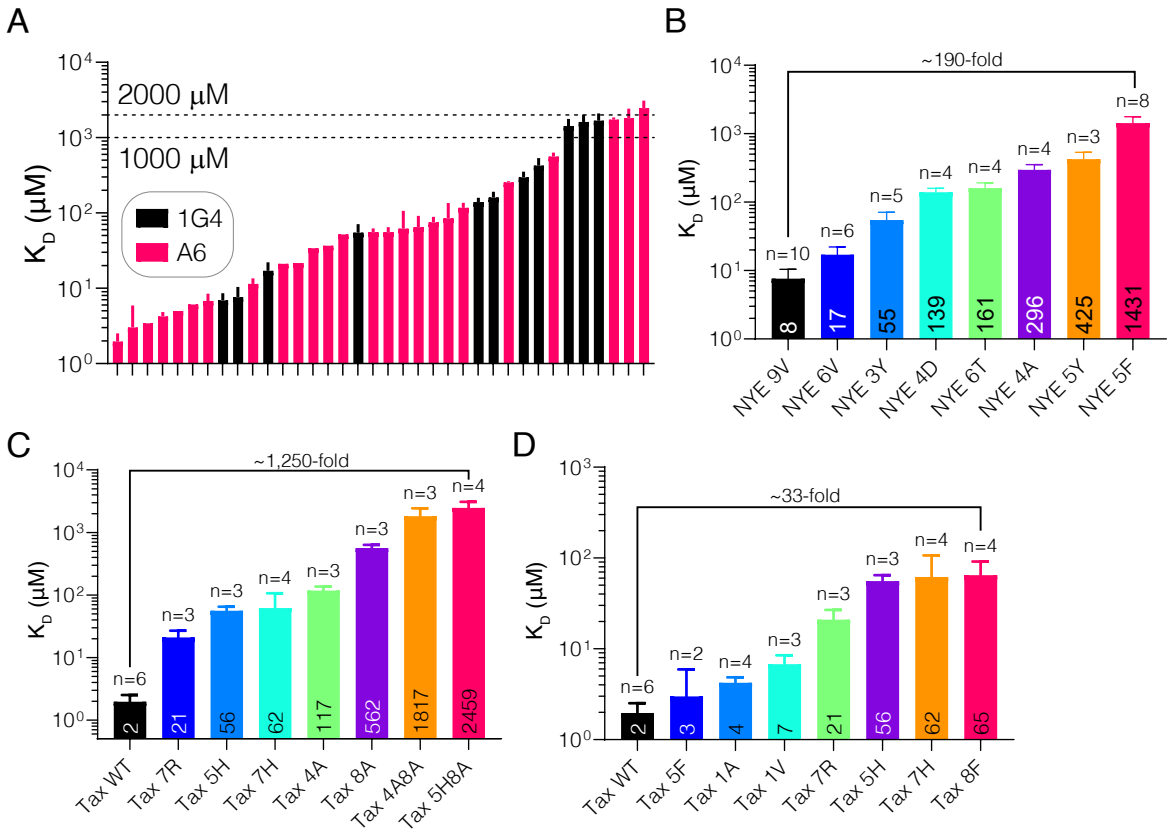


**Figure 3.7: Screening of peptide ligands for the 1G4 and A6 TCRs.**
**(A)** Overview of peptide variants screened for the 1G4 and the A6 TCR. **(B)** Selection of 8 peptides for functional experiments with the 1G4 TCR. **(C)** Selection of 8 peptides for functional experiments with the A6 TCR. **(D)** A6 panel with higher affinities.

When we measured the affinities for all of these peptides, we found a broad range of $K_D$s ranging from 2 $\mu$M to ~2 mM (Figure 3.7A; Table S1 and Table S2). For the 1G4 TCR, we could reproduce the $K_D$s reported previously for high-affinity peptides, but we found some difference to lower affinity ones [78]. When comparing the affinities for the A6 TCR for the Tax WT and the Tax 7R peptide, we find slightly lower affinities [27], potentially due to the difference in temperature used (37°C for us). Based on the range of peptide affinities, I designed a panel for the 1G4 and A6 TCR, each spanning a wide range of affinities (Figure 3.7B–C). Due to limited sensitivity of A6-expressing T cells (see chapter 4 for details), I furthermore designed an additional panel for the A6 TCR that is enriched in higher-affinity peptide variants (Figure 3.7D).

### 3.2.4 Recognition of pMHC by the TCR is characterized by an affinity-floor

Surprisingly, even with double amino acid substitutions, we did not find peptides for either the 1G4 or the A6 TCR that showed $K_D$s significantly larger than 2 mM (Figure 3.7A). We speculated that this might represent an affinity-floor. At this floor, the dominant energetic contribution to binding is expected to come from contacts to the MHC, rather than the peptide. Since for our initial APL screening we changed at most two amino acids, the peptides were still closely related to their ancestral index/cognate peptide. We therefore sought to investigate completely unrelated peptides. First, we used NYE APLs designed for the 1G4 TCR and measured their affinity for the A6 TCR and *vice versa* (cross-reactivity). However, they bound with a similar affinity of about 2 mM to either TCR (Figure 3.8A–B). Next, we tested a minimal peptide that consists only of alanines with conserved anchor residues. Yet, the affinity remained very similar (Figure 3.8A–B). Lastly, we tested a biased peptide library (see Table 6.9), where the primary anchor residues (P2 + P9) are constrained to favor HLA-A*02:01 binding. Secondary anchor residues (P3 + P6) were chosen not to obstruct MHC binding. For TCR-facing positions (P1, P4, P5, P7, P8) only residues were allowed that do not likely contribute to TCR binding (i.e. small uncharged amino acids). When using this biased peptide library, we found a $K_D$ similar to the affinity floor (Figure 3.8A–B). Furthermore, when calculating the average of all affinity-floor peptides, we found it to be very similar for both TCRs (Figure 3.8C). When comparing the affinity floor with binding to NYE 9V, we estimate the loss of binding energy to be around 3.4 kcal/mol* or ~25 % based on a previously estimated total binding energy for the 1G4 of -12.5 kcal/mol [289].

*Calculated using: $\Delta\Delta G = -RT\ln\left(\frac{K_{D\,(\text{affinity floor})}}{K_{D\,(\text{NYE 9V})}}\right)$, where RT is 0.62 kcal/mol at 37°C.

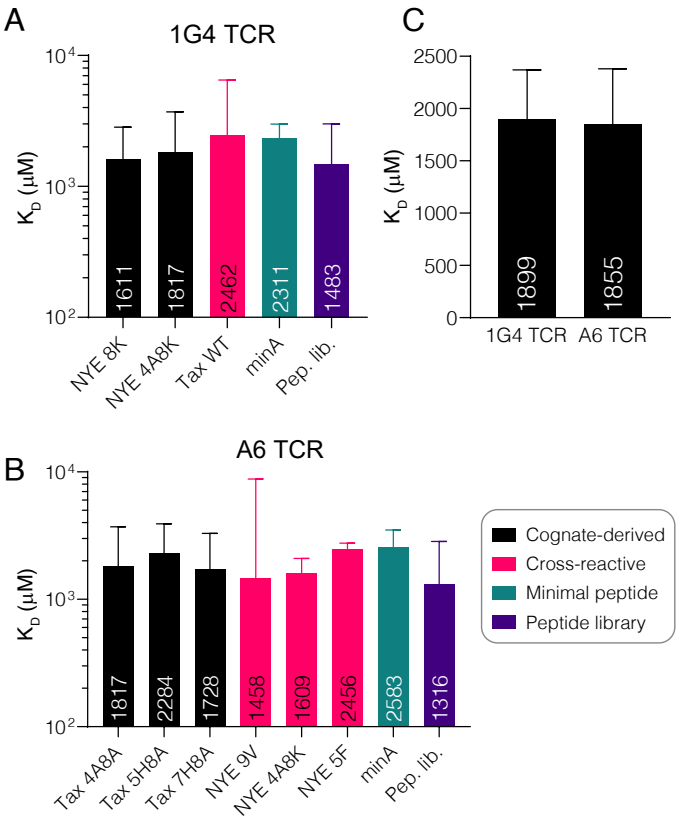


**Figure 3.8: The A6 and 1G4 TCRs exhibit a minimal affinity of about 2 mM to HLA-A*02:01.** Comparison of $K_D$s measured for some ultra-low affinity peptides for the **(A)** 1G4 and **(B)** A6 TCR. This includes peptides derived from the cognate/index peptide by single or double amino acid substitutions, completely unrelated peptides (cross-reactive), a minimal peptide with all alanines (except for the anchor residues), and a peptide library (see Table 6.9 for details). Shown is the geo. mean with 95 % CI. **(C)** Both TCRs show a very similar affinity floor of about 2 mM $K_D$. Displayed is the geo. mean of the geo. means of all peptides shown in (A) and (B) with geo. SD.

It is possible that this affinity-floor is merely an artifact of the control protein we used in the reference flow cell. For example, if CD58 is repulsing the TCR, this would lead to apparent binding to pMHC. To exclude such an effect, we tested additional control proteins. When testing MHC class II and CD86 we found them to be similar to CD58 (Figure 3.9A). Using ICAM1 led to a slightly (non-significantly) higher response than CD58 (Figure 3.9A). However, when we tested the influence of different control proteins on the actual $K_D$ on the example of 1G4 binding NYE 5F from paired experiments, we found the effect to be marginal (Figure 3.9B).

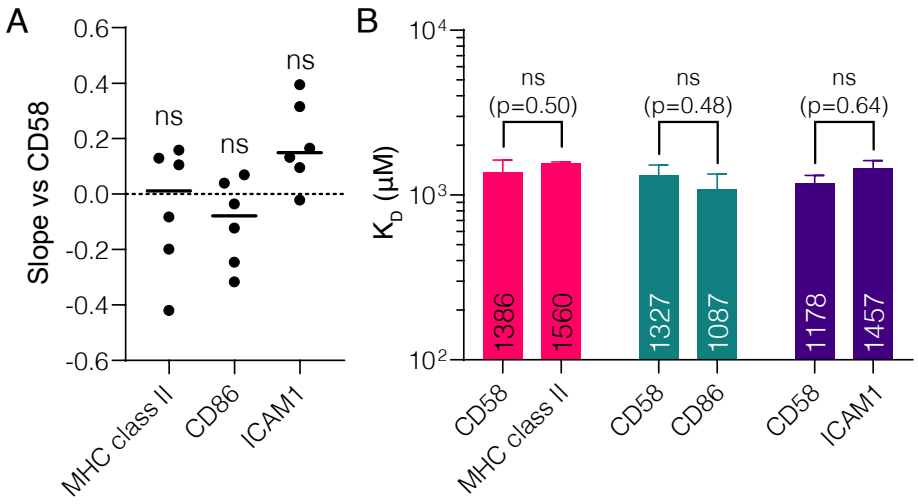


**Figure 3.9: Immobilizing alternative control proteins in the reference flow cell does not change the $K_D$ of ultra-low affinity pMHCs dramatically.**
**(A)** CD58 and MHC class II or CD86 produce a similar baseline. ICAM1 results in slightly more unspecific binding compared to CD58. Shown are the slopes of the binding when using CD58 as reference flow cell. Slopes were determined by fitting a linear function to the [TCR] vs RU data (see Figure 3.5B). Statistical testing by multiple, independent 1-sample Wilcoxon tests versus 0. p=0.84, p=0.31, p=0.06 for MHC class II, CD86, and ICAM1, respectively. **(B)** Using a different control protein for the reference flow cell does not change the $K_D$ of an ultra-low affinity peptide (1G4/NYE 5F) significantly. Statistical testing using mixed effect analysis (paired) with Dunnett's multiple comparison on log-transformed data. Shown are geo. mean + geo. SD. n=2, 4, 3 for MHC class II, CD86, and ICAM1, respectively.

## 3.3 Discussion

SPR has been pivotal in understanding TCR/pMHC interactions. However, due to the naturally low affinity of TCRs, it has been practically impossible to measure the kinetics or affinities for low affinity pMHCs. Here we showed a new SPR method based on steady-state $K_D$ fitting, that allows the determination of $K_D$ values >1 mM; i.e. affinities >10-fold lower than previously possible. To achieve this we used a conformation-specific antibody binding all human class I MHCs to assess the $B_{max}$ independently of reaching saturating concentrations of TCR analyte. We showed that this method correlates well with the traditional approach for high affinity pMHCs. There is currently no independent way to verify our $K_D$s >100 $\mu$M. How-

ever, in contrast to the $B_{max}$ fitted method, we were able to measure $K_D$s reproducibly with a variance similar to that for high affinity pMHCs.

Using this method we screened >40 APLs for the human class I TCRs 1G4 and A6. We found affinities ranging from 2 $\mu$M to over 2 mM. For the first time this allowed us to design a pMHC panel to study the response of T cells to ultra-low affinity pMHCs (see chapter 4). Surprisingly, even with aggressive substitutions, cross-reactive peptides, or a minimal peptide we did not identify pMHC with $K_D$s much lower than 2 mM. When testing pMHC refolded with a peptide library that represents a large diversity, we found a similar $K_D$, defining an affinity floor for TCR/pMHC interactions. Importantly, we tested multiple control proteins to exclude the possibility that this affinity floor is due to a special property of our standard control protein CD58. However, while our class I pMHC ligands are produced in bacteria, all control proteins were produced in mammalian cells. Therefore, further experiments are required to rule out the chance that the difference in glycosylation would result in higher unspecific binding of the TCR to pMHC than the control proteins. Moreover, we did not attempt to change the anchor residues of our peptides, except for the peptide library, where they were allowed to vary within a limited number of amino acids that can bind HLA-A*02:01 well. While they are not expected to contribute much to the binding [290], they could play a role when assessing this affinity floor.

Interestingly, the two TCRs tested by us showed a similar affinity floor. However, further experiments are required to establish if this holds true for other TCRs as well. For example, it would be interesting to investigate TCRs binding to other HLAs than HLA-A*02:01, which is the HLA both the A6 and the 1G4 TCR bind to. Moreover, testing class II MHCs could establish if this threshold is biologically conserved for $CD4^+$ T cells, as well. We hypothesize that this affinity-floor represents the background affinity that a TCR would be exposed to in a physiological settings when interacting with self-peptide on APCs. It is tempting to speculate that this is a direct consequence of positive selection and therefore may vary greatly when TCRs

are tested against MHC allotypes they have not experienced during thymic selection. Further experiments would aid our insight into the importance self pMHC interactions and may provide clues for the mechanisms underlying the development of autoimmunity.

The ability to reliably measure the ultra-low affinity peptides down to the background affinity would open up multiple interesting applications. First, interaction of T cells with self-peptide expressing APCs has been shown to be important for T cell maintenance [71]. Better understanding of this process might help us to improve the persistence of engineered T cells, such as CAR T cells in a therapeutic setting. Next, one could study how strong auto-reactive TCRs bind their self-peptide and how this relates to the background affinity to other peptides. Additionally, this assay could be useful to study cross- or allo-reactivity. In particular, when studying engineered TCRs designed for clinics it would be interesting to exclude the strong cross-reactivity that previously led to fatal auto-reactivity in patients [291]. Lastly, characterizing these really low affinity interactions will help us better understand positive selection, as it happens in the thymus, with the ultimate goal of generating non-auto-reactive TCRs completely *in vitro* to any HLA allotype desired. In conclusion, this method opens up many opportunities for SPR to continue to support the understanding of TCR/pMHC interactions by providing affinities for pMHC ligands that were previously out of reach.

# Chapter 4

---

# Antigen discrimination by primary human T cells

## 4.1 Introduction

T cells fulfill a unique function within the immune system of jawed vertebrates. They can recognize foreign-derived peptide presented on MHC and initiate an immune response where necessary. Unlike the innate immune system, T cells do not rely on genetically-encoded pattern recognition receptor (PRR), but are able to potentially bind any given peptide presented on MHC through their T cell receptor. Since the ligand for a T cell clone (i.e. a specific TCR) is not determined *a priori*, thymic selection after somatic recombination is necessary to prevent binding to self-pMHC (negative selection), while ensuring that each TCR displays some affinity for the MHC scaffolds that will carry potential foreign antigens (positive selection) [40]. Given their peculiar situation, T cells are required to discriminate self and non-self antigens in the periphery with high fidelity. Like any monomeric receptor/ligand interaction, the TCR binding the pMHC can be characterized by its affinity (i.e. $K_D$) and its on- and off-rates. While the on-rate may have some influence on rebinding [292], generally the off-rate ($k_{off}$) is considered the biophysical parameter probed through TCR binding, since it determines the lifetime of the bond ($\tau = 1/k_{off}$).

Based on substituting amino acids in a known cognate peptide, previous research has established the astounding ability for T cells to recognize single amino acid changes. When measuring the affinity or off-rates of the agonistic cognate peptide versus a non-agonistic substituted peptide by SPR, the difference was found to only be 3–10-fold using different murine experimental systems [30, 31, 33–36]. This capacity to translate a <10-fold change in binding into a >1000-fold difference in response (i.e. the difference between responding and not responding at all) is sometimes referred to as 'perfect' or 'near-perfect' discrimination. While this presents currently the dominant view in the field, there are multiple reasons to question such a high level of discrimination. First, it has been difficult to explain such discrimination mathematically, while maintaining a physiological level of sensitivity and speed [37, 256].

Furthermore, it is inconsistent with the idea of a physiological role of cross-reactivity. Since the pool of naïve T cell clones is physically limited, to achieve full coverage of the peptidome, each T cell needs to recognize an estimated one million peptides [45]. As such, it would be expected that there is some flexibility for small differences in binding. Lastly, upon close inspection of the SPR data from these early studies, we found signs of aggregation (i.e. multi-phasic unbinding) and an analyte concentration too low to reliably measure affinities by steady-state fitting (see chapter 3 for details).

Based on these results, I aimed to investigate the question of antigen discrimination quantitatively in more detail. Unlike prior studies, I used a new SPR protocol to reliably measure TCR/pMHC affinities >10 times lower than previously possible. When measuring the discrimination power in primary human $CD8^+$ T cells transduced with one of two natural TCRs, I found it to be much lower than previously reported. Surprisingly, I could not identify any hard affinity threshold after which the T cell response was fully abolished, but rather a gradual, affinity-dependent decline in potency. However, discrimination was still above that of an 'ordinary' receptor and therefore consistent with the physiological role of T cells in balancing discrimination and cross-reactivity. Due to the large range in $K_D$s, I was able to fit a kinetic proofreading model, to determine for the first time the proofreading rate and number of proofreading steps for a TCR binding a physiological antigen.

## 4.2 Results*

### 4.2.1 Defining discrimination power

T cells depend on their ability to differentiate self and foreign to fulfill their function as part of the adaptive immune system. Based on previous work, antigen discrimination is expected to be very good in T cells. In contrast, most other receptors in the body are not predicted to have such discrimination. To allow a quantitative comparison of the level discrimination, I introduced discrimination power ($\alpha$) as the sensitivity of a system/cell to changes in affinity. Calculating the discrimination power requires a measure of potency. Here, I use the antigen dose required to reach 15 % of the activation seen with a high affinity peptide (Figure 4.1A). When correlating potency and affinity on a loglog plot, the slope corresponds to the discrimination power ($\alpha$), while the y-intercept is a measure of sensitivity.

The discrimination power is an empirical measure and therefore independent of the underlying mechanism, such as kinetic proofreading. However, different antigen discrimination models predict the maximum discrimination power that can be reached. In an occupancy model, where activation only depends on the affinity, a discrimination power of 1 or less is expected (Figure 4.1B). In this model, dose and affinity are interchangeable (i.e. a loss of one can be compensated by an equal increase of the other). In contrast, kinetic proofreading can achieve discrimination powers larger than 1 (Figure 4.1B). Here, signaling depends on the lifetime/off-rate, rather than the affinity. In kinetic proofreading, the receptor/ligand-complex needs to undergo a series of irreversible modifications before signaling [252]. Since these steps are independent, they disproportionally favor ligands with longer lifetimes, thereby allowing discrimination surpassing the occupancy model and to explain $\alpha$>1. For a given TCR, introducing substitutions to a peptide mostly changes the off-rate and not the on-rate [78] and there-

*The results in this chapter are published in [4].

fore in my analysis I can use $K_D$ ($K_D = k_{off}/k_{on}$) as a good correlate of the off-rate. Notably, our laboratory previously calculated the discrimination power reported in others studies on T cells to be ~9 [4].

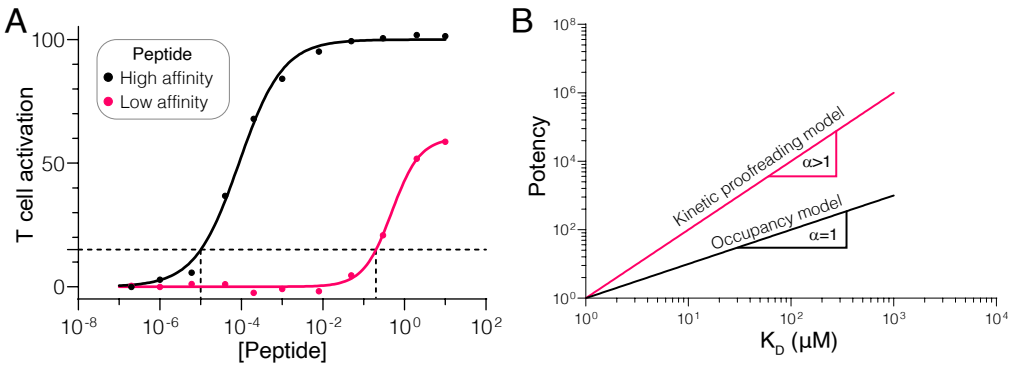


**Figure 4.1: Kinetic proofreading can achieve better discrimination than an occupancy model.** **(A)** When measuring the T cell activation over a titration of peptide, I define potency as the concentration to reach 15 % of the maximum activation of the high affinity/control peptide (dotted line). **(B)** Comparison of discrimination power between occupancy and kinetic proofreading model. In the occupancy model dose and affinity are interchangeable resulting in a power of 1. Kinetic proofreading models can achieve discrimination powers >1, depending on the parameter regime. Note here I plot $K_D$, rather than $k_{off}$, based on the assumption they are closely correlated.

### 4.2.2 Measuring physiological antigen discrimination

One way to study antigen discrimination is to use a panel of peptides spanning a large range of affinities. Using the SPR technology introduced earlier (see chapter 3.2.3), we screened the $K_D$s of previously described [78, 82] single amino acid altered peptide ligands for the 1G4 TCR, a natural human HLA-A*02:01-restricted TCR. Spanning a range of ~190-fold from the index/cognate peptide NYE 9V to the lowest affinity peptide NYE 5F (Figure 4.3A), this allowed me to quantitatively study antigen discrimination. Since the anchor residues were conserved, I did not expect any substantial differences in stability on the MHC to influence how well these peptides can activate T cells. To verify this, I pulsed T2 cells, which are deficient in the TAP transporter. Pulsing leads to displacement of the weakly bound endogenous peptides and

stabilization of MHC class I on the surface. All NYE peptides tested stabilized HLA-A2 to a comparable level (Figure 4.2), indicating that there are no large differences in loading.

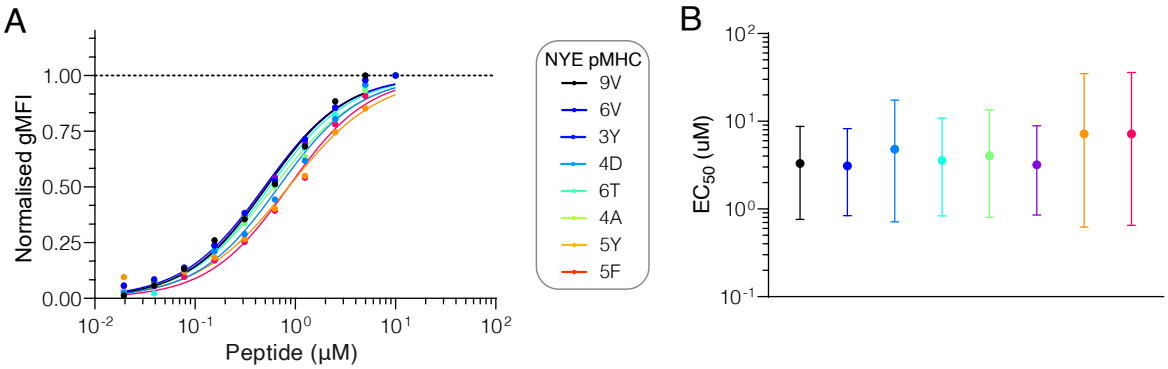


**Figure 4.2: All NYE peptides load similarly on T2 cells.**
T2 cells were pulsed for 90 min with indicated peptides and upregulation of HLA-A2 was measured by flow cytometry. **(A)** Upregulation of HLA-A2 in a peptide-dose dependent manner. **(B)** All NYE peptide load similarly on HLA-A2. Shown is the $EC_{50}$ with 95 % confidence intervals from the fits displayed in (A).

Next, I sought to measure antigen discrimination in a physiological system using T cells in co-culture with peptide-pulsed U87 target cells (a glioblastoma cell line). Briefly, $CD8^+$ T cells were isolated from the blood of healthy donors, transduced with the 1G4 TCR, and expanded (see also Figure 2.6). Surprisingly, when T cell activation was measured after 5 h by upregulation of the activation marker CD69, T cells showed a response even to the lowest affinity peptide NYE 5F with a $K_D$ of ~1,400 $\mu$M (Figure 4.3A–B). Notably, T cells did not produce IL2 in response to NYE 5F and they showed only little ligand-dependent 1G4 TCR downregulation (Figure 4.3C–D). Importantly, this response to ultra-low affinity peptides was specific to the 1G4 TCR, since untransduced cells that only expressed endogenous TCR did not show any response to either the high affinity NYE 9V, nor the low affinity NYE 5F peptide (Figure 4.3E). The potency was calculated as defined above by taking the concentration required to reach 15 % activation. This allows for accurate measurements even in the absence of a clearly defined $E_{max}$, as required for commonly used $EC_{50}$ (defined as the concentration require to reach ½ $E_{max}$). To assess the discrimination power in this system, I plotted the potency of each peptide

ligand against its $K_D$, as measured by SPR. The data follows a power-law relationship (a linear function in loglog space) with no clear threshold upon which there is an over-proportional loss in potency (Figure 4.3F). Notably, I cannot reproduce the complete loss of response with a <10-fold difference in $K_D$. However, T cells exhibit discrimination over baseline levels (i.e. $\alpha$>1), since a ~190-fold decrease in affinity requires a ~10,000–30,000-fold increase in dose to reach the same level of activation (Figure 4.3F–H).

One possible reason for the discrepancy between previous data and my results could be the TCR used. To independently verify these results, I repeated these experiments with a different TCR. Like the 1G4, the A6 TCR is a natural human TCR. However, it recognizes a viral, rather than a self-peptide presented on the same HLA-A*02:01 background [62]. As for the 1G4 TCR, I designed a functional panel of 8 peptides spanning a wide range of affinities by screening variants of the index peptide Tax WT (Figure 4.4A). Surprisingly, unlike 1G4-transduced T cells, those transduced with the A6 TCR stopped responding at a $K_D$ of ~60 $\mu$M (Figure 4.4B). Consistent with their lower sensitivity, these cells stained poorly with tetramers specific for the A6 TCR (Figure 4.4C). To allow direct comparison of expression levels between the 1G4 and the A6 TCR using the same staining reagent, I transduced Jurkat cells lacking $\alpha\beta$TCR with either TCR. Staining with anti-TCR antibody revealed an about 14-fold decrease in expression when comparing the A6 to the 1G4 TCR (Figure 4.4D).

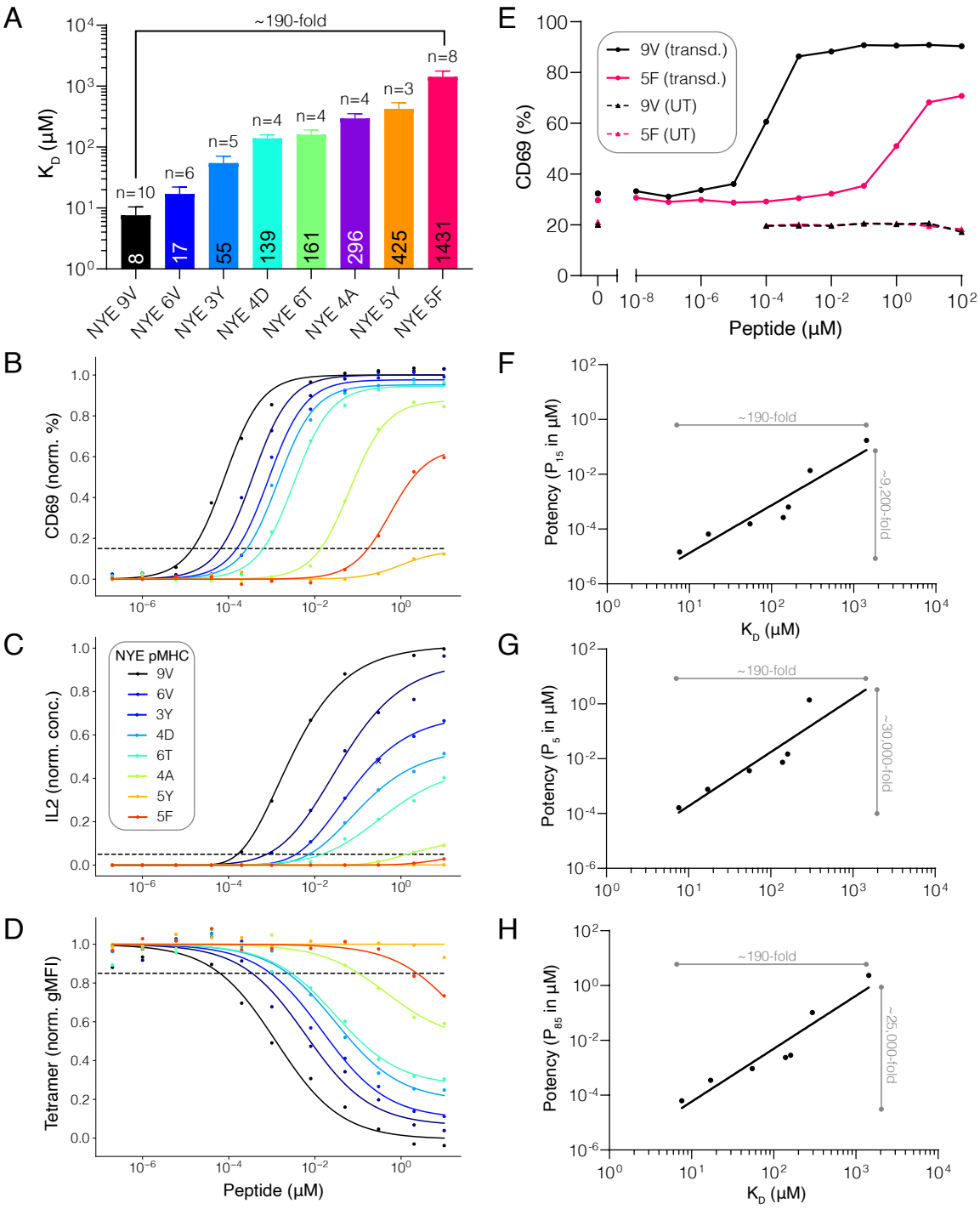


**Figure 4.3: 1G4-transduced T cells respond to pMHC in an affinity-dependent manner.** 1G4-transduced (B–D) or untransduced (E) T cells were stimulated for 5 h in co-culture with peptide-pulsed U87 cells. **(A)** Selection of NYE peptides used for functional experiments. Shown are the geometric means with geo. SD. T cells show CD69 upregulation **(B)**, but no IL2 secretion **(C)** in response to ultra-low affinity peptides. **(D)** TCR downregulation follows the same hierarchy as T cell activation. The dotted lines indicate the potency thresholds used for the following plots. **(E)** 1G4-transduced (transd.), but not untransduced (UT) T cells respond to high and low affinity NYE peptides. The potency of the T cell response is linearly correlated with the affinity of the pMHC for CD69 upregulation **(F)**, IL2 secretion **(G)**, and TCR downregulation **(H)**.

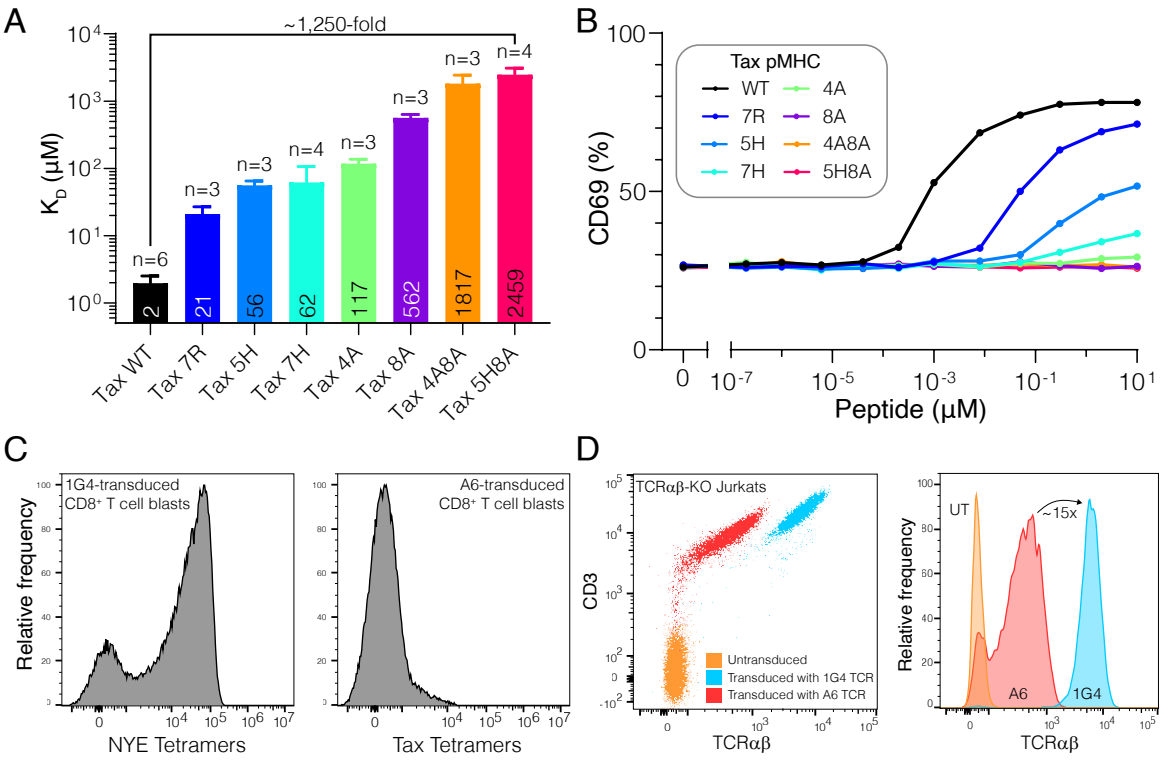


**Figure 4.4: A6-transduced T cells have lower sensitivity due to decreased TCR expression.** A6-transduced T cells were stimulated for 5 h in co-culture with peptide-pulsed U87 cells. **(A)** Selection of Tax peptides spanning a wide affinity range. Shown are the geometric means with geo. SD. **(B)** A6-transduced T cells do not respond to peptides >60 $\mu$M $K_D$. **(C)** Staining of A6-transduced T cells with Tax WT tetramers is much weaker than staining of 1G4-transduced T cells with NYE 9V tetramers, even though the former has a higher affinity. Notably, this is not due to a low transduction efficacy, since a substantial fraction (~30–70 %) of A6-transduced T cells can respond to Tax WT peptide, such as shown in (B). **(D)** Direct comparison of TCR levels when staining with pan-αβTCR antibody in TCR-transduced Jurkat cells that lack endogenous TCR. Indicated is the fold difference in TCRαβ gMFI, when gating on transduced cells (by CD3) and subtracting the untransduced signal (UT).

Since accurate measurement of the discrimination power requires as many data points as possible, I decided to select a peptide panel enriched in higher affinity variants, with the lowest affinity around 60 $\mu$M (Figure 4.5A). T cells stimulated with this panel show a hierarchy very similar to what was seen with 1G4 T cells for a wider panel (Figure 4.5B). As before, when correlating potency and affinity, I find a good correlation in loglog-space (Figure 4.5C). As a measure of sensitivity, I define as $C$ (units of concentrations) the y-intersect of the power function (linear function on loglog plot). This represents the potency of a theoretical peptide with $K_D = 1\,\mu M$ and allows comparison between different conditions. In addition, I define

discrimination power α (dimensionless) as the slope of the linear function (or power of the power function) used to fit the data empirically. As expected, when calculating the sensitivity, I found a >100-fold decrease in sensitivity between the A6 and the 1G4 TCR (Figure 4.5D). Interestingly, the discrimination power is independent of the sensitivity and the specific TCR used (Figure 4.5E).

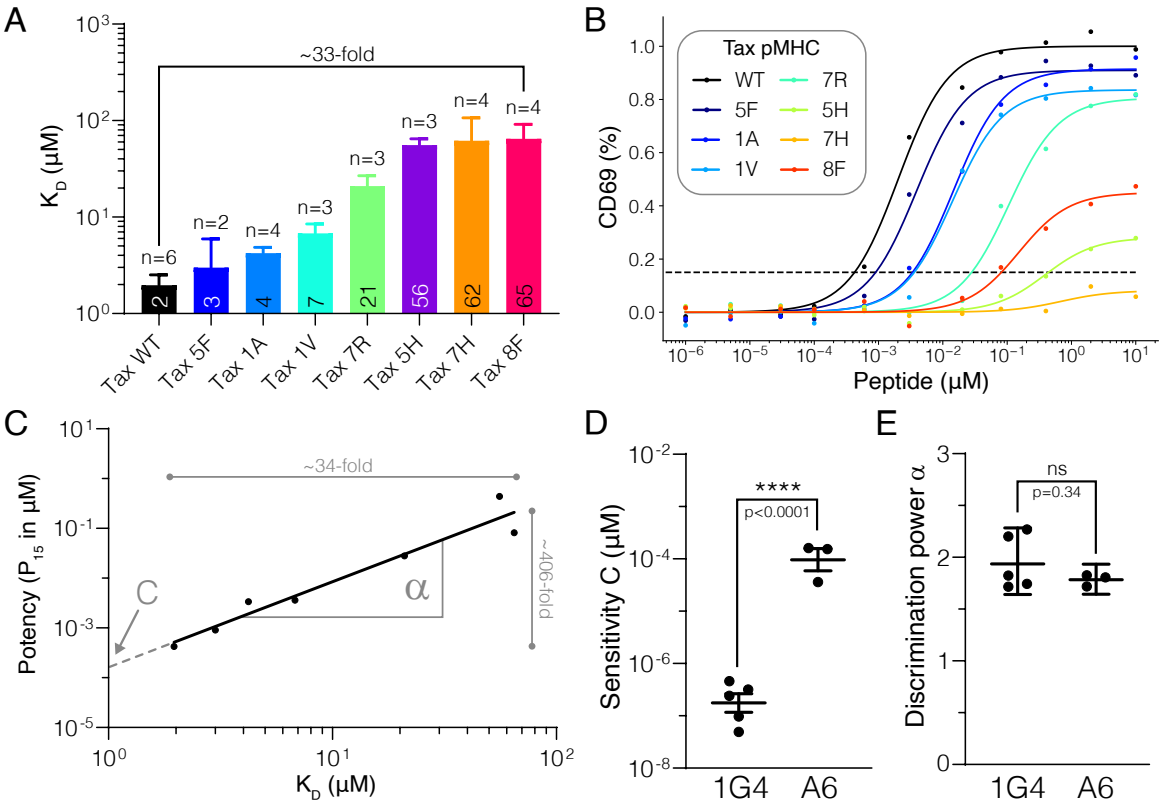


**Figure 4.5: The A6 TCR discriminates with similar accuracy as the 1G4 TCR.**
A6-transduced T cells were stimulated for 5 h in co-culture with peptide-pulsed U87 cells. **(A)** Selection of Tax peptides used for functional antigen discrimination experiments. Shown are the geometric means with geo. SD. **(B)** Example of T cells responding to the A6 peptide panel. The dotted lines indicate the potency thresholds used for the following plot. **(C)** Correlation between potency of CD69 response and TCR/pMHC affinity. Indicated are the sensitivity C and the discrimination power α. The sensitivity is defined as the extrapolated potency to a theoretical 1 mM $K_D$ peptide. The discrimination power (α) corresponds to the slope of the line in loglog space. **(D)** A6-transduced T cells are considerably less sensitive than 1G4-transduced T cells. **(E)** However, their discrimination power is very similar. Shown is the geo. mean with geo. SD for (D) and (E). Geo. mean for α is 1.9 and 1.8 for the 1G4 and A6 TCR, respectively.

### 4.2.3 Factors influencing antigen discrimination

Once I had defined the level of discrimination in a physiological system, I started to investigate what factors might be important to achieve this. I utilized the plate system with immobilized pMHC that I had previously developed to study antigen discrimination in a simplified system, where only the TCR/pMHC interactions are present (see chapter 2.2.2). As before, blasted 1G4-transduced T cells responded to even the lowest affinity pMHC by upregulation of CD69 on the surface (Figure 4.6A) and the potency and affinity correlated well. Notably, the discrimination power was lower when only pMHC was present ($\alpha$=1.1), compared to the co-culture system ($\alpha$=1.9; Figure 4.6D and Figure 4.7B).

Based on my results that the accessory ligands CD58 (ligand to human CD2) and ICAM1 (a ligand to LFA-1) can increase sensitivity dramatically in this system (see chapter 2.2.2), I sought to study their contribution to antigen discrimination. As before, when adding either of these two adhesion ligands, sensitivity to pMHC increased significantly (Figure 4.6A–C and Figure 4.7A). Antigen discrimination was also improved, but did not reach the level seen in the more physiological co-culture system (Figure 4.6E–F and Figure 4.7B). Notably, all but immobilized pMHC alone tested significantly different from the null hypothesis of an occupancy model ($\alpha = 1$).

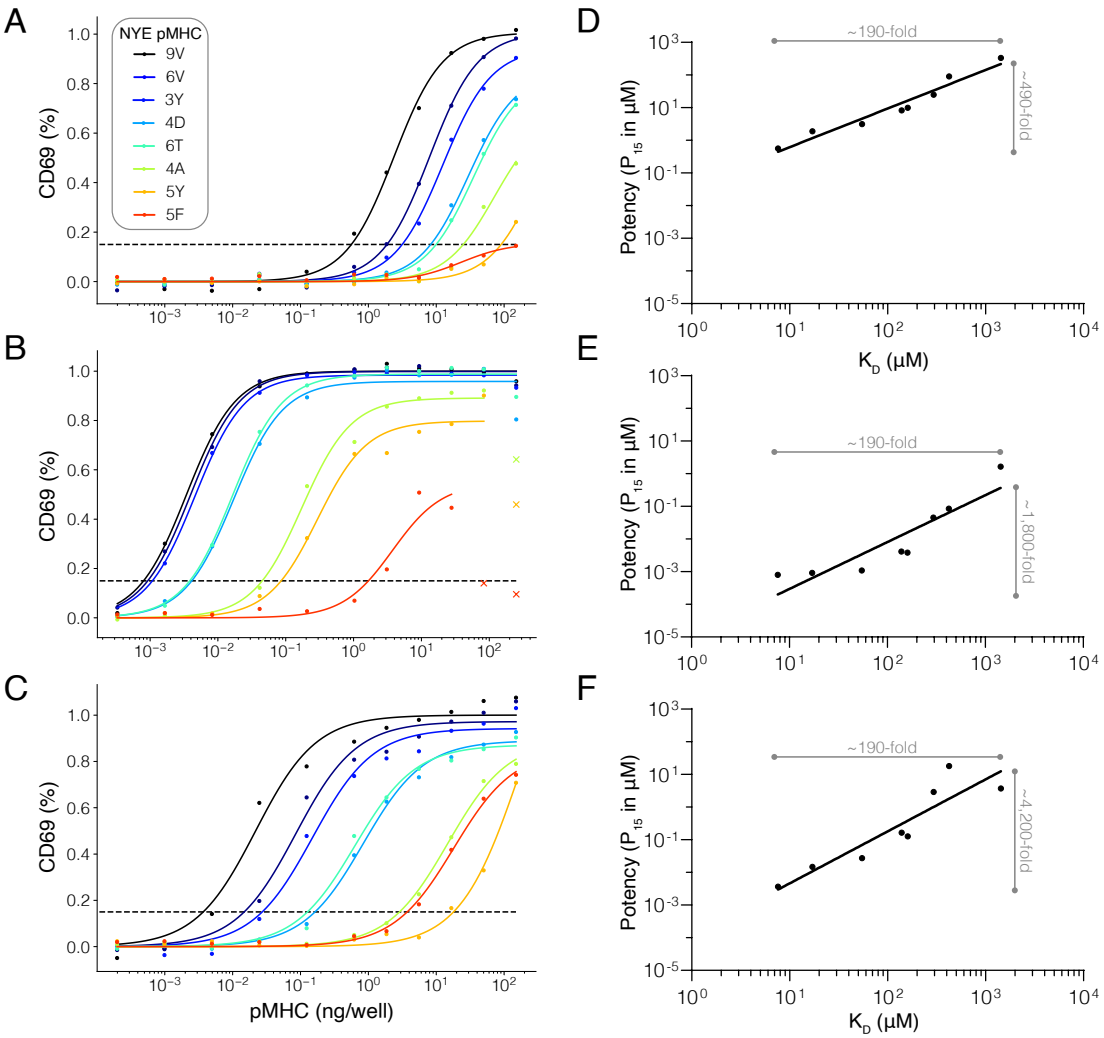


**Figure 4.6: T cells respond to immobilized pMHC in an affinity-dependent manner.**
1G4-transduced T cells were stimulated for 4 h on glass plates with immobilized recombinant ligands. Example of T cells responding to immobilized pMHC alone **(A)**, in the presence of CD58 **(B)**, or in the presence of ICAM1 **(C)**. Potency thresholds are indicated as dotted lines. Correlation of potency with TCR/pMHC affinity for pMHC alone **(D)**, +CD58 **(E)**, or +ICAM1 **(F)**. (A-C) x marks datapoints that were manually excluded as outliers or automatically excluded due to their bell-shape (decrease of activation at very high doses).

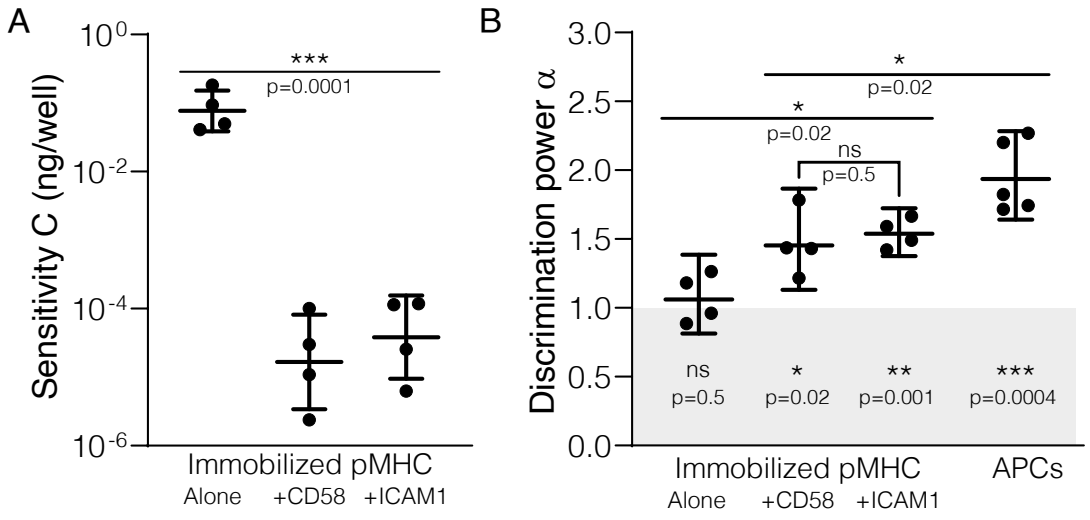


**Figure 4.7: Adhesion ligands improve sensitivity and antigen discrimination.**
**(A)** Sensitivity to pMHC is drastically increased when adding either CD58 or ICAM1. Compared using repeated-measure ANOVA (Geisser-Greenhouse corrected). **(B)** The discrimination power with immobilized pMHC is close to 1 and much lower than in the physiological context of an APC. Addition of CD58 or ICAM1 partially rescues discrimination. Plate data are compared using repeated-measure ANOVA with Sidak's multiple comparison. CD58/ICAM1 condition were compared to APCs using a ordinary 1-way ANOVA. All samples were compared to a discrimination power of 1 (indicated as gray box) using multiple 1-sample t-tests. All tests were performed on log-transformed data.

### 4.2.4 Fitting a kinetic proofreading model

In the previous sections, I chose to fit an empirical model rather than a mechanistic model. Most of the data is fitted well by the empirical model. However, some datasets show saturation at low $K_D$s (e.g. Figure 4.6E). This is observed to some extent for all 1G4 data other than pMHC alone on plates. Such flattening at higher affinities is predicted by kinetic proofreading. I therefore directly fitted the data using a simplified kinetic proofreading model (see Materials & methods for details). Since in kinetic proofreading, potency depends on the lifetime ($\tau = 1/k_{off}$) of the TCR/pMHC interaction and not the affinity, I first estimated off-rates of the 1G4 peptide panel. This is possible since $K_D$ and off-rates are usually closely correlated for peptide variants of a given TCR. I estimated off-rates ($k_{off} = K_D \times k_{on}$) based on previously measured on-rates for the 1G4 TCR at 37°C [78]. As expected, the on-rates reported there do not change strongly for different peptide variants tested (Figure 4.8A). I do not expect this to introduce a significant error. For example, the off-rate previously measured for NYE 9V is 0.33/s [78], whereas I estimated it to be 0.34/s, based on its $K_D$ of 8 $\mu$M and an on-rate of 0.0447 $\mu M^{-1}s^{-1}$. Notably, I did not fit the A6 data with this KP model. First, there is no good estimate of the on-rate at 37°C. Moreover, due to the small difference in $K_D$ in the A6 panel, the A6 data does not include any real saturation, which is required to determine the parameters of a KP model unambiguously.

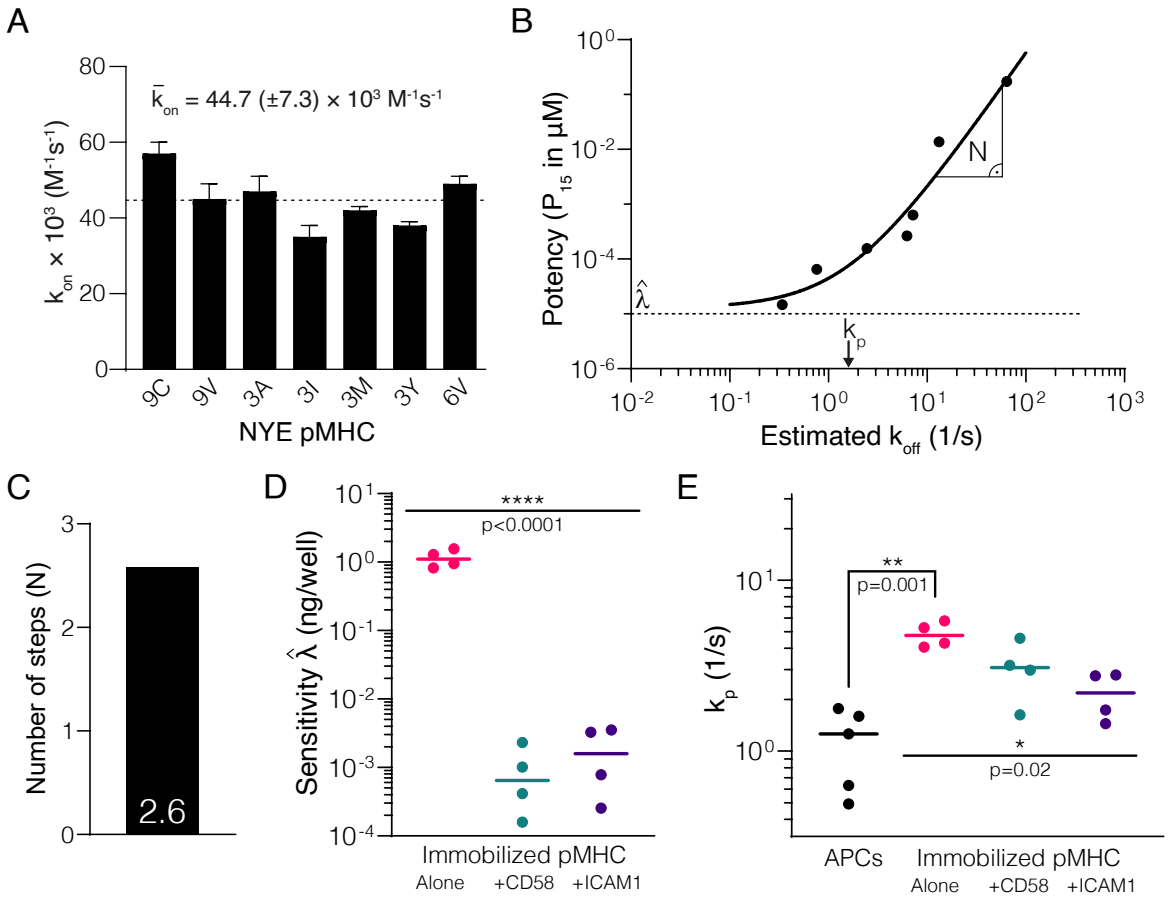


**Figure 4.8: Fitting a kinetic proofreading model to the antigen discrimination data.**
**(A)** On-rates of the 1G4 TCR to different peptide variants, as measured in [78]. Peptides with $K_D$s >50 $\mu$M were excluded, since the kinetics will be more prone to errors. The average on-rate of the 7 peptides shown here was used to estimate the off-rates of the 1G4 peptides in this thesis based on: $k_{off} = k_{on} \times K_D$. **(B)** Example of data fitted with a kinetic proofreading model. Shown are the proofreading rate ($k_p$), the number of steps ($N$), and the sensitivity ($\hat{\lambda}$). **(C)** Result of fitting $N$ globally. No estimate of the variance is available. **(D)** The sensitivity is much higher (i.e. smaller) when CD58 or ICAM1 are added. Since they were generated with different experimental systems, a comparison between APC and plate data would not be sensible. Statistics by a repeated-measure 1-way ANOVA (Geisser-Greenhouse corrected) on log-transformed data. Fold difference of geo. mean to pMHC alone: 1800x (CD58) and 900x (ICAM1). **(E)** If $N$ is fitted globally, the decrease in discrimination power on the plate can be explained by an increase in proofreading rate. This increase is reduced when adding CD58 or ICAM1. APCs and pMHC alone were compared by an unpaired t-test on log-transformed data. Plate data was compared by a repeated-measure 1-way ANOVA (Geisser-Greenhouse corrected) on log-transformed data. Geo. mean of $k_p$: 1.0, 4.8, 2.9, and 2.1 $s^{-1}$ for APCs, pMHC alone, pMHC + CD58, and pMHC + ICAM1, respectively.

The kinetic proofreading model used to fit the data includes 3 parameters: the proofreading rate ($k_p$), the sensitivity ($\hat{\lambda}$), and the number of proofreading steps ($N$). When fitted to the data, N corresponds to the slope of the curve for high off-rates, $k_p$ to the inflection point (Figure 4.8B) and the sensitivity $\hat{\lambda}$ is defined as the potency at saturation. Since the number of proofreading steps is expected to be independent of the condition, I fitted $N$ as a global parameter that is shared for all the 1G4 data. I found the number of proofreading steps to be unexpectedly low with 2.6 steps (Figure 4.8C). As anticipated, the effect of CD58 or ICAM1 on the sensitivity in the empirical model is reproduced by the kinetic proofreading model (Figure 4.8D). Since the APC and plate data were using different measures of dose, I did not attempt to compare the sensitivity between them directly. Lastly, I found the proofreading rate to be 1.0 $s^{-1}$ for the data generated on APCs, corresponding to a proofreading time ($\tau = N/k_p$) of 2.6 s. In this KP model, where $N$ is the same for all conditions, the decrease in discrimination power observed when fitting the empirical model, can be explained by an increase in proofreading rate. This effectively represents moving to the left (i.e. the flatter part) of the curve in Figure 4.8B. Adding CD58 or ICAM1 decreases the proofreading rate, consistent with the results on the discrimination power.

## 4.3 Discussion

Antigen discrimination in T cells is essential for the function of the adaptive immune system. Here I show that antigen discrimination in primary human $CD8^+$ T cells is good, but not as high as previously described in murine systems. In those studies, a 3–10-fold difference in affinity or lifetime resulted in the complete abrogation of the response, when compared to a cognate antigen [30, 31, 33–36]. However, fitting non-saturated data can lead to the introduction of large errors into affinity measurements when using steady-state fitting (as shown in chapter 3). These errors may explain why a complete loss of response was associ-

ated with such a seemingly small difference in binding affinity. Importantly, an analysis from our lab further supports this theory. We determined the discrimination power using the same method described here on previously published data. When analyzing the published original murine data, we found an average discrimination power of ~9, consistent with near-perfect discrimination. However, when reanalyzing some of this published data with independently published, more recent SPR measurements, the discrimination decreased from 'near-perfect' to levels similar to what I found in this work (~2). Moreover, when this analysis is applied to more recent data that was not specifically generated for the purpose of studying antigen discrimination, a power of ~2 is confirmed [4]. The combined evidence of my own data, as well as this meta-analysis, strongly supports the idea that these initial studies overestimated discrimination and the true discrimination power is ~2 for both mouse and human.

Interestingly, I found that T cells can respond to ultra-low affinity peptides (>1 mM $K_D$). However, if this represents a physiological situation is not clear. As a comparison of the A6 and 1G4 impressively illustrates is that sensitivity depends strongly on TCR expression. It would be interesting to directly compare the expression levels of these transgenic TCRs to endogenous ones. When pulsing APCs or immobilizing ligand on plates the dose will be significantly higher than expected during physiological presentation, where each APC presents a large mixture of peptides. For example, the NYE peptide recognized by the 1G4 TCR was found on 10–50 MHC molecules of each cell of a tumor cell line tested that expressed the NY-ESO protein [293]. However, the concentration of self pMHC can be considered as much higher, if the mixture of peptides comprising self pMHC presented on APCs are considered as one entity. Importantly, in my experiments T cells stimulated with ultra low affinity peptides up-regulated CD69, but did not secrete cytokines. Therefore, the activation observed may reflect tonic activation, rather than full-blown activation that would lead to the initiation of an immune response. Such tonic signaling has been shown to be important for T cell maintenance [71].

In my work I am correlating functional T cell responses with binding parameters measured with recombinant proteins in solution (3D $K_D$). However, in the physiological context of the TCR being expressed on a T cell, the receptors and ligands are only mobile in 2D. Consistent with this idea, Huang *et al.* found 2D kinetics, measured directly on the T cell, to be more predictive than 3D kinetics by SPR [88]. However, this conclusion was based on 3D SPR data that likely exhibited protein aggregates. In contrast, another study using a different TCR found both 2D and 3D affinity predicted T cell responses [294]. I showed that the 3D $K_D$ correlates well with functional potency for my data. However, in some experiments, the order of NYE 5Y and 5F for T cell activation and TCR downregulation is reversed. Considering that all peptide loaded similarly, difference in stability seem unlikely to contribute to this phenotype. I measured $K_D$s as a proxy of off-rates and generally this is expected to introduce only a small error [78]. However, if NYE 5Y or 5F were outliers to this trend, differences in on-rate could explain the reversed order. Surprisingly, on plates with pMHC alone, their potency is in line with their $K_D$s. Testing their off-rates directly with a more advanced SPR machine, may reveal why their potency is not perfectly predicted by their $K_D$. Furthermore, I have only tested two TCRs and it is possible that the generally good correlation will not be true for any TCR/pMHC pairs.

More recently, force has been proposed to play a major role for antigen discrimination. By applying force on the TCR/pMHC bond, T cells might enhance the difference in lifetime between ligands [295–297]. This is based on the idea that the bond between the TCR and agonists have an increased lifetime under force (catch bond), while non-agonists show a decreased lifetime under force (slip bond). Such a behavior can also explain T cells that stain with tetramers, but do not respond to the peptide [92]. However, in my data, the potency of ligands correlated well with their 3D affinity, providing no evidence for a role of force. Interestingly, in the plate system, addition of the adhesion ligands CD58 or ICAM1 could partially enhance discrimination. One possible explanation is that these receptors could insulate the TCR from forces. If forces are actually deleterious and not beneficial for discrimination, this could lead to the

observed improvement in presence of the adhesion ligands. It would be interesting if the addition of both CD58 and ICAM1 at the same time would lead to a level of discrimination similar to what I observed in the co-culture system. Furthermore, experiments that aim to directly measure the forces on the TCR/pMHC bond could shed light on this speculative mechanism of force insulation.

In this work, I used T cells blasts to study antigen discrimination. They are produced using a protocol adapted from CAR T cell production [298] and are expected to exhibit an effector/memory T cell phenotype. To ensure that these results are not just limited to blasted T cells, we sought to repeat these experiments in a more physiological setting with professional APCs. We measured antigen discrimination using resting 1G4-electroporated naïve or memory $CD8^+$ T cells that were co-cultured with autologous, peptide-pulsed dendritic cells [4]. Importantly, discrimination was similar between naïve, memory and T cell blasts, with a total average of $\alpha = 2.0$. Given that the structure of the TCR is evolutionarily conserved, it is expected that antigen discrimination would also be conserved in different T cells and species.

When closely inspecting the correlation of $K_D$ with potency, I often found some flattening towards low $K_D$s (see Figure 4.6E for example). This is seen for pMHC + CD58 or +ICAM1 on plates, and also in the co-culture experiments, but it is not clear if there are relevant systematic differences. Such saturation at high affinities is predicted by kinetic proofreading (KP). Previous attempts to explain antigen discrimination by KP for near perfect levels of discrimination failed when using a simple KP model and had to invoke more complicated mechanisms, such as adaptive sorting [258, 259]. However, a recent study could not identify a physiological parameter regime for adaptive sorting that explains discrimination, when they applied realistic restrictions on the limits of the parameters [256]. Due to the limited data and the stringent requirements of near-perfect discrimination, no good estimate for proofreading steps ($N$) and the proofreading rate ($k_p$) existed. When I fitted my data with such a model, rather than the empirical power law model, I could determine the proofreading rate to be 1.0 $s^{-1}$ and the num-

ber of steps 2.6. While I used a simplified model, fitting a full KP model resulted in very similar results with a proofreading rate of 1.3 $s^{-1}$ and a $N$ of 2.7 [4]*. Unlike previous parameter estimates [7], this parameter regime can explain discrimination and ligand sensitivity at the same time [4]. Notably, fitting a KP model is only possible due to the large range in $K_D$s found in the 1G4 panel. Thereby supporting the use of our new SPR-based method to measure ultra-low affinity TCR/pMHC interactions.

In conclusion, I have shown that antigen discrimination is not near-perfect, as previously described, but still above the levels predicted by a pure occupancy model. Furthermore, I was able to directly fit a kinetic proofreading model to the data to determine the proofreading rate and number of steps for a TCR in a physiological system for the first time. Unlike prior work, we employed an improved SPR protocol for reliable measurements of lower affinity pMHC. With this new-found knowledge of discrimination, I hope we will be able to decipher the biological mechanisms that power this remarkable ability to distinguish different antigens. Ultimately, we may apply this to design better artificial antigen receptors like CARs, that avoid some of the side effects, such as cross-reactivity. Moreover, understanding antigen discrimination will further our comprehension of the enigma of TCR signal initiation. The unexpected findings that adhesion interactions improve discrimination may be interpreted as a hint towards a previously unexpected impact of force. Further research will most certainly continue to provide surprising new insights into one of the most sophisticated signaling machineries in biology.

*See Materials & methods for full discussion of the differences in model and data used.

# Chapter 5

# Discussion

Antigen discrimination is a core function of T cells and a key prerequisite for the adaptive immune system. Here I investigated the effect of accessory receptors on T cell activation and quantified antigen discrimination in human $CD8^+$ T cells.

First, I assessed the effects of the accessory receptors CD2 and LFA-1 when interacting with their ligands CD58 and ICAM1, respectively. In line with previous work generated in mice [165, 175, 176, 221–223], I found a dramatic increase in sensitivity in human T cells when either of these adhesion ligands was present. Notably, engagement of these accessory receptors led to an accelerated downregulation of the TCR, indicating that they likely influence the kinetics of TCR/pMHC binding.

Next, we developed a new SPR method to measure affinities that were out of reach for previous assays. Using an antibody to determine the $B_{max}$ independently of reaching saturating concentrations of TCR allowed us to determine for the first time the $K_D$s of TCR/pMHC interactions above 100 $\mu$M $K_D$ reproducibly. We determined the affinities of more than 30 single or double amino acid substitution variants of the cognate peptide NYE 9V and Tax WT, binding the 1G4 and A6 TCR, respectively, with $K_D$s ranging from 2 $\mu$M to about 2 mM.

Lastly, I quantitatively investigated antigen discrimination using the 1G4 and A6 TCRs. Previous work in the 90s and early 2000s produced the notion of near-perfect or absolute discrimination, where very small differences in lifetime or affinity (<10-fold) can convert an agonist into a non-agonist [30, 31, 33–36]. I obtained a very different result here with a larger panel of peptides. Antigen discrimination is good, but below the level previously proposed. Reassuringly, when our laboratory reanalyzed previous data with updated SPR measurements, we found a discriminatory power of ~2, very similar to the results I obtained with the 1G4 and A6 TCR in this thesis [4]. It therefore seems highly likely that previous results came to the wrong conclusion, based on inaccurate SPR measurements.

## 5.1 Antigen discrimination and its implications

My results on antigen discrimination have important implications. First, they put emphasis on mechanisms in the periphery for maintaining tolerance. The negative selection process ensures that no TCR recognizing a self-pMHC expressed during selection will make it into the periphery. However, as a consequence of the lower discrimination, antigens that do not negatively select at a low concentration in the thymus, may still activate T cells in the periphery if presented at a high dose (Figure 5.1). Consistently, the human immune system includes various ways to support peripheral tolerance. For example, regulatory T cells play an important role in maintaining immune tolerance in the periphery and their absence results in severe autoimmunity [299]. Furthermore, the expression of co-stimulatory or co-inhibitory molecules on professional APCs and the secretion of cytokines by APCs and adjacent cells are important to determine if a T cell is activated [300]. Modulating accessory interactions is now one of the most actively researched fields in the battle against cancer and autoimmunity [301].

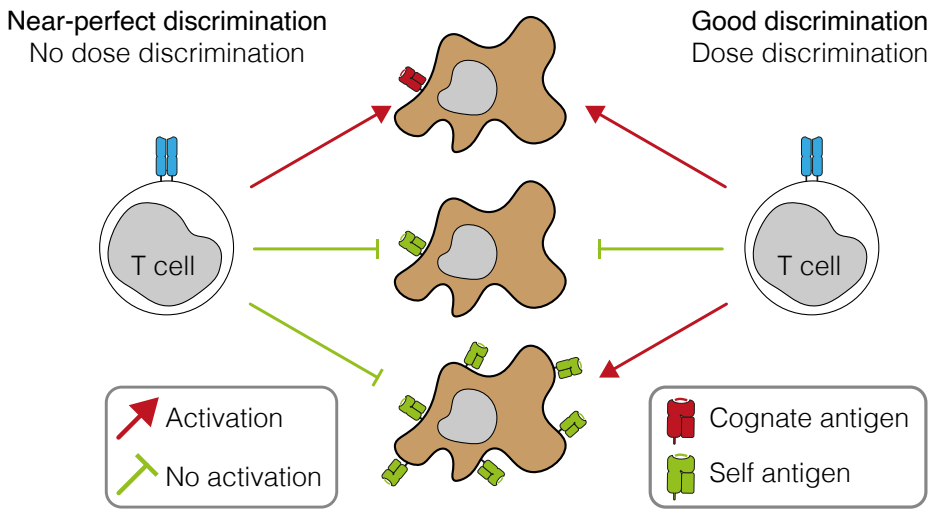


**Figure 5.1: Discrimination based on antigen dose.**
A lower discrimination power renders T cells more sensitive to dose. They may activate to low affinity or self antigens if presented at high doses. The immune system might exploit this sensitivity to dose for the control of its endocrine tissues [302]. In this theory, autoimmunity serves a physiological role to eliminate hyper-secretive clones to avoid the negative effects of hormonal dysregulation.

While a decrease in discriminatory power leads to less sensitivity for the affinity, it also increases the ability of the T cell to sense differences in dose. Generally, this was thought to be counter-productive, since a large quantity of a low affinity peptide may still be able to activate T cells in the periphery (Figure 5.1). However, dose-sensitivity allows T cells to identify cells with differences in expression levels. Recently, it was postulated that such dose-discrimination is important to kill hyper-secretive clones in endocrine tissues, therefore offering a physiological role for auto-reactivity [302]. Furthermore, dose-discrimination may be important to recognize cancer cells that overexpress a wild type protein. My findings are consistent with dose-discrimination, but further research will be required to show that this is actively exploited by T cells *in vivo*.

Lastly, my results support the concept of cross-reactivity (i.e the number of peptides a single TCR can be activated by). The necessity for a single T cell to recognize a large number of antigens has been known for a long time, based on theoretical calculations [303] and experimental work [304]. Cross-reactivity depends both on the discrimination power and the sensitivity and *vice versa* (Figure 5.2). For example, affinity-enhanced TCRs have been shown to be more cross-reactive [305, 306], but this is likely a consequence of increased sensitivity and not decreased discrimination power. Furthermore, the TCRs used in these particular studies included mutations in the CDR2 region and therefore may have an increase affinity to the MHC backbone. Conversely, at the same level of sensitivity, a T cell exhibiting the level of discrimination power described here will be significantly more cross-reactive than one that exhibits near-perfect discrimination. Consequently, the relatively low discrimination power of T cells may have evolved to preserve the cross-reactivity required to give full immune coverage. It would be interesting to conduct theoretical calculations to decide if the antigen discrimination described here is compatible with the physiological requirements. It is possible that species with less physical capacity to hold and maintain naïve T cells (i.e. smaller body size) may have decreased discrimination to boost cross-reactivity and therefore ensure full

immune coverage. However, a control of cross-reactivity by the co-receptor, as proposed previously [120], would offer a simpler solution. In this model, the co-receptor regulates cross-reactivity by changing the sensitivity of the T cell to pMHC without affecting the discrimination power.

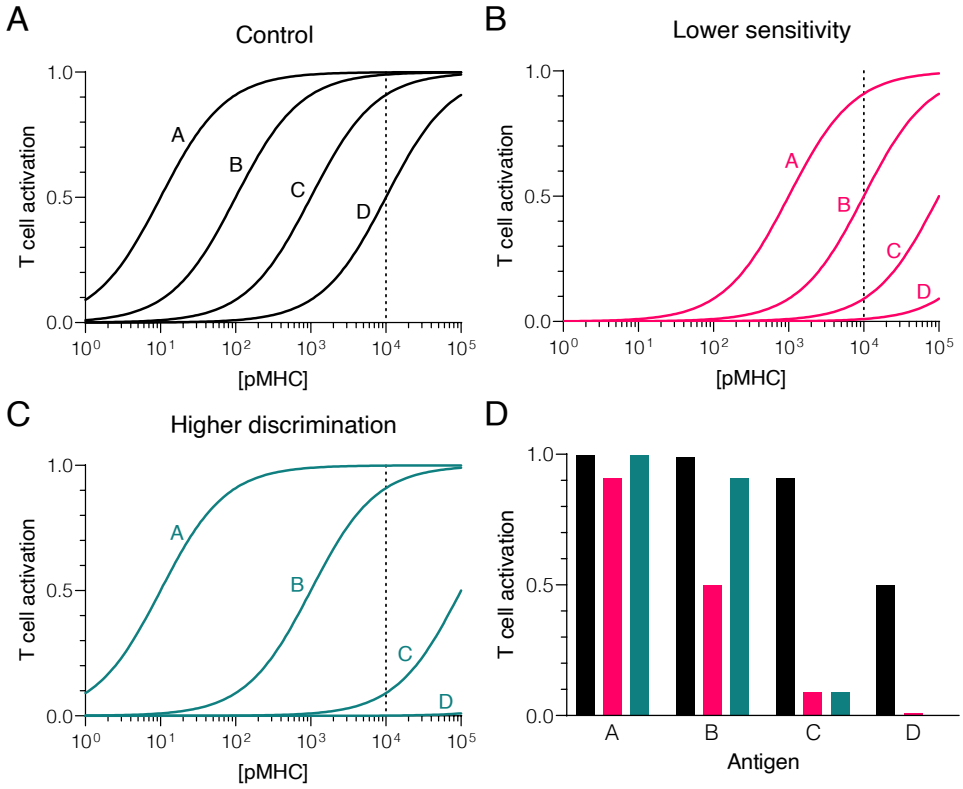


**Figure 5.2: Impact of sensitivity and discrimination on cross-reactivity.**
Cross-reactivity is often measured by counting the number of antigens that T cells with a given TCR respond to. Simulated sigmoidal dose responses for **(A)** low discrimination + high sensitivity, **(B)** low discrimination + low sensitivity, and **(C)** high discrimination + high sensitivity. **(D)** Lowering the sensitivity or increasing the discrimination decreases cross-reactivity. Shown is the activation at a dose of $10^4$ as shown as dotted lines in (A–C).

## 5.2 The affinity floor and its implications

We initially developed a new SPR-based method to allow the generation of a large panel of peptide variants to study antigen discrimination. However, when we measured $K_D$s of many different peptide variants, we were surprised that we did not identify peptides with $K_D$s significantly higher than 2 mM. Using different controls did not change this result, indicating that this is not due to binding to the control protein CD58. Even drastic mutations did not further lower the affinity. For example, a biased peptide library exhibited an affinity close to 2 mM for two TCRs tested. Previously, the contribution of the MHC to the total binding energy of 1G4 TCR was estimated to be around ~40 % [289]. This is somehow lower than our calculation of ~75 % based on the difference in $K_D$s between NYE 9V and the affinity floor, indicating that even at 2 mM $K_D$, TCR/peptide interactions may still contribute to the total binding energy. This possibly is a consequence of positive selection and consistent with the idea, that this minimal affinity may represent the intrinsic affinity of the TCR to MHC of positively selected T cells. It would be interesting to compare the functional phenotype of freshly isolated T cells, with those in culture and stimulated with ultra-low affinity peptides. In my experiments, T cells stimulated with ultra-low affinity peptides expressed CD69, but did not secrete cytokines. However, it should be noted that the peptides I tested were variants of the cognate peptide, and not the more drastic substitutions including cross-reactive peptides, the minimal alanine peptide, or the biased peptide library. Testing these variants directly would shine light on whether similar functional responses can also be caused by non-related peptides.

In the future, it would be interesting to measure the affinity floor of other TCRs and HLA allotypes. Correlating the maximal $K_D$ with a marker of the strength of the signal received during positive selection would provide an interesting insight into the range of affinity thresholds used during positive selection. For example, CD5 is a negative regulator of TCR signaling and its expression levels depend on the strength of the positive selection interactions and interac-

tions with self pMHC in the periphery [307–311]. Furthermore, testing TCRs derived from regulatory T cells would be interesting. Thymic regulatory T cells are thought to be enriched for T cells that respond more strongly to positively selecting ligands, compared to conventional T cells [299]. Consequently, their TCRs may exhibit a higher affinity floor when measured in SPR. Knowing their affinity to self-pMHC might help us to engineered artificial regulatory T cells to treat autoimmune disease.

## 5.3 Implications for TCR triggering

In my experiments, affinity and potency of the T cell response were well correlated. Since the on-rate of the TCRs to peptide variants with one substitution is not expected to change very much [78], this correlation should hold true for off-rate versus potency. Importantly, I did not find strong outliers that would support alternative models, such as conformational change or mechano-sensing by the TCR. Such outliers would be expected if antigen discrimination is not only dependent on the off-rate. However, binding kinetics could be non-linearly changed (i.e. not the same for all peptide variants) in the 2D environment of cellular contact through the effect of force on the TCR/pMHC bonds (also Figure 5.4). For example, Sibener *et al.* found that responses correlated poorly with affinities measured by SPR. This correlation improved dramatically when the off-rates were measured under force [92]. However, the authors failed to exclude peptide stability on the MHC or loading efficiency as a possible cause of a bad correlation. Furthermore, their force assay depends on repetitive testing of the same cells. Specifically, agonists may induce TCR triggering that could influence subsequent probing of the lifetime, for example by clustering of TCR, a classical hallmark of T cell activation [73, 74]. It would be interesting to repeat the experiments described in this thesis with the TCRs and ligands used in their study to understand how such different results emerged.

## 5.4 Kinetic proofreading

My data support the idea of kinetic proofreading (KP). While it has been difficult to explain near-perfect discrimination by kinetic proofreading or its variants, it is possible for the level of discrimination I described here [4]. Notably, KP can explain why some data points diverge from the linear fit I used in my thesis (e.g. Figure 4.6E). At high affinity/long lifetimes, no further increase in potency is possible and therefore the curve flattens (Figure 5.3A). The value it converges to is the maximal sensitivity this T cell can reach. For the first time, we were able to identify parameters for kinetic proofreading by fitting a KP model to the data. From fitting my data, I found the number of steps to be 2.6 and the proofreading rate ($k_p$) to be 1.0 $s^{-1}$. In a more sophisticated analysis with overlapping, but not identical data, we found very similar values, with 2.67 steps and a proofreading rate of 1.3 $s^{-1}$ [4].

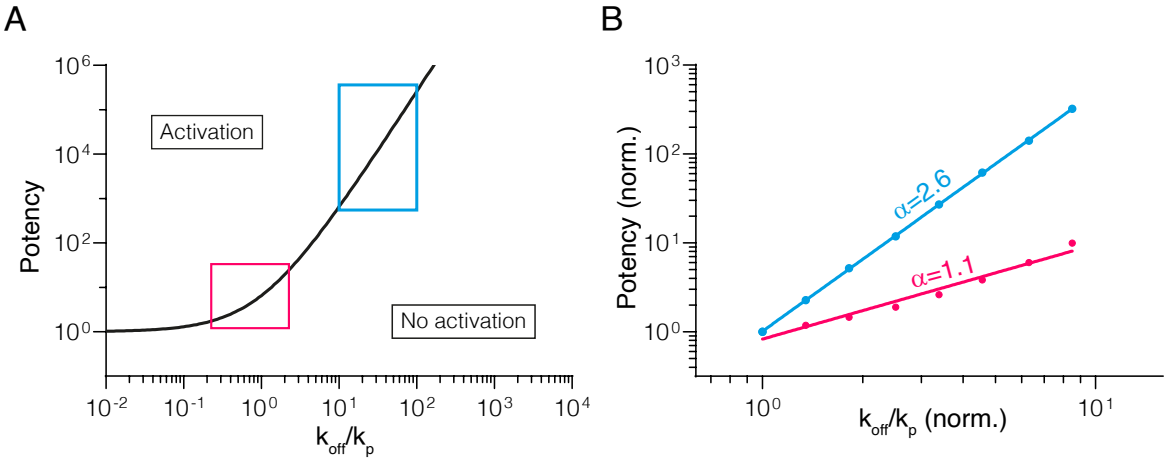


**Figure 5.3: Comparison between the kinetic proofreading and empirical power law models.** **(A)** The number of ligands required to activate a T cell (i.e. potency) as predicted by a kinetic proofreading model with good discrimination ($N = 2.7$). The curve can be shifted to the right by increasing the proofreading rate ($k_p$) and *vice versa*. **(B)** When analyzing the discrimination power by fitting a power law to the data (i.e. a linear fit in loglog space), the results can vary significantly depending on the regime within the KP curve. Data corresponds to boxes shown in (A) and was normalized for both axes to aid visualization. The discrimination power (α) and number of proofreading steps are virtually identical for high $k_{off} : k_p$ ratios (blue), but can be much lower if data is obtained from the saturated part of the curve (red). This might explain the effect of improving discrimination with CD2 and LFA-1, and why CAR T cells exhibit poor discrimination.

Notably, our number of steps is significantly lower than the number of steps required to explain near-perfect discrimination. For example, to reach a specificity* of 99 % for a 2-fold change in lifetime between agonist and non-agonist, one would require a unfeasible 53 proofreading steps and the resulting toll on the sensitivity and/or speed would be dramatic [7]. The lower number of steps in our analysis is consistent with the lower discrimination observed by us. Interestingly, a similar number ($N = 2.7$) was found using an opto-genetic CAR system [312]. This is particularly remarkable, given that there is no co-receptor in the CAR system, a component that has previously been implied to participate in proofreading [116]. Other potential steps include Lck binding, phosphorylation of the ten different CD3 ITAMs, ZAP-70 binding and phosphorylation, and LAT phosphorylation [116, 257]. For the phosphorylation of ITAMs there is evidence that some of these steps occur in parallel, rather than in sequence and therefore may not contribute more than as a single step [313]. This is also consistent with the similar number of steps found in the CAR system, where only six of ten ITAMs are present [312].

In addition to the number of steps, I also estimated the proofreading rate ($k_p = 1.0\,s^{-1}$), and the closely related proofreading time ($\tau_{KP} = N/k_p = 2.6\,s$). This short time is consistent with the high speed of ligand recognition that is required for efficient APC scanning. For example, LAT phosphorylation was reported to occur only 4 s after ligand engagement [25]. A recent study using an opto-genetically activated TCR found a somehow larger proofreading time of around 8 s [314]. However, as Yousefi *et al.* suggest, the lack of co-receptor could be the cause of the longer proofreading time in their work. The estimates provided here for $k_p$ and $N$ will be particularly helpful for the antigen discrimination modeling field. In the future, new modeling studies will not depend on satisfying qualitative requirements of antigen discrimination, but they can rather test their hypotheses and models based on the quantitative data presented here.

*Defined as $truepositive/(truepositive + falsepositive)$.

### 5.4.1 How do CD2 and LFA-1 fit into kinetic proofreading?

In my study, antigen discrimination on plates was severely impaired ($\alpha \approx 1.0$), but partially rescued ($\alpha \approx 1.5$) by the addition of the adhesion ligands CD58 or ICAM1. It seems unlikely that placing T cells on plates or the engagement of adhesion receptors could change the number of proofreading steps. If we define the discrimination power ($\alpha$) as previously in this thesis, then the same KP model can support very different levels of $\alpha$. This is due to the fact that the KP curve flattens at small off-rates (Figure 5.3A). When the discrimination power is measured, unsurprisingly, it is much lower at the left part than the right part of the KP curve (Figure 5.3B). Where the TCR operates on this curve depends on 2 factors: the off-rate ($k_{off}$) and the proofreading rate ($k_p$). One possible explanation is that engagement of CD2 or LFA-1 decreases the proofreading rate, thereby moving into a more favorable regime (i.e. to the right) on the KP curve. Since T cells have evolved in a setting in which cell-cell contact is required, it seems possible that if adhesion is removed, T cells may operate in a sub-optimal regime of their kinetic proofreading signaling machinery.

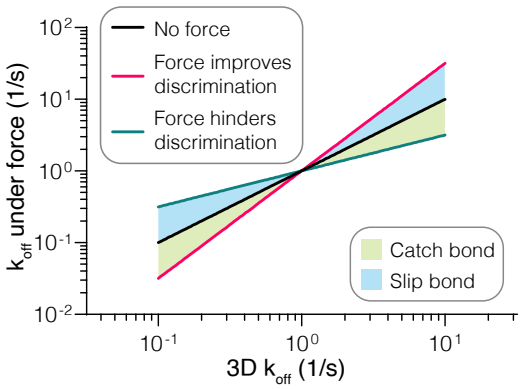


**Figure 5.4: Effect of force on the TCR/pMHC off-rate.**
Currently the effect of force on antigen discrimination is still not fully understood. Assuming a correlation between the sensitivity to force and the 3D off-rate, force can either improve or decrease antigen discrimination. For example, force may strengthen bonds with small off-rates (catch bond), while weaken those with large off-rates (slip bonds). In such a case, antigen discrimination would be improved, since the fold-difference in the off-rates between the antigens when bound to the TCR increases. However, if the opposite relationship is true, antigen discrimination would decrease under force.

An alternative hypothesis is that these adhesion interactions insulate the TCR from forces. If forces, unlike the currently held view in the field [269], decrease the difference in off-rates between ligands (Figure 5.4), insulating from force could improve discrimination without directly changing KP. This would require a non-linear susceptibility of pMHC ligands, wherein the agonists' off-rate becomes larger (i.e their lifetime decreases) under force (slip bond), and the non-agonists' off-rate stays constant or even decreases (catch bond). Finally, adhesion may also influence discrimination purely by changing the effective kinetics. Measurements of 2D kinetics between the TCR and pMHC found both the effective off- and on-rate to be much faster than when measured by SPR in 3D [87]. If it is adhesion that accelerated both*, it could explain improved discrimination based on the same argument as above: moving into a more favorable regime on the KP curve (i.e. to the right on Figure 5.3A). Unlike an effect on $k_p$, however, this mechanism of action would not require changing the rates of the proofreading reactions taking place intracellularly. Rather, this effect can be explained purely by changing the binding of the TCR and does not require any signaling of LFA-1 or CD2. It is easy to imagine how CD2 or LFA-1 increase the effective on-rate by bringing the adjacent membranes close to each other, thereby facilitating TCR/pMHC binding. CD2 can create close contacts perfectly suited to allow binding between the TCR and pMHC [72, 133]. Since LFA-1/ICAM1 is somehow larger [215], it is not expected to create these close contacts directly, but still bring the membrane much closer together than in a thermodynamic equilibrium driven by the repulsive forces of the adjacent glycocalyces (see also Figure 1.2). It is less clear how they would increase the off-rate. Directly measuring the molecular force on the TCR/pMHC bond in the absence or presence of CD2/LFA-1, could reveal the mechanism underlying their effect on discrimination. Very recently, the tools to do so became available, i.e. a force-spring that can be used to measure the force on the TCR/pMHC bond using FRET [315].

*The effect on the on-rate should be larger than on the off-rate to be consistent with the increased sensitivity when CD2 or LFA-1 is engaged.

### 5.4.2 Putting the model back into the cell

The exact biological implementation of proofreading remains unsolved and will require further research to uncover. For example, it would be interesting to repeat these antigen discrimination experiments with MHC that is mutated to abrogate binding to CD8. If antigen discrimination is impaired, this would support a role of co-receptors in the proofreading chain. To assess the influence of intracellular signaling molecules is technically more challenging. One option is to inhibit the kinases and phosphatases involved chemically. However, often this is not particularly specific to one target. Genetic deletions or RNA knock-downs offer a specific alternative, but may allow the T cells to adapt between the targeting and the experiment. An alternative is the use of signaling proteins that are engineered to be specifically inhibited by a chemical compound, such as shown for the inhibitory kinase Csk [316, 317].

Interestingly, neither the estimate produced from analyzing CAR T cells [312] nor our estimate [4] of $N$ is an integer. This is unexpected given the biological limitation of having discrete proofreading steps. One possible explanation is population heterogeneity on a cellular or even molecular level within each cell, causing an apparent fractional number of steps. An alternative hypothesis is the existence of a short circuit in the proofreading chain. For example, a proofreading chain with 3 steps and some short circuiting can lead to our observed fractional number of steps [5]. ZAP-70 binding was shown to have a longer lifetime than normal pMHC ligands and could therefore represent the not easily reversible step causing a fractional $N$ [266–268]. Interestingly, homeostatic contacts between T cells and professional APCs can lead to some phosphorylation of ITAMs and ZAP-70 binding without T cells getting activated [318, 319]. If these constitute KP steps, then partial pre-activation (tonic signaling) may represent a short-cut resulting in a fractional $N$.

## 5.5 Antigen discrimination in non-TCR receptors

In this thesis I focused on antigen discrimination of the TCR. It would be interesting to test this in other immune and non-immune receptors. The most relevant comparison is a family of receptors referred to as non-catalytic tyrosine-phosphorylated receptors (NTRs), which includes the TCR, BCR, and other receptors such as Fc receptors [246]. They share a number of important features, for example, having small extracellular domains and tails with tyrosine motifs, such as ITAMs, and binding anchored (i.e. non-soluble) ligands. Furthermore, their activation is controlled by a balance of kinases such as Lck and phosphatases such as CD45 [246]. Consequently, kinetic proofreading might be a common feature of their signaling. However, it is not clear why cells would utilize an energy-consuming process if good discrimination was not relevant to the receptor's function. For example, Fc receptors need to discriminate between different isotypes of antibodies. However, they probably do not require kinetic proofreading. Instead these receptors more likely co-evolved with their ligands to maximize the difference in affinity between agonistic and non-agonistic ligands. For instance, Fc$\gamma$RI binds $IgG_1$, $IgG_3$, and $IgG_4$ with a high affinity ($K_D \approx 10^{-8} M^{-1}$), but $IgG_2$ with much lower affinity ($K_D$ not measurable) [320]. The BCR may be an exception, in that B cells as part of the adaptive immune system are also required to exhibit antigen discrimination. Notably, B cells have a complex receptor-proximal signaling chain [321], that shares many similarities with the TCR and therefore could also rely on kinetic proofreading. In a meta-analysis from our laboratory on the limited published data available, we found a discrimination power of about 1.3 for the BCR [4]. This is lower than the TCR, but higher than any other receptor investigated. B cells bind previously unknown antigen and in some instances can be activated without T cell help. However, the generation of high affinity antibodies and immunological memory is dependent on interactions with T cells [6]. It therefore seems possible that B cells 'outsourced' the complex task of antigen discrimination to T cells altogether.

### 5.5.1 Antigen discrimination in CAR T cells

Lastly, CARs are an interesting class of receptors to study. Classical CARs are comprised of a single-chain variable fragment derived from an antibody, an extracellular hinge, a transmembrane domain, and an intracellular tail that is usually based on CD3ζ and sometimes CD28 and/or 41BB signaling elements. CARs are larger than TCRs, typically bind with much higher affinities, and their sensitivity seems to be lower by around 1000-fold [267]. In the meta-analysis from our lab, they showed a discrimination power of 0.9 and were therefore significantly worse than TCRs in antigen discrimination [4]. However, Tischer *et al.* found the number of proofreading steps (i.e. 2.7) using a system based on CARs [312] to be similar to the number I measured for the TCR. It is therefore possible that CARs are generally capable of good discrimination, but when using high affinity/low off-rates scFvs they operate in a saturating parameter regime of kinetic proofreading (i.e. left side of the curve in Figure 5.3A; red in B). Consequently, affinity-enhanced TCRs may also exhibit lower discrimination. Further research directly comparing TCRs, affinity-enhanced TCRs, CARs, and BCRs will be required to untangle the specific components and cellular requirements of discrimination.

## 5.6 Conclusion

Here I studied the effect of the accessory receptors CD2 and LFA-1 on T cell activation. We also developed a new SPR protocol to measure very low affinity TCR/pMHC interactions that allowed me to study the response of T cells to very low affinity antigens and their discriminatory power. Unlike previous work, I found antigen discrimination to be good, but not near-perfect. In the future, it would be interesting to replicate these results in $CD4^+$ T cells and potentially species other than human. Considering this is such an important process, I would expect antigen discrimination to be conserved. However, it might be possible that there are small differences. For example, regulatory T cells may be less discriminatory, since at least some of them exhibit stronger binding to MHC in the thymus. Future research will shed light on the complicated signaling machinery that drives antigen discrimination by T cells. We should strive to learn as much as we can from T cell receptors and incorporate this knowledge into the next generation of therapeutics. Very recently, for example, a CAR based on a TCR scaffold was shown to outperform a traditional CAR [322].

# Chapter 6

# Materials & methods

## 6.1 Reagents

**Table 6.1: Antibodies for flow cytometry.**
RRIDs can be found on Resource Identification Portal. For flow cytometry, all antibodies were used at a dilution of 1:200 if not indicated otherwise.

| Target | Clone | Conjugation | Supplier | RRID |
|---|---|---|---|---|
| CD69 | FN50 | AF488<br>BV421<br>AF647 | Biolegend | RRID:AB_528869<br>RRID:AB_2561909<br>RRID:AB_528871 |
| 41BB | 4B4-1 | PerCP-Cy5<br>AF647 | Biolegend | RRID:AB_2205686<br>RRID:AB_2566258 |
| CD45 | HI30 | BV421<br>BV510<br>BV711<br>AF647 | Biolegend | RRID:AB_2561357<br>RRID:AB_2561940<br>RRID:AB_2563466<br>RRID:AB_389336 |
| HLA-A2 | BB7.2 | BV421<br>PE | Biolegend | RRID AB_2721523<br>RRID AB_1877227 |
| CD2 | TS1/8 | BV421 | Biolegend | RRID:AB_2561832 |
| CD2 | RPA-2.10 | BUV395 | BD Biosciences | RRID:AB_2744356 |
| CD2 | RPA-2.10 | BV605<br>APC | Biolegend | RRID:AB_2687243<br>RRID:AB_10895925 |
| ICAM1 | HCD54 | PE | Biolegend | RRID:AB_535979 |
| CD80 | 2D10 | BV421 | Biolegend | RRID:AB_10899567 |
| CD86 | BU63 | BV421 | Biolegend | RRID:AB_2728393 |
| Isotype Ctrl | MOPC-21 | BV421<br>PE | Biolegend | RRID:AB_11150232<br>RRID:AB_326435 |
| Isotype Ctrl | MOPC-173 | APC | Biolegend | RRID:AB_326468 |
| CD3 | UCHT1 | APC | Biolegend | RRID:AB_314066 |
| CD3 | OKT3 | AF488 | Biolegend | RRID:AB_571877 |
| TCR$\alpha\beta$ | IP26 | PE | Biolegend | RRID:AB_314646 |
| CD8 | HIT8a | PE | Biolegend | RRID:AB_314112 |

**Table 6.2: Unconjugated antibodies.**
RRIDs can be found on Resource Identification Portal.

| Target | Clone | Supplier | RRID | Notes |
|---|---|---|---|---|
| HLA-A/B/C | W6/32 | Biolegend | RRID:AB_314871 | Lot: B233942 |
| CD58 | TS2/9 | Biolegend | RRID:AB_2075983 | For blocking experiments. Azide- and endotoxin-free. |
| ICAM1 | HA58 | Thermo Fisher Scientific | RRID:AB_467304 | For blocking experiments. |
| ICAM1 | 15.2 | Thermo Fisher Scientific | RRID:AB_929068 | For blocking experiments. |
| Isotype Ctrl | MOPC-21 | Biolegend | RRID:AB_2890215 | Ctrl for blocking experiments. Azide- and endotoxin-free. |

**Table 6.3: Cell lines.**
RRIDs can be found on Resource Identification Portal.

| Name | Source | RRID | Notes |
|---|---|---|---|
| HEK293T | Previously obtained | N/A | Identity was not verified. |
| Lenti-X 293T | Takara Bio | RRID:CVCL_4401 | For production of lentivirus. |
| Freestyle 293F | Nicole Zitzmann University of Oxford | RRID:CVCL_D603 | For protein production. |
| CHO-A2 | Jesús Siller Farfán | N/A | CHO K1 cells transduced with lentivirus encoding HLA-A2 single chain dimer. |
| CHO-A2 CD58 | Jesús Siller Farfán | N/A | CHO-A2 cells transduced with lentivirus encoding CD58-FLAG. Sorted to have a similar expression of HLA-A2. |
| U87 | Vincenzo Cerundolo University of Oxford | RRID:CVCL_0022 | Identity was not verified. |
| U87 CD58 KO | This thesis | N/A | CRISPR KO with CD58 G1 of parental U87. FAC sorted. |
| U87 ICAM1 KO | This thesis | N/A | CRISPR KO with ICAM1 G2 of parental U87. FAC sorted. |
| U87 Double KO | This thesis | N/A | CRISPR KO with ICAM1 G2 of U87 CD58 KO. FAC sorted. |
| Jurkat TCR$\alpha\beta$-KO | Edward Jenkins | N/A | |
| CHO ecdCD58 | Simon Davis University of Oxford | N/A | Express soluble CD58 (secretion signal + amino acids 29–213 + BirA biotinylation site). |
| CHO ecdCD86 | Simon Davis University of Oxford | N/A | Express soluble CD86 (secretion signal + amino acids 18–232 + BirA biotinylation site). |
| T2 | Jesús Siller Farfán | RRID:CVCL_2211 | Identity was not verified. |

**Table 6.4: Plasmids.**
RRIDs can be found on Resource Identification Portal. N/A: not applicable.

| Name | Source | Notes |
|---|---|---|
| pTT3-ecdCD58 | This thesis | Plasmid for production of recombinant, soluble CD58 through transient transfection of mammalian cells. See sequence 10. |
| pTT3-ecdCD86 | This thesis | Plasmid for production of recombinant, soluble CD86 through transient transfection of mammalian cells. See sequence 11. |
| pTT3-ecdICAM1 | This thesis | Plasmid for production of recombinant, soluble ICAM1 through transient transfection of mammalian cells. See sequence 12. |
| pTT3-BirA-FLAG | Addgene | Plasmid for in-flask biotinylation by co-transfection. See also [323]. RRID:Addgene_64395. |
| pET-sA6α | This thesis | For production of soluble A6 α chain in *E. coli.* and *in vitro* refolding. See sequence 3. |
| pET-sA6β-His | This thesis | For production of soluble A6 β chain in *E. coli.* and *in vitro* refolding. See sequence 4. |
| pET-HLA-A2-AT | This thesis | For production of soluble HLA-A*02:01 heavy chain in *E. coli.* and *in vitro* refolding. See sequence 1. |
| β2M plasmid | Previously obtained | β-2 microglobulin for production in *E. coli.* and *in vitro* refolding. See sequence 2. |
| pLEX-A6 | This thesis | pLEX307-based transfer plasmid for lentivirus production encoding the full-length A6 TCR. See sequence 9. |
| pHR-1G4 | Previously obtained | Transfer plasmid for lentivirus production encoding the full-length 1G4 TCR. See sequence 7. |
| pHR-1G4hi | Previously obtained | Transfer plasmid for lentivirus production encoding the full-length, affinity-enhanced 1G4 TCR. See sequence 8. |

**Table 6.5: General reagents.**
N/A: not applicable.

| Name | Supplier | Catalog number |
|---|---|---|
| Retronectin | Takara Bio | T100B |
| Streptavidin-PE | Biolegend | 405245 |
| Biotinylated BSA | Thermo Fisher Scientific | 29130 |
| Streptavidin | Thermo Fisher Scientific | 434301 |
| IL2 | PeproTech | 200-02 |
| RosetteSep Human $CD8^+$ T Cell Enrichment Cocktail | Stemcell Technologies | 15063 |
| Fixable Viability Dye eFluor 780 | Thermo Fisher Scientific | 65-0865-14 |
| Zombie Fixable UV viability kit | Biolegend | 423107 |
| Zombie Fixable NIR viability kit | Biolegend | 423105 |
| 96 well streptavidin Coated High Capacity Plates | Thermo Fisher Scientific | 15500 |
| 96 Well SensoPlate | Greiner | 655892 |
| CM5 sensor chips | GE Healthcare Life Sciences | N/A |
| Amine coupling kit | GE Healthcare Life Sciences | BR100050 |
| CD3/CD28 Human T-activator dynabeads | Thermo Fisher Scientific | 11132D |
| X-tremeGENE 9 | Sigma-Aldrich | 6365809001 |
| X-tremeGENE HP | Sigma-Aldrich | 6366546001 |
| IL-2 Human Uncoated ELISA Kit | Thermo Fisher Scientific | 88-7025-77 |
| TNF Human Uncoated ELISA Kit | Thermo Fisher Scientific | 88-7346-77 |
| LDH Cytotoxicity Assay Kit | Thermo Fisher Scientific | 88954 |
| Lipofectamine CRISPRMAX Cas9 Transfection Reagent | Thermo Fisher Scientific | CMAX00001 |
| TrueCut Cas9 Protein v2 | Thermo Fisher Scientific | A36497 |
| tracrRNA | Thermo Fisher Scientific | A35506 |
| BirA biotin-protein ligase bulk reaction kit | Avidity | N/A |
| Nunc MaxiSorp 96-well plates | Thermo Fisher Scientific | 442404 |
| GSEM supp | Sigma-Aldrich | G9785 |
| Biotin | Avidity | N/A |
| Methionine Sulfoximine (MSX) | Previously obtained | N/A |
| Accutase | Biolegend | 423201 |
| Goat anti-mouse 680RD | LI-COR Biosciences | 926-68070 |
| Streptavidin 800CW | LI-COR Biosciences | 926-32230 |

**Table 6.6: Cell culture media & buffers.**

| Name | Content |
|---|---|
| Complete RPMI | RPMI<br>10 % FCS<br>1 % Penicillin/Streptomycin |
| Complete DMEM | DMEM<br>10 % FCS<br>1 % Penicillin/Streptomycin |
| Complete OptiMEM | OptiMEM<br>5 % FCS<br>1 % Penicillin/Streptomycin |
| HBS-EP | pH 7.4<br>0.01 M HEPES<br>0.15 M NaCl<br>3 mM EDTA<br>0.005 % v/v Tween20 |
| CHO selection medium | DMEM<br>10 % dialysed FCS<br>1X GSEM supplement<br>20–50 $\mu$M MSX<br>1 % Penicillin/Streptomycin |
| CHO production medium | DMEM<br>2–5 % FCS<br>1X GSEM supplement<br>20 $\mu$M MSX<br>2 mM sodium butyrate<br>1 % Penicillin/Streptomycin |
| 5X annealing buffer | pH 7.4 with KOH<br>Nuclease-free water<br>30 mM HEPES<br>100 mM Potassium acetate<br>2 mM Magnesium acetate |

**Table 6.7: Instruments and equipment.**

| Name | Company |
|---|---|
| Biacore T200 SPR machine | GE Healthcare |
| ÄKTA pure FPLC | GE Healthcare |
| Superdex 75 column | GE Healthcare |
| Superdex 200 column | GE Healthcare |
| X-20 flow cytometer | BD Biosciences |
| CytoFlex flow cytometer | Beckman Coulter |
| Odyssey Sa Imager | LI-COR Biosciences |

**Table 6.8: Software and packages.**

| Name | Version | Company |
|---|---|---|
| FlowJo | v10 | BD Biosciences |
| GraphPad Prism | v7–9 | GraphPad Software |
| BIAevaluation | v4.1 | GE Healthcare |
| Python | v3.7–3.9 | N/A |
| lmfit | v0.9.13 | N/A |

## 6.2 Sequences

**Sequence 1:** Soluble HLA-A2 heavy chain with AviTag for expression in *E. coli*.
Sequence of heavy chain: GenBank: AAA98727.1 (amino acids 25–298).

```
MGSHSMRYFF TSVSRPGRGE PRFIAVGYVD DTQFVRFDSD AASQRMEPRA PWIEQEGPEY
WDGETRKVKA HSQTHRVDLG TLRGYYNQSE AGSHTVQRMY GCDVGSDWRF LRGYHQYAYD
GKDYIALKED LRSWTAADMA AQTTKHKWEA AHVAEQLRAY LEGTCVEWLR RYLENGKETL
QRTDAPKTHM THHAVSDHEA TLRCWALSFY PAEITLTWQR DGEDQTQDTE LVETRPAGDG
TFQKWAAVVV PSGQEQRYTC HVQHEGLPKP LTLRWEPGSG GGLNDIFEAQ KIEWHE*
```

**Sequence 2:** β2M for expression in *E. coli*.

```
>sp|P61769|21--119
MIQRTPKIQV YSRHPAENGK SNFLNCYVSG FHPSDIEVDL LKNGERIEKV EHSDLSFSKDW
SFYLLYYTEF TPTEKDEYAC RVNHVTLSQP KIVKWDRDM*
```

**Sequence 3:** Soluble A6 α chain for expression in *E. coli*.
An additional cysteine was introduced (TRAC T48C) to improve the stability of the protein.

```
MQKEVEQNSG PLSVPEGAIA SLNCTYSDRG SQSFFWYRQY SGKSPELIMS IYSNGDKEDG
RFTAQLNKAS QYVSLLIRDS QPSDSATYLC AVTTDSWGKL QFGAGTQVVV TPDIQNPDPA
VYQLRDSKSS DKSVCLFTDF DSQTNVSQSK DSDVYITDKC VLDMRSMDFK SNSAVAWSNK
SDFACANAFN NSIIPEDTFF PSPESS*
```

**Sequence 4:** Soluble A6 β chain with His-tag for expression in *E. coli*.
An additional cysteine was introduced (TRBC2 S57C) to improve the stability of the protein.

```
MNAGVTQTPK FQVLKTGQSM TLQCAQDMNH EYMSWYRQDP GMGLRLIHYS VGAGITDQGE
VPNGYNVSRS TTEDFPLRLL SAAPSQTSVY FCASRPGLAG GRPEQYFGPG TRLTVTEDLK
NVFPPEVAVF EPSEAEISHT QKATLVCLAT GFYPDHVELS WWVNGKEVHS GVCTDPQPLK
EQPALNDSRY ALSSRLRVSA TFWQDPRNHF RCQVQFYGLS ENDEWTQDRA KPVTQIVSAE
AWGRADHHHH HH*
```

**Sequence 5:** Soluble 1G4 α chain with His-tag for expression in *E. coli*.
No egineered cysteines. Not sequence verified.

```
MQEVTQIPAA LSVPEGENLV LNCSFTDSAI YNLQWFRQDP GKGLTSLLLI QSSQREQTSG
RLNASLDKSS GRSTLYIAAS QPGDSATYLC AVRPTSGGSY IPTFGRGTSL IVHPYIQNPD
PAVYQLRDSK SSDKSVCLFT DFDSQTNVSQ SKDSDVYITD KTVLDMRSMD FKSNSAVAWS
NKSDFACANA FNNSIIPEDT FFPSPENDGG GCKLEHHHHH H
```

**Sequence 6:** Soluble 1G4 β chain for expression in *E. coli*.
No egineered cysteines. Not sequence verified.

```
MGVTQTPKFQ VLKTGQSMTL QCAQDMNHEY MSWYRQDPGM GLRLIHYSVG AGITDQGEVP
NGYNVSRSTT EDFPLRLLSA APSQTSVYFC ASSYVGNTGE LFFGEGSRLT VLEDLKNVFP
PEVAVFEPSE AEISHTQKAT LVCLATGFYP DHVELSWWVN GKEVHSGVST DPQPLKEQPA
LNDSRYCLSS RLRVSATFWQ NPRNHFRCQV QFYGLSENDE WTQDRAKPVT QIVSAEAWGR
AD*
```

**Sequence 7:** Insert of pHR-1G4 lentiviral transfer plasmid.
Contains 1G4 α-linker-P2A-β. No cysteines were removed or introduced.

```
METLLGLLIL WLQLQWVSSK QEVTQIPAAL SVPEGENLVL NCSFTDSAIY NLQWFRQDPG
KGLTSLLLIQ SSQREQTSGR LNASLDKSSG RSTLYIAASQ PGDSATYLCA VRPTSGGSYI
PTFGRGTSLI VHPYIQNPDP AVYQLRDSKS SDKSVCLFTD FDSQTNVSQS KDSDVYITDK
TVLDMRSMDF KSNSAVAWSN KSDFACANAF NNSIIPEDTF FPSPESSCDV KLVEKSFETD
TNLNFQNLSV IGFRILLLKV AGFNLLMTLR LWSSGSRAKR SGSGATNFSL LKQAGDVEEN
PGPRMSIGLL CCAALSLLWA GPVNAGVTQT PKFQVLKTGQ SMTLQCAQDM NHEYMSWYRQ
DPGMGLRLIH YSVGAGITDQ GEVPNGYNVS RSTTEDFPLR LLSAAPSQTS VYFCASSYVG
NTGELFFGEG SRLTVLEDLK NVFPPEVAVF EPSEAEISHT QKATLVCLAT GFYPDHVELS
WWVNGKEVHS GVSTDPQPLK EQPALNDSRY CLSSRLRVSA TFWQNPRNHF RCQVQFYGLS
ENDEWTQDRA KPVTQIVSAE AWGRADCGFT SESYQQGVLS ATILYEILLG KATLYAVLVS
ALVLMAMVKR KDSRG*
```

**Sequence 8:** Insert of pHR-1G4hi lentiviral transfer plasmid.
Contains affinity enhanced c61c58 1G4 β-linker-P2A-α. No cysteines were removed or introduced.

```
MACGSATMSI GLLCCAALSL LWAGPVNAGV TQTPKFQVLK TGQSMTLQCA QDMNHEYMSW
YRQDPGMGLR LIHYSVAIQT TDRGEVPNGY NVSRSTIEDF PLRLLSAAPS QTSVYFCASS
YLGNTGELFF GEGSRLTVLE DLKNVFPPEV AVFEPSEAEI SHTQKATLVC LATGFYPDHV
ELSWWVNGKE VHSGVSTDPQ PLKEQPALND SRYCLSSRLR VSATFWQNPR NHFRCQVQFY
GLSENDEWTQ DRAKPVTQIV SAEAWGRADC GFTSESYQQG VLSATILYEI LLGKATLYAV
LVSALVLMAM VKRKDFSRGA AAGPSGPDPA TNFSLLKQAG DVEENPGPME TLLGLLILWL
QLQWVSSKQE VTQIPAALSV PEGENLVLNC SFTDSAIYNL QWFRQDPGKG LTSLLLITPW
QREQTSGRLN ASLDKSSGRS TLYIAASQPG DSATYLCAVR PLLDGTYIPT FGRGTSLIVH
PYIQNPDPAV YQLRDSKSSD KSVCLFTDFD SQTNVSQSKD SDVYITDKTV LDMRSMDFKS
NSAVAWSNKS DFACANAFNN SIIPEDTFFP SPESSCDVKL VEKSFETDTN LNFQNLSVIG
FRILLLKVAG FNLLMTLRLW SS*
```

**Sequence 9:** Insert of pLEX-A6 lentiviral transfer plasmid.
Contains A6 β-P2A-α. Two native cysteines (TRAC C95S and TRBC2 C131C) were removed and 2 additional cysteines introduced (TRAC T48C and TRBC2 S57C). This engineered cysteine was shown to reduce mispairing with endogenous TCR [324]. TRBC2 contains also a N89D mutation and a second, but unnecessary methionine at the beginning of the β leader sequence.

```
MSIGLLCCAA LSLLWAGPVN AGVTQTPKFQ VLKTGQSMTL QCAQDMNHEY MSWYRQDPGM
GLRLIHYSVG AGITDQGEVP NGYNVSRSTT EDFPLRLLSA APSQTSVYFC ASRPGLAGGR
PEQYFGPGTR LTVTEDLKNV FPPEVAVFEP SEAEISHTQK ATLVCLATGF YPDHVELSWW
VNGKEVHSGV CTDPQPLKEQ PALNDSRYCL SSRLRVSATF WQDPRNHFRC QVQFYGLSEN
DEWTQDRAKP VTQIVSAEAW GRADSGFTSE SYQQGVLSAT ILYEILLGKA TLYAVLVSAL
VLMAMVKRKD SRGATNFSLL KQAGDVEENP GPMMKSLRVL LVILWLQLSW VWSQQKEVEQ
NSGPLSVPEG AIASLNCTYS DRGSQSFFWY RQYSGKSPEL IMSIYSNGDK EDGRFTAQLN
KASQYVSLLI RDSQPSDSAT YLCAVTTDSW GKLQFGAGTQ VVVTPDIQNP DPAVYQLRDS
KSSDKSVCLF TDFDSQTNVS QSKDSDVYIT DKCVLDMRSM DFKSNSAVAW SNKSDFACAN
AFNNSIIPED TFFPSPESSS DVKLVEKSFE TDTNLNFQNL SVIGFRILLL KVAGFNLLMT
LRLWSS*
```

**Sequence 10:** Soluble CD58 for expression in mammalian cells.
Contains chicken RPTPσ signal peptide-CD58 ECD-AviTag-His.

```
MGILPSPGMP ALLSLVSLLS VLLMGCVAET GFSQQIYGVV YGNVTFHVPS NVPLKEVLWK
KQKDKVAELE NSEFRAFSSF KNRVYLDTVS GSLTIYNLTS SDEDEYEMES PNITDTMKFF
LYVLESLPSP TLTCALTNGS IEVQCMIPEH YNSHRGLIMY SWDCPMEQCK RNSTSIYFKM
ENDLPQKIQC TLSNPLFNTT SSIILTTGLN DIFEAQKIEW HEHHHHHH*
```

**Sequence 11:** Soluble CD86 for expression in mammalian cells.
Contains chicken RPTPσ signal peptide-CD86 isoform 2 ECD-AviTag-His.

```
MGILPSPGMP ALLSLVSLLS VLLMGCVAET GAPLKIQAYF NETADLPCQF ANSQNQSLSE
LVVFWQDQEN LVLNEVYLGK EKFDSVHSKY MGRTSFDSDS WTLRLHNLQI KDKGLYQCII
HHKKPTGMIR IHQMNSELSV LANFSQPEIV PISNITENVY INLTCSSIHG YPEPKKMSVL
LRTKNSTIEY DGIMQKSQDN VTELYDVSIS LSVSFPDVTS NMTIFCILET DKTRLLSSPF
SIELEDGLND IFEAQKIEWH EHHHHHH*
```

**Sequence 12:** Soluble ICAM1 for expression in mammalian cells.
Contains chicken RPTP$\sigma$ signal peptide-ICAM1 ECD-AviTag-His.

```
MGILPSPGMP ALLSLVSLLS VLLMGCVAET GQTSVSPSKV ILPRGGSVLV TCSTSCDQPK
LLGIETPLPK KELLLPGNNR KVYELSNVQE DSQPMCYSNC PDGQSTAKTF LTVYWTPERV
ELAPLPSWQP VGKNLTLRCQ VEGGAPRANL TVVLLRGEKE LKREPAVGEP AEVTTTVLVR
RDHHGANFSC RTELDLRPQG LELFENTSAP YQLQTFVLPA TPPQLVSPRV LEVDTQGTVV
CSLDRLFPVS EAQVHLALGD QRLNPTVTYG NDSFSAKASV SVTAEDEGTQ RLTCAVILGN
QSQETLQTVT IYSFPAPNVI LTKPEVSEGT EVTVKCEAHP RAKVTLNGVP AQPLGPRAQL
LLKATPEDNG RSFSCSATLE VAGQLIHKNQ TRELRVLYGP RLDERDCPGN WTWPENSQQT
PMCQAWGNPL PELKCLKDGT FPLPIGESVT VTRDLEGTYL CRARSTQGEV TREVTVNVLS
PRYEGLNDIF EAQKIEWHEH HHHHH*
```

**Sequence 13:** RNA guides for KO of human CD58.

```
>Guide 1|CRISPR758411_CR
GUCAAUGCACAAGUUAGUGU

>Guide 2|CRISPR758416_CR
UUCCAUAGGACCUCUUUUAA

>Guide 3|CRISPR758434_CR
GUUUAUUUAGACACUGUGUC
```

**Sequence 14:** RNA guides for KO of human ICAM1.

```
>Guide 1|CRISPR845341_CR
GGUCUCUAUGCCCAACAACU

>Guide 2|CRISPR845351_CR
GCUAUUCAAACUGCCCUGAU

>Guide 3|CRISPR845343_CR
UACACCUUCCGGUUGUUCCC
```

## 6.3 Experimental methods

### 6.3.1 Peptides and loading

We used altered peptide ligands (APLs) that were either described previously [27, 78, 82, 286–288, 325] or designed by me based on the published crystal structures of these TCRs in complex with MHC (1G4: PDB 2BNQ, A6: PDB 1AO7). We also used a peptide library, which was designed to bind HLA-A*02:01, but avoid residues that could likely interact with the TCR (Table 6.9). Minimal alanine peptide (minA) is a peptide with 2L9V anchor residues and alanine at all other positions.

Peptides were synthesized at a purity of >95 % (Peptide Protein Research, UK). The peptide library was previously obtained at a unknown purity. Tax WT is a 9 amino acid, class I peptide derived from HTLV-1 $Tax_{11–19}$ [62, 326]. NYE 9V refers to a heteroclitic (improved stability on MHC), 9 amino acid, class I peptide derived from the wild type NYE-$ESO_{157–165}$ 9C peptide [47]. See Table S1 and Table S2 for a list of peptides.

Loading efficiency was evaluated by pulsing T2 cells for 1–2 h at 37°C with a titration of peptides. Loading was assessed as upregulation of HLA-A2 by flow cytometry. Data was normalized and fitted with a sigmoidal model, where the top and bottom were constrained to 1 and 0, respectively and $EC_{50}$ values were reported.

**Table 6.9: Biased peptide library.**
For each position it is indicated with this amino acid is a primary anchor residue (⚓), predominantly binding MHC (secondary anchor residues), or predominantly binding TCR. This peptide was designed by Milos Aleksic based on the crystal structure of 1G4 TCR with HLA-A*02:01 [47]. For position 3 + 6, all amino acids that did not prevent MHC binding were allowed [327]. For TCR facing positions, small hydrophilic or hydrophobic residues were allowed, since they are not expected to contribute strongly to TCR binding. Cysteines were excluded at all positions to prevent the formation of peptide multimers.

| 1 | 2 | 3 | 4 | 5 | 6 | 7 | 8 | 9 |
|---|---|---|---|---|---|---|---|---|
| TCR | ⚓ | MHC | TCR | TCR | MHC | TCR | TCR | ⚓ |
| Ser | Leu | Tyr | Ser | Ser | Tyr | Ser | Ser | Val |
| Thr | Ile | Phe | Thr | Thr | Phe | Thr | Thr | Leu |
| Ala | Met | Trp | Ala | Ala | Trp | Ala | Ala | |
| Val | | Thr | Val | Val | Thr | Val | Val | |
| Gly | | Leu | Gly | Gly | Leu | Gly | Gly | |
| | | Ile | | | Ile | | | |
| | | Met | | | Met | | | |
| | | Ala | | | Ala | | | |
| | | Pro | | | Pro | | | |
| | | Gly | | | Gly | | | |
| | | Gln | | | Gln | | | |
| | | Asn | | | Asn | | | |
| | | | | | Glu | | | |
| | | | | | Asp | | | |

## 6.3.2 Protein production

Class I pMHCs were refolded as previously described [328]. Briefly, human HLA-A*0201 heavy chain (sequence 1) with a C-terminal AviTag/BirA recognition sequence and human β-2 microglobulin were expressed in *Escherichia coli* and isolated from inclusion bodies. Trimer was refolded by consecutively adding peptide, β2M and heavy chain into refolding buffer and incubating for 2-3 days at 4°C. Protein was filtered, concentrated using centrifugation, biotinylated with the BirA biotin-protein ligase bulk reaction kit and purified by size exclusion chro-

matography (Superdex 75 column) in HBS-EP. Purified protein was aliquoted and stored at -80°C until use.

Biotinylated class II pMHC (HLA-DPB1*04:01) containing a MAGE-A3$_{243–258}$ peptide (KKLLTQ–HFVQENYLEY) was obtained from the NIH Tetramer Facility.

Soluble $\alpha$ and $\beta$ subunits of 1G4 and A6 TCRs were produced in *E. coli*, isolated from inclusion bodies, refolded *in vitro* and purified using size exclusion chromatography in HBS-EP, as described previously [78].

Soluble extracellular domains (ECDs) of human CD58 (UniProt residues 29–204 or 29–213) and human CD86 (isoform 2; UniProt residues 18–232) were produced either in Freestyle 293F suspension cells or adherent, stable GS CHO cell lines. For the latter, cells were expanded in selection medium for at least 1 week. Production was performed in production medium continuously for a few weeks with regular medium exchanges. Production in 293F was performed according to manufacturer's instructions. Human ICAM1 ECD (UniProt residues 28–480) was either produced by transient transfection, lentiviral transduction of adherent 293T, or by transient expression in 293F, as described above. All supernatants were 0.45 $\mu$m filtered and 100 $\mu$M PMSF was added. Proteins were purified using standard Ni-NTA agarose columns, followed by *in vitro* biotinylation as described above. Alternatively, ligands were biotinylated by co-transfection (1:10) of a secreted BirA-encoding plasmid and adding 100 $\mu$M D-biotin to the medium, as described before [329]. Proteins were further purified and excess biotin removed from proteins biotinylated *in vitro* by size exclusion chromatography (Superdex 75 or 200 column) in HBS-EP. Purified proteins were aliquoted and stored at -80°C until use.

Biotinylation levels of pMHC and accessory ligands were routinely tested by gel shift on SDS-PAGE upon addition of saturating amounts of streptavidin.

### 6.3.3 SPR

TCR–pMHC interactions were analyzed on a Biacore T200 instrument at 37°C and a flow rate of 10 $\mu$l/min with HBS-EP as running buffer. Streptavidin was coupled to CM5 sensor chips using an amino coupling kit to near saturation, typically 10000–12000 response units (RU). Biotinylated pMHCs (47 kDa, no glycosylation) were injected into the experimental flow cells (FCs) for different lengths of time to produce desired immobilization levels (typically 500–1500 RU), which were matched as closely as feasible in each chip. Excess streptavidin was blocked with two 40 s injections of 250 $\mu$M biotin. Before TCR injections, the chip surface was conditioned with 8 injections of the running buffer. Dilution series of TCRs were injected simultaneously in all FCs for 30–70 s. Buffer was also injected (conditioning) for the same length as TCR after every 2 or 3 TCR injections to allow double referencing (see below). After the final TCR injection and an additional conditioning cycle, W6/32 antibody (10 $\mu$g/ml) was injected for 10 min.

Each experiment included at least 1 reference flow cell (usually FC1 out of 4 on a CM5 chip). Biotinylated CD58 ECD (23 kDa + ~25 kDa glycosylation) was immobilized in FC1 at a level matching those of pMHCs in the other FCs. In some experiments, the CD58 ECD was replaced with those of CD86 (28 kDa + glycosylation), ICAM1 (53 kDa + glycosylation), or class II pMHC loaded with MAGE peptide (~60 kDa with glycosylation).

Steady-state binding was measured >10 s post-injection. In addition to subtracting the signal from the reference FC with immobilized CD58 (single referencing), all TCR binding data was double referenced versus the average of the closest buffer injections before and after TCR injection [285]. This allows to exclude small differences in signal between flow cells (e.g. drifts). TCR binding versus TCR concentration was fitted with the following model:

$$B = \frac{B_{max} \times [TCR]}{K_D + [TCR]}$$

Where $B$ is the response/binding, $B_{max}$ the maximal binding (this parameter is either kept free or is fixed with the W6/32 derived $B_{max}$), and $[TCR]$ the injected TCR concentration. Maximal W6/32 binding ($R_{max}$) was used to generate the empirical standard curve and to infer the $B_{max}$ of TCRs from the standard curve. $R_{max}$ was derived by fitting the W6/32 binding data after double referencing with the following, empirically chosen, model: $R = R_{max} * t/(K_t + t)$, where $t$ is time (s), $R$ the sensogram response after single referencing, and $K_t$ a nuisance parameter. The empirical standard curve only contained data where the ratio of the highest concentration of TCR to the fitted $K_D$ value (obtained using the standard method with $B_{max}$ fitted) was 2.5 or more. This threshold ensured that the binding response curves saturated so that only accurate measurements of $B_{max}$ were included. $K_D$ values reported are from unconstrained fits ($B_{max}$ fitted) for $K_D$s <20 $\mu$M and otherwise from constrained fits.

### 6.3.4 pMHC tetramers

Tetramers were produced in-house using refolded monomeric, biotinylated pMHC and streptavidin-PE at a 1:4 molar ratio. Streptavidin-PE was added in 10 steps and incubated for 10 min while shaking at room temperature. Insoluble proteins were removed by brief centrifugation at 13,000 $g$ and 0.05-0.1 % sodium azide added for preservation. Tetramers were kept for up to 3 months at 4°C. For the 1G4 TCR, tetramers produced with NYE 9V were used. For the A6 TCR, tetramers loaded with either Tax WT or Tax 5F were used.

### 6.3.5 Lentivirus production

HEK 293T or Lenti-X 293T were seeded in complete DMEM in 6-well plate to reach 60–80 % confluency after one day. Cells were either transfected with 0.95 $\mu$g pRSV-Rev, 0.37 $\mu$g pVSV-G (pMD2.G), 0.95 $\mu$g pGAG (pMDLg/pRRE), and 0.8 $\mu$g of a pHR-1G4, pHR-1G4hi, or pLEX-A6 with 9 $\mu$l X-tremeGENE 9 or HP. Lentiviral supernatant was harvested after 20–30 h and fil-

tered through a 0.45 $\mu$m cellulose acetate filter. In an updated version, LentiX cells were transfected with 0.25 $\mu$g pRSV-Rev, 0.53 $\mu$g pGAG, 0.35 $\mu$g pVSV-G, and 0.8 $\mu$g transfer plasmid using 5.8 $\mu$l X-tremeGENE HP. Medium was replaced after 12–18 h and supernatant harvested as above after 30–40 h. Supernatant from one well of a 6-well plate was used to transduce 1 Mio T cells. Sequence for the A6 TCR lacked one natural cysteine per chain and included engineered cysteines ($\alpha$T48C and $\beta$S57C) to reduce the formation of mixed TCR dimers with endogenous TCR [324]. The 1G4 TCR was expressed from the WT sequences without engineered cysteines.

### 6.3.6 T cell blasts

All cell culture of human T cells was done using complete RPMI at 37°C, 5 % $CO_2$. T cells were isolated from whole blood from healthy donors or leukocyte cones purchased from the NHS Blood and Transplantation service at the John Radcliffe Hospital. For whole blood donations, a maximum of 50 ml was collected by a trained phlebotomist after informed consent had been given. This project has been approved by the Medical Sciences Inter-Divisional Research Ethics Committee of the University of Oxford (R51997/RE001) and all samples were anonymised in compliance with the Data Protection Act.

For plate stimulations and experiments with U87 target cells, $CD8^+$ T cells were isolated using RosetteSep Human $CD8^+$ enrichment cocktail at 6 $\mu$l/ml for whole blood or 150 $\mu$l/ml for leukocyte cones. After 20 min incubation at room temperature, blood cone samples were diluted 3.125-fold with PBS, while whole blood samples were used directly. Samples were layered on Ficoll Paque Plus (GE) at a 0.8:1.0 ficoll:sample ratio and spun at 1200 g for 20–30 min at room temperature . Buffy coats were collected, washed twice, counted and cells were resuspended in complete RMPI with 50 U/ml IL2 (PeproTech) and CD3/CD28 Human T-activator dynabeads (Thermo Fisher) at a 1:1 bead:cell ratio. Aliquots of 1 Mio cells in 1 ml medium were grown overnight in 12- or 24-well plates (either TC-treated or coated with 5 $\mu g/cm^2$

retronectin) and then transduced with VSV-pseudotyped lentivirus encoding for either the 1G4 or the A6 TCR. After 2 days (4 days after transduction), 1 ml of medium was exchanged, and IL2 was added to a final concentration of 50 U/ml. Beads were magnetically removed at day 5 post-transduction and T cells from thereon were resuspended at 1 Mio/ml with 50 U/ml IL2 every other day. For functional experiments, T cells between 10–16 days after transduction were used.

### 6.3.7 Plate stimulation

96-well glass-bottom Sensoplates were washed with 1 M HCl/70 % EtOH, thoroughly rinsed twice with PBS and coated overnight at 4°C with 100 $\mu$l/well of 1 mg/ml biotinylated BSA in PBS. Plates were washed with PBS twice and incubated for at least 1 h with 20 $\mu$g/ml streptavidin in 1 % BSA/PBS at room temperature. Plates were washed again with PBS and biotinylated pMHC (in-house) was added for at least 1 h at room temperature or overnight at 4°C. Plates were emptied and accessory ligand (50–125 ng/well CD58 or 30–50 ng/well ICAM1, in-house) or PBS was added for the same duration as pMHC. Upon completion, plates were washed once and stored for up to 1 day in PBS at 4°C.

Alternatively, commercial streptavidin-coated plates were used for all experiments involving the 1G4$^{hi}$. Due to the different surface, generally more pMHC and accessory ligands were required with these plates. Ligands were added sequentially as described above.

For stimulation on either plates, T cells were counted, washed once to remove excess IL2, and 75,000 cells in 180–200 $\mu$l complete RMPI were dispensed per well. Cells were briefly spun down at 50 g to settle to the bottom and subsequently incubated for 4 h at 37°C. At the end of the experiment, 10 mM EDTA was added and cells were detached by vigorous pipetting. Cells were stained for flow cytometry and analyzed immediately, or fixed and stored for up to 1 day. Supernatants were saved for cytokine ELISAs.

### 6.3.8 CRISPR knock-out

tracrRNA:crRNA complexes were produced according to the manufacturer's instructions. Guide RNAs and tracrRNA were resuspended at 100 $\mu$M in TE. Both were diluted to 20 $\mu$M in annealing buffer and annealed in a thermocycler: 5 min at 95°C; cooled-down to 78°C at -2°C/s; 10 min at 78°C; cooled-down to 25°C at 0.1°C/s; 5 min at 25°C. Annealed guides were further 1:5 diluted in annealing buffer (final concentration: 5 $\mu$M = 5 pmol/µl) and used immediately or stored at -20°C.

CD58 and ICAM1 CRISPR knock-outs were generated according to the manufacturer's instructions. For each target, 3 guides were selected. ICAM1 KOs were generated from sorted G1 CD58-KO U87 or WT U87 to generate double-KOs or single-KO, respectively. 50,000 U87 cells were seeded in a 24-well plate and incubated overnight. Mix 1 was prepared as: 25 $\mu$l OptiMEM; 1.25 $\mu$l Cas9 protein (1.25 $\mu$g = 7.5 pmol); 1.5 $\mu$l annealed gRNA (240 ng = 7.5 pmol); 2.5 $\mu$l Lipofectamine Cas9 Plus per reaction. Mix 2 was prepared as: 25 $\mu$l OptiMEM; 1.5 $\mu$l Lipofectamine CRISPRMAX per reaction. Mix 2 was incubated for 1 min and then mixed with mix 1. After 10–15 min, 50 $\mu$l was added to each well. Cells were screened by flow cytometry and sorted by FACS. All guides for CD58 and ICAM1 produced some fraction of KO cells. All experiments shown in this thesis were performed with guide 1 for CD58 and guide 2 for ICAM1, after FAC sorting.

### 6.3.9 U87 co-culture of T cell blasts

For co-culture experiments with U87, 30,000 target cells were seeded in a TC-coated 96-well F-bottom plate and incubated overnight. Peptides were diluted in complete DMEM to their final concentration and incubated with U87 cells for 1–2 h at 37°C. Peptide-containing medium was removed and 60,000 1G4 or A6 TCR-transduced primary human $CD8^+$ T cell blasts were

added in complete RPMI. For antibody blocking experiments, T cells were added in medium containing control or blocking antibodies, after preincubating the T cells with the antibodies for 10–20 min. Plates were spun for 2 min at 50 g to settle cells, and incubated for 4–6 h at 37°C. At the end of the experiment, 10 mM EDTA/PBS was added and cells were detached by vigorous pipetting. Cells were stained for flow cytometry and analyzed immediately, or fixed and stored for up to 1 day before running. Supernatants were saved for cytokine ELISAs. U87 and T cells were distinguished by staining for CD45.

### 6.3.10 CHO co-culture of T cell blasts

20,000 CHO-A2 (expressing HLA-A2 single chain dimer) or CHO-A2 CD58 (additionally expressing human CD58) target cells were seeded per well in a 96-well TC-coated F-bottom plate and incubated overnight. Peptides were diluted in complete OptiMEM to their final concentration and incubated with U87 cells for 1–2 h at 37°C. Peptide-containing medium was removed and 50,000 1G4 TCR-transduced primary human $CD8^+$ T cell blasts in 200 $\mu$l complete OptiMEM were added. Plates were spun for 2 min at 50 g to settle cells, and incubated for 20–24 h at 37°C. At the end of the experiment, the medium was removed and saved. Accutase was added to the cells, the cells incubated for 2–5 min at 37°C, and then detached by pipetting. Medium and detached cells were pooled again, spun, and supernatant and cell fraction were separated. Cells were stained for flow cytometry and analyzed immediately, or fixed and stored for up to 1 day before running. Supernatants were saved for cytokine ELISAs. CHO and T cells were distinguished by staining for CD45.

### 6.3.11 Flow cytometry

Cells were washed once in PBS by spinning for 5 min at 300–500 g. Cells were stained for antibodies (1:200) and/or tetramers (1:300–1:1000) in the presence of 1:1000 fixable viability

dye for >30 min in PBS at 4°C. 1 % BSA/PBS was added on top, spun and cells were washed one more time in BSA/PBS, before a final resuspension in PBS. Samples were analyzed within 3 h using a X-20 or a CytoFlex flow cytometer and data analysis was performed using FlowJo.

### 6.3.12 ELISAs

IL-2 Human uncoated ELISA kit, TNF Human uncoated ELISA kit, or LDH cytotoxicity assay kit and Nunc MaxiSorp 96-well plates were used according to the manufacturer's instructions. For cytokine ELISAs, supernatant was appropriately diluted (commonly 4–30-fold).

Data was analyzed after fitting a 4 parameter sigmoidal curve on untransformed data and interpolating the concentration (c) using either Prism or Python + lmfit:

$$OD(c) = E_{min} + \frac{E_{max} - E_{min}}{1 + (\frac{EC_{50}}{c})^H}$$

### 6.3.13 Quantification of protein immobilization

A glass plate coated with biotinylated BSA, streptavidin, and a titration of 1–250 ng/well NYE 9V was prepared as described above. Additional control included 0 pMHC wells, and no streptavidin wells. pMHC wells and 0 pMHC control were stained by incubating with W6/32 (1:500) overnight at 4°C, washed 3 times in PBS, followed by 1 h anti-mouse 680RD secondary antibody (1:500) at room temperature. Biotinylated BSA only wells were stained in parallel with streptavidin 800CW (20 $\mu$g/ml). After a final 3 PBS washes, fluorescent signals in the 700 and 800 nm channels were measured on a Odyssey Sa scanner and the resulting images and integrated intensities per well were exported.

### 6.3.14 TCR expression

TCR$\alpha\beta$-KO Jurkat cells were transduced with 1G4 or A6 lentivirus and TCR expression was measured by staining for CD3 and TCR$\alpha\beta$, or specific tetramers. TCR expression of each transduced batch of primary T cells was tested with specific tetramers during culture to assess transduction efficiency, and after each experiment as a measure of TCR downregulation.

## 6.4 Data analysis & fitting

Details of statistical methods for comparisons can be found in the figure legends. All tests were 2-tailed, if not stated otherwise. All fitting was done using least squares optimization (Levenberg–Marquardt), if not stated otherwise. All statistics on discrimination power and sensitivity were performed on log-transformed data, unless stated otherwise. All data analysis was performed using GraphPad Prism, if not stated otherwise.

### 6.4.1 Fitting dose response curves

Quantitative analysis of antigen discrimination was performed by first fitting dose response data with a 4-parameter sigmoidal model on a linear scale using Python and lmfit with either leastsq or Nelder-Mead:

$$R(x) = bottom + \frac{top - bottom}{1 + (\frac{EC_{50}}{x})^{hill}} \tag{6.1}$$

where $x$ refers to the peptide concentration used to pulse the target cells (in $\mu$M) or the amount of pMHC used to coat the well of a plate (in ng/well). Rather than using the $EC_{50}$ as a metric for potency, I decided to calculate an activation threshold based on the control condition in each

experiment. For antigen discrimination experiments, the index peptide was the control condition (i.e. NYE 9V or Tax WT). This avoids unreliable results, when the top of the response is not reached, i.e. for low affinity peptides. Thresholds to measure potency were chosen based on noise levels and feasibility (see Table 6.10 and Table 6.11 for details). Potency or $EC_{50}$ values exceeding doses used for pulsing or coating by more than 10 % (on log) were excluded from the analysis. For plate experiments, data from wells with over-saturation of the binding capacity of the plates were excluded. For IL2, some responses showed a bell shape and therefore decreasing data was excluded from dose response fitting. The $E_{max}$ reported in this thesis is not identical with the top parameter of the fits, but represents the maximum value of the curve within the x-limits. For dose responses where saturation is reached, top and $E_{max}$ will be very similar, while they can diverge significantly for non-saturating activation curves. For some data, bell shaped data points were automatically or manually removed.

**Table 6.10: Details of dose response fitting in chapter 2.**
Shared refers to parameters that were shared for all curves within one marker and experiment. Norm. cond.: The normalization condition used to define 0–1. Threshold: Threshold used as a measure of potency (e.g. $P_{15}$).

| **1G4 plate – Figure 2.3 + Figure 2.4 + Figure 2.5** | | | |
|---|---|---|---|
| | **CD69 (%)** | **IL2/TNF** | **Tetramers (gMFI)** |
| Top | [0; 100] | [0; 100,000] | shared |
| Bottom | shared | fixed to 0 | unconstrained |
| $EC_{50}$ | unconstrained | unconstrained | unconstrained |
| Hill | [0.3; 3.0] | [0.2; 3.0]; shared | [-1.5; -0.3] |
| Norm. cond. | N/A | N/A | NYE 9V |
| Threshold | N/A | N/A | 60 % |

| **1G4 U87 – Figure 2.8 + Figure 2.9** | | | |
|---|---|---|---|
| | **CD69 (%)** | **TNF (KOs)** | **TNF (ABs)** |
| Top | unconstrained | [0; 100,000] | [0; 100,000] |
| Bottom | unconstrained | fixed to 0 | fixed to 0 |
| $EC_{50}$ | unconstrained | unconstrained | unconstrained |
| Hill | unconstrained | [0.2; 3.0]; shared | [0.2; 3.0]; shared |
| Norm. cond. | N/A | Parental | 1x Isotype Ctrl |
| Threshold | N/A | 15 % | 15 % |

| **1G4 CHO – Figure 2.12** | | |
|---|---|---|
| | **41BB (%)** | **LDH (OD)** |
| Top | unconstrained | [0; 100,000] |
| Bottom | shared | shared |
| $EC_{50}$ | unconstrained | unconstrained |
| Hill | [0.3; 3.0] | [0.3; 3.0] |
| Norm. cond. | N/A | N/A |
| Threshold | N/A | N/A |

| **$1G4^{hi}$ plate – Figure 2.15 + Figure 2.17** | | |
|---|---|---|
| | **CD69 (%)** | **IL2** |
| Top | unconstrained | unconstrained |
| Bottom | shared | shared |
| $EC_{50}$ | unconstrained | unconstrained |
| Hill | [0.3; 3.0] | [0.3; 3.0]; shared |
| Norm. cond. | N/A | 0 CD58 |
| Threshold | N/A | 10 % |

**Table 6.11: Details of dose response fitting in chapter 4.**
Shared refers to parameters that were shared for all curves within one marker and experiment. Norm. cond.: The normalization condition used to define 0–1. Threshold: Threshold used as a measure of potency (e.g. $P_{15}$).

| **1G4 & A6 U87 – Figure 4.3 + Figure 4.5** | | | |
|---|---|---|---|
| | **CD69 (%)** | **IL2** | **Tetramers (gMFI)** |
| Top | unconstrained | unconstrained | shared |
| Bottom | shared | fixed to 0 | unconstrained |
| $EC_{50}$ | unconstrained | unconstrained | unconstrained |
| Hill | [0.3; 3.0]; shared | [0.3; 3.0]; shared | [-2.0; -0.3]; shared |
| Norm. cond. | NYE 9V or Tax WT | NYE 9V or Tax WT | NYE 9V or Tax WT |
| Threshold | 15 % | 5 % | 85 % |

| **1G4 plate – Figure 4.6** | |
|---|---|
| | **CD69 (%)** |
| Top | unconstrained |
| Bottom | shared |
| $EC_{50}$ | unconstrained |
| Hill | [0.3; 3.0]; shared |
| Norm. cond. | NYE 9V |
| Threshold | 15 % |

### 6.4.2 Fitting empirical antigen discrimination model

For empirical antigen discrimination fitting, I fitted a linear function in loglog space to our data, corresponding to the following power function:

$$P_{15}(K_D) = K_D^{\alpha} + 10^C$$

where $\alpha$ is a measure of discrimination power and $C$ a correlate of sensitivity. Fits and reported values are per experiment.

### 6.4.3 Fitting kinetic proofreading model*

Given a kinetic proofreading model with $N$ steps, the concentration of the $N^{th}$ complex depends on the total amount of complex ($C_T$), the kinetic proofreading rate ($k_p$) and the off-rate of the ligand ($k_{off}$):

$$C_N = (\frac{k_p}{k_p + k_{off}})^N \times C_T$$

The total amount of complex is a function of the total amount of receptor ($R_0$), the total amount of ligand ($L_0$) and the binding affinity between receptor and ligand ($K_D$):

$$C_T = \frac{R_0 + L_0 + K_D - \sqrt{(R_0 + L_0 + K_D)^2 - 4R_0L_0}}{2}$$

We furthermore define an activation threshold $\lambda$ as a the fraction of total receptor that needs to be in a complex for the cell to become activated. Since when fitting we do not directly fit his activation threshold, but rather some correlated of it, we will use the term $\hat{\lambda}$ in the following.

$$\lambda = \frac{C_N}{R_0}$$

Additionally, the concentration of ligand, relative to the total amount of receptors, shall be the potency $\rho$:

$$\rho = \frac{L_0}{R_0}$$

*See also supplementary of [253] for details and the derivation of the kinetic proofreading equations used here.

I solve for $\rho$, by substituting :

$$\frac{C_N}{R_0} = (\frac{k_p}{k_p + k_{off}})^N \times \frac{1 + \frac{L_0}{R_0} + \frac{K_D}{R_0} - \sqrt{(1 + \frac{L_0}{R_0} + \frac{K_D}{R_0})^2 - 4\frac{L_0}{R_0}}}{2}$$

$$\frac{2\hat{\lambda}}{(\frac{k_p}{k_p+k_{off}})^N} = 1 + \rho + \frac{K_D}{R_0} - \sqrt{(1 + \rho + \frac{K_D}{R_0})^2 - 4x}$$

$$\rho = \alpha(1 - \frac{K_D}{R_0}(\frac{1}{\alpha - 1})); \text{ where } \alpha = \frac{\hat{\lambda}}{(\frac{k_p}{k_p+k_{off}})^N}$$

For the limit where every ligand engages ($\frac{K_D}{R_0} << 1$), above can be simplified to:

$$\rho = \alpha = \frac{\hat{\lambda}}{(\frac{k_p}{k_p+k_{off}})^N} = \hat{\lambda}(1 + \frac{k_{off}}{k_p})^N$$

$$\log \rho = \log \hat{\lambda} + N \log(1 + \frac{k_{off}}{k_p}) \tag{6.2}$$

I fit the data using least squared in GraphPad Prism. To support convergence, I fit the parameters $\hat{\lambda}$ and $k_p$ in log-space. I calculated the off-rates for different 1G4 peptide variants using their $K_D$ and constant, estimated on-rate of 0.0447 $\mu M^{-1}s^{-1}$ ($k_{off} = K_D \times k_{on}$). This on-rate was calculated as the average on-rate of the 1G4 TCR to different NYE peptides at 37°C as reported in [78]. On-rates from peptide with $K_D$s larger than 50 $\mu$M were excluded.

In comparison to the kinetic proofreading found in our paper about antigen discrimination [4], there is several differences: (1) Small differences in $K_D$s based on using geo. mean rather than arithmetic mean and including extra data points in this thesis. (2) Unlike here, no simplification regarding the receptors occupancy ($\frac{K_D}{R_0}$) is made. (3) Plate and APC data are fitted separately and the APC data includes additional experiments performed with naïve or memory T cells co-cultured with dendritic cells. (4) In the paper, we use a more sophisticated fit-

ting algorithm (approximate Bayesian computation-sequential Monte Carlo; ABC-SMC) to fit the data. One benefit is, that unlike here, this allows us to estimate the variance of $N$.

### 6.4.4 Simulating kinetic proofreading

I generated potency versus off-rate simulations of different kinetic proofreading models using Equation 6.2 with $\lambda = \hat{\lambda}$. For all stimulations:

$$k_{on} = 10,000\ M^{-1}$$

$$\lambda = 10^{-4}\ M$$

$$k_p = 1.0\ s^{-1}$$

To simulate dose responses, I generated sigmoidal data using the same model as for fitting data (Equation 6.1). These sigmoidal functions simulate the heterogeneity within a population of T cells that get activated. I calculated the expected $EC_{50}$ based on:

$$EC_{50} = \rho \left( \frac{top - bottom}{threshold - bottom} - 1 \right)^{1/hill}$$

I set bottom to 0, used 10 % as a potency threshold, and arbitrarily chose decreasing top values for higher off-rates. Such a decrease is expected, but the details depend on the threshold* cells use to get activated.

*This threshold refers to λ in the KP model and should not be confused with the potency threshold I chose when fitting dose response curves.

# References


[1] J. Pettmann et al. “Membrane Ultrastructure and T Cell Activation.” In: *Front Immunol* (2018). DOI: 10.3389/fimmu.2018.02152.

[2] P. Kruger. “On the Role of Receptor Downregulation and Costimulation in Shaping the T Cell Response.” University of Oxford, 2018.

[3] E. Abu-Shah et al. “Human CD8 T Cells Exhibit a Shared Antigen Threshold for Different Effector Responses.” In: *Journal of Immunology* (2020). DOI: 10.4049/jimmunol.2000525.

[4] J. Pettmann et al. “The discriminatory power of the T cell receptor.” In: *eLife* (2021). DOI: 10.7554/elife.67092.

[5] J. Pettmann et al. “T Cells Exhibit Unexpectedly Low Discriminatory Power and Can Respond to Ultra-low Affinity Peptide-MHC Ligands.” In: *bioRxiv* (2020). DOI: 10.1101/2020.11.14.382630.

[6] F. D. Batista and N. E. Harwood. “The Who, How and Where of Antigen Presentation to B Cells.” In: *Nature Reviews Immunology* (2009). DOI: 10.1038/nri2454.

[7] C. Chan, A. J. T. George, and J. Stark. “T Cell Sensitivity and Specificity - Kinetic Proofreading Revisited.” In: *Discrete & Continuous Dynamical Systems - B* (2003). DOI: 10.3934/dcdsb.2003.3.343.

[8] L. Wooldridge et al. “CD8 Controls T Cell Cross-reactivity.” In: *Journal of Immunology* (2010). DOI: 10.4049/jimmunol.1001480.

[9] D. Tortorella et al. “Viral Subversion of the Immune System.” In: *Annual Review of Immunology* (2000). DOI: 10.1146/annurev.immunol.18.1.861.

[10] S. Spranger and T. F. Gajewski. “Mechanisms of Tumor Cell–intrinsic Immune Evasion.” In: *Annual Review of Cancer Biology* (2018). DOI: 10.1146/annurev-cancerbio-030617-050606.

[11] D. J. Irvine et al. “Direct Observation of Ligand Recognition by T Cells.” In: *Nature* (2002). DOI: 10.1038/nature01076.

[12] J. Huang et al. “A Single Peptide-major Histocompatibility Complex Ligand Triggers Digital Cytokine Secretion in CD4(+) T Cells.” In: *Immunity* (2013). DOI: 10.1016/j.immuni.2013.08.036.

[13] Y. Sykulev et al. “Evidence That a Single Peptide-MHC Complex on a Target Cell Can Elicit a Cytolytic T Cell Response.” In: *Immunity* (1996). DOI: 10.1016/s1074-7613(00)80483-5.

[14] M. A. Purbhoo et al. “T Cell Killing Does Not Require the Formation of a Stable Mature Immunological Synapse.” In: *Nature Immunology* (2004). DOI: 10.1038/ni1058.

[15] M. Gunzer et al. “Antigen Presentation in Extracellular Matrix: Interactions of T Cells with Dendritic Cells Are Dynamic, Short Lived, and Sequential.” In: *Immunity* (2000). DOI: 10.1016/s1074-7613(00)00032-7.

[16] M. J. Miller et al. “Autonomous T Cell Trafficking Examined in Vivo with Intravital Two-photon Microscopy.” In: *Proc Natl Acad Sci USA* (2003). DOI: 10.1073/pnas.2628040100.

[17] M. J. Miller et al. “Imaging the Single Cell Dynamics of CD4+ T Cell Activation by Dendritic Cells in Lymph Nodes.” In: *The Journal of Experimental Medicine* (2004). DOI: 10.1084/jem.20041236.

[18] M. J. Miller et al. “T Cell Repertoire Scanning Is Promoted by Dynamic Dendritic Cell Behavior and Random T Cell Motility in the Lymph Node.” In: *Proceedings of the National Academy of Sciences* (2004). DOI: 10.1073/pnas.0306407101.

[19] E. Cai et al. “Visualizing Dynamic Microvillar Search and Stabilization during Ligand Detection by T Cells.” In: *Science* (2017). DOI: 10.1126/science.aal3118.

[20] P. A. van der Merwe and A. N. Barclay. “Transient Intercellular Adhesion: The Importance of Weak Protein-protein Interactions.” In: *Trends in Biochemical Sciences* (1994). DOI: 10.1016/0968-0004(94)90109-0.

[21] S. Stoll et al. “Dynamic Imaging of T Cell-dendritic Cell Interactions in Lymph Nodes.” In: *Science* (2002). DOI: 10.1126/science.1071065.

[22] T. R. Mempel, S. E. Henrickson, and U. H. Von Andrian. “T-cell Priming by Dendritic Cells in Lymph Nodes Occurs in Three Distinct Phases.” In: *Nature* (2004). DOI: 10.1038/nature02238.

[23] T. Zell et al. “Single-cell Analysis of Signal Transduction in CD4 T Cells Stimulated by Antigen in Vivo.” In: *Proc Natl Acad Sci USA* (2001). DOI: 10.1073/pnas.191567898.

[24] J. C. D. Houtman et al. “Early Phosphorylation Kinetics of Proteins Involved in Proximal TCR-mediated Signaling Pathways.” In: *Journal of Immunology* (2005). DOI: 10.4049/jimmunol.175.4.2449.

[25] M. Huse et al. “Spatial and Temporal Dynamics of T Cell Receptor Signaling with a Photoactivatable Agonist.” In: *Immunity* (2007). DOI: 10.1016/j.immuni.2007.05.017.

[26] A. Brodovitch, P. Bongrand, and A. Pierres. “T Lymphocytes Sense Antigens within Seconds and Make a Decision within One Minute.” In: *J Immunol* (2013). DOI: 10.4049/jimmunol.1300523.

[27] Y. H. Ding et al. “Four A6-TCR/peptide/HLA-A2 Structures That Generate Very Different T Cell Signals Are Nearly Identical.” In: *Immunity* (1999). DOI: 10.1016/s1074-7613(00)80080-1.

[28] M. Degano et al. “A Functional Hot Spot for Antigen Recognition in a Superagonist TCR/MHC Complex.” In: *Immunity* (2000). DOI: 10.1016/s1074-7613(00)80178-8.

[29] D. Dong et al. “Structural Basis of Assembly of the Human T Cell Receptor–CD3 Complex.” In: *Nature* (2019). DOI: 10.1038/s41586-019-1537-0.

[30] D. S. Lyons et al. “A TCR Binds to Antagonist Ligands with Lower Affinities and Faster Dissociation Rates Than to Agonists.” In: *Immunity* (1996).

[31] G. J. Kersh and P. M. Allen. “Structural Basis for T Cell Recognition of Altered Peptide Ligands: A Single T Cell Receptor Can Productively Recognize a Large Continuum of Related Ligands.” In: *J Exp Med* (1996).

[32] G. Altan-Bonnet and R. N. Germain. “Modeling T Cell Antigen Discrimination Based on Feedback Control of Digital Erk Responses.” In: *Plos Biol* (2005). DOI: 10.1371/journal.pbio.0030356.

[33] K. A. Hogquist, S. C. Jameson, and M. J. Bevan. “Strong Agonist Ligands for the T Cell Receptor Do Not Mediate Positive Selection of Functional CD8+ T Cells.” In: *Immunity* (1995).

[34] S. M. Alam et al. “T-cell-receptor Affinity and Thymocyte Positive Selection.” In: *Nature* (1996). DOI: 10.1038/381616a0.

[35] G. J. Kersh et al. “High- and Low-potency Ligands with Similar Affinities for the TCR: The Importance of Kinetics in TCR Signaling.” In: *Immunity* (1998).

[36] S. M. Alam et al. “Qualitative and Quantitative Differences in T Cell Receptor Binding of Agonist and Antagonist Ligands.” In: *Immunity* (1999).

[37] P. François and G. Altan-Bonnet. “The Case for Absolute Ligand Discrimination: Modeling Information Processing and Decision by Immune T Cells.” In: *J Stat Phys* (2016). DOI: 10.1007/s10955-015-1444-1.

[38] A. Allam and D. Kabelitz. “TCR Trans-rearrangements: Biological Significance in Antigen Recognition Vs the Role As Lymphoma Biomarker.” In: *Journal of Immunology* (2006). DOI: 10.4049/jimmunol.176.10.5707.

[39] D. G. Pellicci et al. “The Molecular Bases of $\Delta/\alpha\beta$ T Cell-mediated Antigen Recognition.” In: *The Journal of Experimental Medicine* (2014). DOI: 10.1084/jem.20141764.

[40] L. N. Schoettle, M. E. Poindexter, and J. N. Blattman. “T-cell Receptors.” In: *eLS*. American Cancer Society, 2015. DOI: 10.1002/9780470015902.a0000915.pub2.

[41] M. M. Davis and P. J. Bjorkman. “T-cell Antigen Receptor Genes and T-cell Recognition.” In: *Nature* (1988). DOI: 10.1038/334395a0.

[42] V. I. Zarnitsyna et al. “Estimating the Diversity, Completeness, and Cross-reactivity of the T Cell Repertoire.” In: *Frontiers in Immunology* (2013). DOI: 10.3389/fimmu.2013.00485.

[43] T. P. Arstila et al. “A Direct Estimate of the Human Alphabeta T Cell Receptor Diversity.” In: *Science* (1999). DOI: 10.1126/science.286.5441.958.

[44] Q. Qi et al. “Diversity and Clonal Selection in the Human T-cell Repertoire.” In: *Proc Natl Acad Sci USA* (2014). DOI: 10.1073/pnas.1409155111.

[45] A. K. Sewell. “Why Must T Cells Be Cross-reactive?” In: *Nat Rev Immunol* (2012). DOI: 10.1038/nri3279.

[46] M. Attaf et al. “The T Cell Antigen Receptor: The Swiss Army Knife of the Immune System.” In: *Clinical and Experimental Immunology* (2015).

[47] J.-L. Chen et al. “Structural and Kinetic Basis for Heightened Immunogenicity of T Cell Vaccines.” In: *The Journal of Experimental Medicine* (2005). DOI: 10.1084/jem.20042323.

[48] M. Reth. “Antigen Receptor Tail Clue.” In: *Nature* (1989). DOI: 10.1038/338383b0.

[49] A. Alcover et al. “Lysine 271 in the Transmembrane Domain of the T-cell Antigen Receptor Beta Chain Is Necessary for Its Assembly with the CD3 Complex but Not for Alpha/beta Dimerization.” In: *The Journal of Biological Chemistry* (1990).

[50] M. E. Call et al. “The Organizing Principle in the Formation of the T Cell Receptor-CD3 Complex.” In: *Cell* (2002). DOI: 10.1016/s0092-8674(02)01194-7.

[51] M. E. Call et al. “The Structure of the Zetazeta Transmembrane Dimer Reveals Features Essential for Its Assembly with the T Cell Receptor.” In: *Cell* (2006). DOI: 10.1016/j.cell.2006.08.044.

[52] G. Werlen, B. Hausmann, and E. Palmer. “A Motif in the Alphabeta T-cell Receptor Controls Positive Selection by Modulating Erk Activity.” In: *Nature* (2000). DOI: 10.1038/35019094.

[53] C. Xu, M. E. Call, and K. W. Wucherpfennig. “A Membrane-proximal Tetracysteine Motif Contributes to Assembly of CD3deltaepsilon and CD3gammaepsilon Dimers with the T Cell Receptor.” In: *The Journal of Biological Chemistry* (2006). DOI: 10.1074/jbc.M607164200.

[54] M. S. Kuhns and M. M. Davis. “Disruption of Extracellular Interactions Impairs T Cell Receptor-CD3 Complex Stability and Signaling.” In: *Immunity* (2007). DOI: 10.1016/j.immuni.2007.01.015.

[55] R. Platzer and J. B. Huppa. “T-cell Antigen Recognition – Lessons from the Past and Projections into the Future.” In: *eLS*. 2020. DOI: 10.1002/9780470015902.a0001229.pub3.

[56] A. Mallabiabarrena, M. Fresno, and B. Alarcón. “An Endoplasmic Reticulum Retention Signal in the CD3 Epsilon Chain of the T-cell Receptor.” In: *Nature* (1992). DOI: 10.1038/357593a0.

[57] J. S. Bonifacino, P. Cosson, and R. D. Klausner. “Colocalized Transmembrane Determinants for Er Degradation and Subunit Assembly Explain the Intracellular Fate of TCR Chains.” In: *Cell* (1990). DOI: 10.1016/0092-8674(90)90447-m.

[58] F. Letourneur and R. D. Klausner. “A Novel Di-leucine Motif and a Tyrosine-based Motif Independently Mediate Lysosomal Targeting and Endocytosis of CD3 Chains.” In: *Cell* (1992). DOI: 10.1016/0092-8674(92)90636-q.

[59] J. B. Huppa and H. L. Ploegh. “In Vitro Translation and Assembly of a Complete T Cell Receptor-CD3 Complex.” In: *The Journal of Experimental Medicine* (1997). DOI: 10.1084/jem.186.3.393.

[60] J. P. H. Lauritsen et al. “Masking of the CD3 Gamma Di-leucine-based Motif by Zeta Is Required for Efficient T-cell Receptor Expression.” In: *Traffic* (2004). DOI: 10.1111/j.1600-0854.2004.00211.x.

[61] J. Rossjohn et al. “T Cell Antigen Receptor Recognition of Antigen-presenting Molecules.” In: *Annu Rev Immunol* (2015). DOI: 10.1146/annurev-immunol-032414-112334.

[62] D. N. Garboczi et al. “Assembly, Specific Binding, and Crystallization of a Human TCR-alphabeta with an Antigenic Tax Peptide from Human T Lymphotropic Virus Type 1 and the Class I MHC Molecule HLA-A2.” In: *Journal of Immunology* (1996). DOI: 10.2210/pdb1bd2/pdb.

[63] D. X. Beringer et al. “T Cell Receptor Reversed Polarity Recognition of a Self-antigen Major Histocompatibility Complex.” In: *Nature Immunology* (2015). DOI: 10.1038/ni.3271.

[64] S. Gras et al. “Reversed T Cell Receptor Docking on a Major Histocompatibility Class I Complex Limits Involvement in the Immune Response.” In: *Immunity* (2016). DOI: 10.1016/j.immuni.2016.09.007.

[65] K. Matsui et al. “Kinetics of T-cell Receptor Binding to Peptide/i-ek Complexes: Correlation of the Dissociation Rate with T-cell Responsiveness.” In: *Proc Natl Acad Sci Usa* (1994). DOI: 10.1073/pnas.91.26.12862.

[66] J. D. Stone, A. S. Chervin, and D. M. Kranz. “T-cell Receptor Binding Affinities and Kinetics: Impact on T-cell Activity and Specificity.” In: *Immunology* (2009). DOI: 10.1111/j.1365-2567.2008.03015.x.

[67] F. D. Batista and M. S. Neuberger. “Affinity dependence of the B cell response to antigen: a threshold, a ceiling, and the importance of off-rate.” In: *Immunity* (1998). DOI: 10.1016/s1074-7613(00)80580-4.

[68] Y. Li et al. “Directed Evolution of Human T-cell Receptors with Picomolar Affinities by Phage Display.” In: *Nat Biotechnol* (2005). DOI: 10.1038/nbt1070.

[69] M. N. Duong et al. “Chronic TCR-MHC (self)-interactions Limit the Functional Potential of TCR Affinity-increased CD8 T Lymphocytes.” In: *Journal for Immunotherapy of Cancer* (2019). DOI: 10.1186/s40425-019-0773-z.

[70] D. K. Cole et al. “Human TCR-binding Affinity Is Governed by MHC Class Restriction.” In: *J Immunol* (2007).

[71] D. R. Myers, J. Zikherman, and J. P. Roose. “Tonic Signals: Why Do Lymphocytes Bother?” In: *Trends Immunol* (2017). DOI: 10.1016/j.it.2017.06.010.

[72] V. T. Chang et al. “Initiation of T Cell Signaling by CD45 Segregation at ’close Contacts’.” In: *Nat Immunol* (2016). DOI: 10.1038/ni.3392.

[73] G. Campi, R. Varma, and M. L. Dustin. “Actin and Agonist MHC-peptide Complex-dependent T Cell Receptor Microclusters As Scaffolds for Signaling.” In: *J Exp Med* (2005). DOI: 10.1084/jem.20051182.

[74] T. Yokosuka et al. “Newly Generated T Cell Receptor Microclusters Initiate and Sustain T Cell Activation by Recruitment of Zap70 and Slp-76.” In: *Nat Immunol* (2005). DOI: 10.1038/ni1272.

[75] W. W. Schamel et al. “Coexistence of Multivalent and Monovalent TCRs Explains High Sensitivity and Wide Range of Response.” In: *J Exp Med* (2005). DOI: 10.1084/jem.20042155.

[76] B. F. Lillemeier et al. “TCR and Lat Are Expressed on Separate Protein Islands on T Cell Membranes and Concatenate during Activation.” In: *Nat Immunol* (2010). DOI: 10.1038/ni.1832.

[77] S. V. Pageon et al. “Functional Role of T-cell Receptor Nanoclusters in Signal Initiation and Antigen Discrimination.” In: *Proc Natl Acad Sci* (2016). DOI: 10.1073/pnas.1607436113.

[78] M. Aleksic et al. “Dependence of T Cell Antigen Recognition on T Cell Receptor-peptide MHC Confinement Time.” In: *Immunity* (2010). DOI: 10.1016/j.immuni.2009.11.013.

[79] S. Valitutti et al. “Serial Triggering of Many T-cell Receptors by a Few Peptide-MHC Complexes.” In: *Nature* (1995). DOI: 10.1038/375148a0.

[80] A. M. Kalergis et al. “Efficient T Cell Activation Requires an Optimal Dwell-time of Interaction between the TCR and the pMHC Complex.” In: *Nat Immunol* (2001). DOI: 10.1038/85286.

[81] D. A. Schmid et al. “Evidence for a TCR Affinity Threshold Delimiting Maximal CD8 T Cell Function.” In: *Journal of Immunology* (2010). DOI: 10.4049/jimmunol.1000173.

[82] M. Lever et al. “Architecture of a Minimal Signaling Pathway Explains the T-cell Response to a 1 Million-fold Variation in Antigen Affinity and Dose.” In: *Proc Natl Acad Sci USA* (2016). DOI: 10.1073/pnas.1608820113.

[83] G. I. Bell, M. Dembo, and P. Bongrand. “Cell Adhesion. Competition between Nonspecific Repulsion and Specific Bonding.” In: *Biophys J* (1984). DOI: 10/b26sjz.

[84] W. T. Coakley and D. Gallez. “Membrane-membrane Contact: Involvement of Interfacial Instability in the Generation of Discrete Contacts.” In: *Biosci Rep* (1989). DOI: 10.1007/BF01114806.

[85] M. J. Footer et al. “Direct Measurement of Force Generation by Actin Filament Polymerization Using an Optical Trap.” In: *Proc Natl Acad Sci Usa* (2007). DOI: 10.1073/pnas.0607052104.

[86] N. J. Burroughs et al. “Boltzmann Energy-based Image Analysis Demonstrates That Extracellular Domain Size Differences Explain Protein Segregation at Immune Synapses.” In: *Plos Comput Biol* (2011). DOI: 10.1371/journal.pcbi.1002076.

[87] J. B. Huppa et al. “TCR-peptide-MHC Interactions in Situ Show Accelerated Kinetics and Increased Affinity.” In: *Nature* (2010). DOI: 10.1038/nature08746.

[88] J. Huang et al. “The Kinetics of Two-dimensional TCR and pMHC Interactions Determine T-cell Responsiveness.” In: *Nature* (2010). DOI: 10.1038/nature08944.

[89] J. Hong et al. “Force-regulated in Situ TCR-peptide-bound MHC Class II Kinetics Determine Functions of CD4+ T Cells.” In: *Journal of Immunology* (2015). DOI: 10.4049/jimmunol.1501407.

[90] M. Axmann et al. “Determination of Interaction Kinetics between the T Cell Receptor and Peptide-loaded MHC Class II Via Single-molecule Diffusion Measurements.” In: *Biophys J* (2012). DOI: 10.1016/j.bpj.2012.06.019.

[91] G. P. O’Donoghue et al. “Direct Single Molecule Measurement of TCR Triggering by Agonist pMHC in Living Primary T Cells.” In: *Elife* (2013). DOI: 10.7554/eLife.00778.

[92] L. V. Sibener et al. “Isolation of a Structural Mechanism for Uncoupling T Cell Receptor Signaling from Peptide-MHC Binding.” In: *Cell* (2018). DOI: 10.1016/j.cell.2018.06.017.

[93] L. E. Samelson et al. “Antigen Activation of Murine T Cells Induces Tyrosine Phosphorylation of a Polypeptide Associated with the T Cell Antigen Receptor.” In: *Cell* (1986). DOI: 10.1016/0092-8674(86)90708-7.

[94] J. E. Smith-Garvin, G. A. Koretzky, and M. S. Jordan. “T Cell Activation.” In: *Annual Review of Immunology* (2009). DOI: 10.1146/annurev.immunol.021908.132706.

[95] A. Veillette et al. “The CD4 and CD8 T Cell Surface Antigens Are Associated with the Internal Membrane Tyrosine-protein Kinase P56lck.” In: *Cell* (1988). DOI: 10.1016/0092-8674(88)90053-0.

[96] E. K. Barber et al. “The CD4 and CD8 Antigens Are Coupled to a Protein-tyrosine Kinase (p56lck) That Phosphorylates the CD3 Complex.” In: *Proc Natl Acad Sci USA* (1989). DOI: 10.1073/pnas.86.9.3277.

[97] A. M. Mørch et al. “Coreceptors and TCR Signaling – the Strong and the Weak of It.” In: *Frontiers in Cell and Developmental Biology* (2020). DOI: 10.3389/fcell.2020.597627.

[98] M. L. Hermiston, Z. Xu, and A. Weiss. “CD45: A Critical Regulator of Signaling Thresholds in Immune Cells.” In: *Annual Review of Immunology* (2003). DOI: 10.1146/annurev.immunol.21.120601.140946.

[99] S. J. Davis and P. A. van der Merwe. “The Kinetic-segregation Model: TCR Triggering and Beyond.” In: *Nat Immunol* (2006). DOI: 10.1038/ni1369.

[100] A. C. Chan et al. “Zap-70: A 70 Kd Protein-tyrosine Kinase That Associates with the TCR Zeta Chain.” In: *Cell* (1992). DOI: 10.1016/0092-8674(92)90598-7.

[101] M. Iwashima et al. “Sequential Interactions of the TCR with Two Distinct Cytoplasmic Tyrosine Kinases.” In: *Science* (1994). DOI: 10.1126/science.7509083.

[102] T. S. Finco et al. “Lat Is Required for TCR-mediated Activation of Plcgamma1 and the Ras Pathway.” In: *Immunity* (1998). DOI: 10.1016/s1074-7613(00)80659-7.

[103] W. Zhang et al. “Essential Role of Lat in T Cell Development.” In: *Immunity* (1999). DOI: 10.1016/s1074-7613(00)80032-1.

[104] W. Zhang et al. “Functional Analysis of Lat in TCR-mediated Signaling Pathways Using a Lat-deficient Jurkat Cell Line.” In: *International Immunology* (1999). DOI: 10.1093/intimm/11.6.943.

[105] N. H. Shah et al. “An Electrostatic Selection Mechanism Controls Sequential Kinase Signaling Downstream of the T Cell Receptor.” In: *eLife* (2016). Ed. by P. A. Cole. DOI: 10.7554/eLife.20105.

[106] L. Li et al. “Ionic CD3-lck Interaction Regulates the Initiation of T-cell Receptor Signaling.” In: *Proc Natl Acad Sci* (2017). DOI: 10.1073/pnas.1701990114.

[107] X. Su et al. “Phase Separation of Signaling Molecules Promotes T Cell Receptor Signal Transduction.” In: *Science* (2016). DOI: 10.1126/science.aad9964.

[108] F. Macián et al. “Transcriptional Mechanisms Underlying Lymphocyte Tolerance.” In: *Cell* (2002). DOI: 10.1016/s0092-8674(02)00767-5.

[109] D. Aivazian and L. J. Stern. “Phosphorylation of T Cell Receptor $\zeta$ Is Regulated by a Lipid Dependent Folding Transition.” In: *Nat Struct Biol* (2000). DOI: 10.1038/80930.

[110] C. Xu et al. “Regulation of T Cell Receptor Activation by Dynamic Membrane Binding of the CD3epsilon Cytoplasmic Tyrosine-based Motif.” In: *Cell* (2008). DOI: 10.1016/j.cell.2008.09.044.

[111] H. Zhang et al. “Basic Residues in the T-cell Receptor Zeta Cytoplasmic Domain Mediate Membrane Association and Modulate Signaling.” In: *Proc Natl Acad Sci USA* (2011). DOI: 10.1073/pnas.1108052108.

[112] X. Guo et al. “Lipid-dependent Conformational Dynamics Underlie the Functional Versatility of T-cell Receptor.” In: *Cell Res* (2017). DOI: 10.1038/cr.2017.42.

[113] R. A. Fernandes et al. “What Controls T Cell Receptor Phosphorylation?” In: *Cell* (2010). DOI: 10.1016/j.cell.2010.08.018.

[114] X. Shi et al. “Ca 2+ Regulates T-cell Receptor Activation by Modulating the Charge Property of Lipids.” In: *Nature* (2013). DOI: 10.1038/nature11699.

[115] O. Stepanek et al. “Coreceptor Scanning by the T Cell Receptor Provides a Mechanism for T Cell Tolerance.” In: *Cell* (2014). DOI: 10.1016/j.cell.2014.08.042.

[116] A. H. Courtney, W. L. Lo, and A. Weiss. “TCR Signaling: Mechanisms of Initiation and Propagation.” In: *Trends Biochem Sci* (2018). DOI: 10.1016/j.tibs.2017.11.008.

[117] T. R. Müller et al. “A T-cell Reporter Platform for High-throughput and Reliable Investigation of TCR Function and Biology.” In: *Clinical & Translational Immunology* (2020). DOI: 10.1002/cti2.1216.

[118] B. Laugel et al. “Different T Cell Receptor Affinity Thresholds and CD8 Coreceptor Dependence Govern Cytotoxic T Lymphocyte Activation and Tetramer Binding Properties.” In: *The Journal of Biological Chemistry* (2007). DOI: 10.1074/jbc.M700976200.

[119] P. Jonsson et al. “Remarkably Low Affinity of CD4/peptide-major Histocompatibility Complex Class II Protein Interactions.” In: *Proc Natl Acad Sci USA* (2016). DOI: 10.1073/pnas.1513918113.

[120] D. K. Cole et al. “The Molecular Determinants of CD8 Co-receptor Function.” In: *Immunology* (2012). DOI: 10.1111/j.1365-2567.2012.03625.x.

[121] D. Gangadharan and H. Cheroutre. “The CD8 Isoform CD8$\alpha\alpha$ Is Not a Functional Homologue of the TCR Co-receptor CD8$\alpha\beta$.” In: *Current Opinion in Immunology* (2004). DOI: 10.1016/j.coi.2004.03.015.

[122] R. Bosselut et al. “Unraveling a Revealing Paradox.” In: *Journal of Experimental Medicine* (2003). DOI: 10.1084/jem.20030170.

[123] R. Maile et al. “Peripheral CD8 Tuning Dynamically Modulates the Size and Responsiveness of an Antigen-specific T Cell Pool in Vivo.” In: *The Journal of Immunology* (2005). DOI: 10.4049/jimmunol.174.2.619.

[124] M. A. Daniels et al. “CD8 Binding to MHC Class I Molecules Is Influenced by T Cell Maturation and Glycosylation.” In: *Immunity* (2001). DOI: 10.1016/s1074-7613(01)00252-7.

[125] A. M. Moody et al. “Developmentally Regulated Glycosylation of the CD8$\alpha\beta$ Coreceptor Stalk Modulates Ligand Binding.” In: *Cell* (2001). DOI: 10.1016/s0092-8674(01)00577-3.

[126] M. A. Daniels, K. A. Hogquist, and S. C. Jameson. "Sweet 'n' Sour: The Impact of Differential Glycosylation on T Cell Responses." In: *Nat Immunol* (2002). DOI: 10.1038/ni1002-903.

[127] T. A. Springer et al. "The Lymphocyte Function-associated LFA-1, CD2, and LFA-3 Molecules: Cell Adhesion Receptors of the Immune System." In: *Annual Review of Immunology* (1987). DOI: 10.1146/annurev.iy.05.040187.001255.

[128] M. E. Sanders et al. "Human Memory T Lymphocytes Express Increased Levels of Three Cell Adhesion Molecules (LFA-3, CD2, and LFA-1) and Three Other Molecules (uchl1, Cdw29, and Pgp-1) and Have Enhanced Ifn-gamma Production." In: *Journal of Immunology* (1988).

[129] S. Ikemizu et al. "Crystal Structure of the CD2-binding Domain of CD58 (lymphocyte Function-associated Antigen 3) at 1.8-a Resolution." In: *Proc Natl Acad Sci USA* (1999).

[130] J. H. Wang et al. "Structure of a Heterophilic Adhesion Complex between the Human CD2 and CD58 (LFA-3) Counterreceptors." In: *Cell* (1999). DOI: 10.1016/s0092-8674(00)80790-4.

[131] P. A. van der Merwe et al. "Human Cell-adhesion Molecule CD2 Binds CD58 (LFA-3) with a Very Low Affinity and an Extremely Fast Dissociation Rate but Does Not Bind CD48 or CD59." In: *Biochemistry* (1994).

[132] D. Leckband et al. "Molecular Mechanisms Determining the Strength of Receptor-mediated Intermembrane Adhesion." In: *Biophys J* (1995). DOI: 10.1016/S0006-3495(95)79990-8.

[133] S. J. Davis and P. A. van der Merwe. "The Structure and Ligand Interactions of CD2: Implications for T-cell Function." In: *Immunol Today* (1996).

[134] D. M. Zhu et al. "Analysis of Two-dimensional Dissociation Constant of Laterally Mobile Cell Adhesion Molecules." In: *Biophys J* (2007). DOI: 10.1529/biophysj.106.089649.

[135] V. Junghans et al. "Effects of a Local Auxiliary Protein on the Two-dimensional Affinity of a TCR-peptide MHC Interaction." In: *Journal of cell science* (2020). DOI: 10.1242/jcs.245985.

[136] W. C. Hahn, S. J. Burakoff, and B. E. Bierer. "Signal Transduction Pathways Involved in T Cell Receptor-induced Regulation of CD2 Avidity for CD58." In: *J Immunol* (1993).

[137] D. M. Zhu et al. "Mechanisms of Cellular Avidity Regulation in CD2-CD58-mediated T Cell Adhesion." In: *Acs Chem Biol* (2006). DOI: 10.1021/cb6002515.

[138] P. Y. Chan et al. "Influence of Receptor Lateral Mobility on Adhesion Strengthening between Membranes Containing LFA-3 and CD2." In: *The Journal of Cell Biology* (1991). DOI: 10.1083/jcb.115.1.245.

[139] A. Brossay et al. "Porcine CD58: Cdna Cloning and Molecular Dissection of the Porcine CD58-human CD2 Interface." In: *Biochemical and Biophysical Research Communications* (2003). DOI: 10.1016/j.bbrc.2003.08.099.

[140] T. Shao et al. "Costimulatory Function of CD58/CD2 Interaction in Adaptive Humoral Immunity in a Zebrafish Model." In: *Front Immunol* (2018). DOI: 10.3389/fimmu.2018.01204.

[141] K. Kato et al. “CD48 Is a Counter-receptor for Mouse CD2 and Is Involved in T Cell Activation.” In: *J Exp Med* (1992).

[142] M. L. Dustin et al. “Low Affinity Interaction of Human or Rat T Cell Adhesion Molecule CD2 with Its Ligand Aligns Adhering Membranes to Achieve High Physiological Affinity.” In: *The Journal of Biological Chemistry* (1997). DOI: 10.1074/jbc.272.49.30889.

[143] M. H. Brown et al. “The CD2 Antigen Associates with the T-cell Antigen Receptor CD3 Antigen Complex on the Surface of Human T Lymphocytes.” In: *Nature* (1989). DOI: 10.1038/339551a0.

[144] A. D. Beyers, L. L. Spruyt, and A. F. Williams. “Molecular Associations between the T-lymphocyte Antigen Receptor Complex and the Surface Antigens CD2, CD4, or CD8 and CD5.” In: *Proc Natl Acad Sci USA* (1992).

[145] W. J. Kivens et al. “Identification of a Proline-rich Sequence in the CD2 Cytoplasmic Domain Critical for Regulation of Integrin-mediated Adhesion and Activation of Phosphoinositide 3-kinase.” In: *Molecular and Cellular Biology* (1998). DOI: 10.1128/mcb.18.9.5291.

[146] K. Nishizawa et al. “Identification of a Proline-binding Motif Regulating CD2-triggered T Lymphocyte Activation.” In: *Proc Natl Acad Sci USA* (1998).

[147] G. Moncalián et al. “Atypical Polyproline Recognition by the CMS N-terminal Src Homology 3 Domain.” In: *The Journal of Biological Chemistry* (2006). DOI: 10.1074/jbc.M606411200.

[148] K. H. Kirsch et al. “CMS: An Adapter Molecule Involved in Cytoskeletal Rearrangements.” In: *Proceedings of the National Academy of Sciences* (1999). DOI: 10.1073/pnas.96.11.6211.

[149] N. J. Hutchings et al. “Linking the T Cell Surface Protein CD2 to the Actin-capping Protein CAPZ Via CMS and CIN85.” In: *Journal of Biological Chemistry* (2003). DOI: 10.1074/jbc.m302540200.

[150] E. V. Tibaldi. “CD2BP3, CIN85 and the Structurally Related Adaptor Protein CMS Bind to the Same CD2 Cytoplasmic Segment, but Elicit Divergent Functional Activities.” In: *International Immunology* (2003). DOI: 10.1093/intimm/dxg032.

[151] G. M. Bell et al. “The Sh3 Domain of p56lck Binds to Proline-rich Sequences in the Cytoplasmic Domain of CD2.” In: *J Exp Med* (1996).

[152] M. L. Dustin et al. “A Novel Adaptor Protein Orchestrates Receptor Patterning and Cytoskeletal Polarity in T-cell Contacts.” In: *Cell* (1998).

[153] C. Freund et al. “Dynamic Interaction of CD2 with the GYF and the SH3 Domain of Compartmentalized Effector Molecules.” In: *Embo J* (2002). DOI: 10.1093/emboj/cdf602.

[154] J. Li et al. “A Cdc15-like Adaptor Protein (CD2BP1) Interacts with the CD2 Cytoplasmic Domain and Regulates CD2-triggered Adhesion.” In: *Embo J* (1998). DOI: 10.1093/emboj/17.24.7320.

[155] C. Freund et al. “The GYF Domain Is a Novel Structural Fold That Is Involved in Lymphoid Signaling through Proline-rich Sequences.” In: *Nature Structural Biology* (1999). DOI: 10.1038/10712.

[156] W. C. Hahn et al. “A Distinct Cytoplasmic Domain of CD2 Regulates Ligand Avidity and T-cell Responsiveness to Antigen.” In: *Proc Natl Acad Sci USA* (1992).

[157] W. C. Hahn and B. E. Bierer. “Separable Portions of the CD2 Cytoplasmic Domain Involved in Signaling and Ligand Avidity Regulation.” In: *The Journal of Experimental Medicine* (1993). DOI: 10.1084/jem.178.5.1831.

[158] J. Leitner et al. “CD58/CD2 Is the Primary Costimulatory Pathway in Human CD28-CD8+ T Cells.” In: *J Immunol* (2015). DOI: 10.4049/jimmunol.1401917.

[159] J. M. Green et al. “Coordinate Regulation of T Cell Activation by CD2 and CD28.” In: *J Immunol* (2000).

[160] E. Parra et al. “Costimulation by B7-1 and LFA-3 Targets Distinct Nuclear Factors That Bind to the Interleukin-2 Promoter: B7-1 Negatively Regulates LFA-3-induced NFAT Dna Binding.” In: *Mol Cell Biol* (1997). DOI: 10.1128/MCB.17.3.1314.

[161] M. E. Kalland et al. “T Cell-signaling Network Analysis Reveals Distinct Differences between CD28 and CD2 Costimulation Responses in Various Subsets and in the Mapk Pathway between Resting and Activated Regulatory T Cells.” In: *Journal of Immunology* (2011). DOI: 10.4049/jimmunol.1101804.

[162] V. Zurli et al. “Phosphoproteomics of CD2 Signaling Reveals Ampk-dependent Regulation of Lytic Granule Polarization in Cytotoxic T Cells.” In: *Sci Signal* (2020). DOI: 10.1126/scisignal.aaz1965.

[163] S. J. Davis et al. “The Nature of Molecular Recognition by T Cells.” In: *Nat Immunol* (2003). DOI: 10.1038/ni0303-217.

[164] S. K. Bromley et al. “The Immunological Synapse and CD28-CD80 Interactions.” In: *Nat Immunol* (2001). DOI: 10.1038/ni737.

[165] M. F. Bachmann, M. Barner, and M. Kopf. “CD2 Sets Quantitative Thresholds in T Cell Activation.” In: *The Journal of Experimental Medicine* (1999).

[166] K. Singleton et al. “A Large T Cell Invagination with CD2 Enrichment Resets Receptor Engagement in the Immunological Synapse.” In: *J Immunol* (2006).

[167] Y. Kaizuka et al. “The Coreceptor CD2 Uses Plasma Membrane Microdomains to Transduce Signals in T Cells.” In: *J Cell Biol* (2009). DOI: 10.1083/jcb.200809136.

[168] P. Demetriou et al. “A Dynamic CD2-rich Compartment at the Outer Edge of the Immunological Synapse Boosts and Integrates Signals.” In: *Nature Immunology* (2020). DOI: 10.1038/s41590-020-0770-x.

[169] O. Milstein et al. “Nanoscale Increases in CD2-CD48-mediated Intermembrane Spacing Decrease Adhesion and Reorganize the Immunological Synapse.” In: *The Journal of Biological Chemistry* (2008). DOI: 10.1074/jbc.M804756200.

[170] B. A. Kyewski et al. “The Effects of Anti-CD2 Antibodies on the Differentiation of Mouse Thymocytes.” In: *European Journal of Immunology* (1989). DOI: 10.1002/eji.1830190526.

[171] N. Killeen, S. G. Stuart, and D. R. Littman. “Development and Function of T Cells in Mice with a Disrupted CD2 Gene.” In: *Embo J* (1992).

[172] C. F. Evans et al. “CD2-deficient Mice Generate Virus-specific Cytotoxic T Lymphocytes upon Infection with Lymphocytic Choriomeningitis Virus.” In: *J Immunol* (1993).

[173] B. Guckel et al. “Anti-CD2 Antibodies Induce T Cell Unresponsiveness in Vivo.” In: *J Exp Med* (1991).

[174] S. J. Teh et al. “CD2 Regulates the Positive Selection and Function of Antigen-specific CD4- CD8+ T Cells.” In: *Blood* (1997). DOI: 10.1182/blood.v89.4.1308.

[175] T. Sasada and E. L. Reinherz. “A Critical Role for CD2 in Both Thymic Selection Events and Mature T Cell Function.” In: *Journal of Immunology* (2001). DOI: 10.4049/jimmunol.166.4.2394.

[176] T. Sasada, H. Yang, and E. L. Reinherz. “CD2 Facilitates Differentiation of CD4 Th Cells without Affecting Th1/th2 Polarization.” In: *Journal of Immunology* (2002). DOI: 10.4049/jimmunol.168.3.1113.

[177] A. Rolle et al. “CD2-CD58 Interactions Are Pivotal for the Activation and Function of Adaptive Natural Killer Cells in Human Cytomegalovirus Infection.” In: *European Journal of Immunology* (2016).

[178] E. C. Y. Wang et al. “Suppression of Costimulation by Human Cytomegalovirus Promotes Evasion of Cellular Immune Defenses.” In: *Proc Natl Acad Sci USA* (2018). DOI: 10.1073/pnas.1720950115.

[179] S. J. Patel et al. “Identification of Essential Genes for Cancer Immunotherapy.” In: *Nature* (2017). DOI: 10.1038/nature23477.

[180] E. J. Cheadle et al. “Ligation of the CD2 Co-stimulatory Receptor Enhances IL-2 Production from First-generation Chimeric Antigen Receptor T Cells.” In: *Gene Ther* (2012). DOI: 10.1038/gt.2011.192.

[181] “Uncovering a Culprit in CAR-T Resistance.” In: *Cancer discovery* (2020). DOI: 10.1158/2159-8290.CD-NB2020-111.

[182] M. Challa-Malladi et al. “Combined Genetic Inactivation of $\beta$ 2-microglobulin and CD58 Reveals Frequent Escape from Immune Recognition in Diffuse Large B Cell Lymphoma.” In: *Cancer Cell* (2011). DOI: 10.1016/j.ccr.2011.11.006.

[183] F. R. Abdul Razak et al. “CD58 Mutations Are Common in Hodgkin Lymphoma Cell Lines and Loss of CD58 Expression in Tumor Cells Occurs in Hodgkin Lymphoma Patients Who Relapse.” In: *Genes and immunity* (2016). DOI: 10.1038/gene.2016.30.

[184] P. L. De Jager et al. “The Role of the CD58 Locus in Multiple Sclerosis.” In: *Proc Natl Acad Sci Usa* (2009). DOI: 10.1073/pnas.0813310106.

[185] J. Y. Kim et al. “CD58 Polymorphisms Associated with the Risk of Neuromyelitis Optica in a Korean Population.” In: *BMC Neurology* (2014). DOI: 10.1186/1471-2377-14-57.

[186] S. Raychaudhuri et al. “Genetic Variants at CD28 , Prdm1 and CD2/CD58 Are Associated with Rheumatoid Arthritis Risk.” In: *Nat Genet* (2009). DOI: 10.1038/ng.479.

[187] H. I. Fraser et al. “Ptpn22 and CD2 Variations Are Associated with Altered Protein Expression and Susceptibility to Type 1 Diabetes in Nonobese Diabetic Mice.” In: *Journal of Immunology* (2015). DOI: 10.4049/jimmunol.1402654.

[188] C. Jenneck and N. Novak. “The Safety and Efficacy of Alefacept in the Treatment of Chronic Plaque Psoriasis.” In: *Therapeutics and Clinical Risk Management* (2007).

[189] M. R. Rigby et al. “Alefacept Provides Sustained Clinical and Immunological Effects in New-onset Type 1 Diabetes Patients.” In: *The Journal of Clinical Investigation* (2015).

[190] T. R. Spitzer et al. “Nonmyeloablative Haploidentical Stem-cell Transplantation Using Anti-CD2 Monoclonal Antibody (medi-507)-based Conditioning for Refractory Hematologic Malignancies.” In: *Transplantation* (2003). DOI: 10.1097/01.tp.0000064211.23536.ad.

[191] C. Koenecke et al. “Nk Cell Recovery, Chimerism, Function, and Recognition in Recipients of Haploidentical Hematopoietic Cell Transplantation Following Nonmyeloablative Conditioning Using a Humanized Anti-CD2 Mab, Medi-507.” In: *Experimental Hematology* (2003). DOI: 10.1016/s0301-472x(03)00224-8.

[192] T. L. Pruett et al. “Safety Profile, Pharmacokinetics, and Pharmacodynamics of Siplizumab, a Humanized Anti-CD2 Monoclonal Antibody, in Renal Allograft Recipients.” In: *Transplantation Proceedings* (2009). DOI: 10.1016/j.transproceed.2009.06.226.

[193] D. Adkins et al. “Safety Profile and Clinical Outcomes in a Phase I, Placebo-controlled Study of Siplizumab in Acute Graft-versus-host Disease.” In: *Transplantation* (2009). DOI: 10.1097/tp.0b013e3181abfbf7.

[194] R. G. Langley et al. “Safety Profile of Intravenous and Subcutaneous Siplizumab, an Anti-CD2 Monoclonal Antibody, for the Treatment of Plaque Psoriasis: Results of Two Randomized, Double-blind, Placebo-controlled Studies.” In: *International Journal of Dermatology* (2010). DOI: 10.1111/j.1365-4632.2010.04512.x.

[195] J. Roswarski et al. “Phase I Dose Escalation Study of the Anti-CD2 Monoclonal Antibody, Siplizumab, with Da-epoch-r in Aggressive Peripheral T-cell Lymphomas.” In: *Leukemia & Lymphoma* (2017). DOI: 10.1080/10428194.2017.1387908.

[196] A. Gokhale et al. “Immunosuppression by Co-stimulatory Molecules: Inhibition of CD2-CD48/CD58 Interaction by Peptides from CD2 to Suppress Progression of Collagen-induced Arthritis in Mice.” In: *Chemical Biology & Drug Design* (2013). DOI: 10.1111/cbdd.12138.

[197] A. S. Gokhale et al. “Inhibition of Cell Adhesion and Immune Responses in the Mouse Model of Collagen-induced Arthritis with a Peptidomimetic That Blocks CD2-CD58 Interface Interactions.” In: *Biopolymers* (2015). DOI: 10.1002/bip.22692.

[198] J. T. Pribila et al. “Integrins and T Cell–mediated Immunity.” In: *Annu Rev Immunol* (2004). DOI: 10.1146/annurev.immunol.22.012703.104649.

[199] T. K. Kishimoto et al. “Heterogeneous Mutations in the Beta Subunit Common to the LFA-1, Mac-1, and P150,95 Glycoproteins Cause Leukocyte Adhesion Deficiency.” In: *Cell* (1987). DOI: 10.1016/0092-8674(87)90215-7.

[200] B.-H. Luo, C. V. Carman, and T. A. Springer. “Structural Basis of Integrin Regulation and Signaling.” In: *Annual Review of Immunology* (2007). DOI: 10.1146/annurev.immunol.25.022106.141618.

[201] P. L. Reilly et al. “The Native Structure of Intercellular Adhesion Molecule-1 (icam-1) Is a Dimer. Correlation with Binding to LFA-1.” In: *Journal of Immunology* (1995).

[202] J. Miller et al. “Intercellular Adhesion Molecule-1 Dimerization and Its Consequences for Adhesion Mediated by Lymphocyte Function Associated-1.” In: *The Journal of Experimental Medicine* (1995). DOI: 10.1084/jem.182.5.1231.

[203] M. Uhlén et al. “Proteomics. Tissue-based Map of the Human Proteome.” In: *Science* (2015). DOI: 10.1126/science.1260419.

[204] M. E. Labadia et al. “Molecular Regulation of the Interaction between Leukocyte Function-associated Antigen-1 and Soluble ICAM-1 by Divalent Metal Cations.” In: *Journal of Immunology* (1998).

[205] M. Shimaoka et al. “Reversibly Locking a Protein Fold in an Active Conformation with a Disulfide Bond: Integrin Alphal I Domains with High Affinity and Antagonist Activity in Vivo.” In: *Proc Natl Acad Sci Usa* (2001). DOI: 10.1073/pnas.101130498.

[206] J. R. Woska et al. “Characterization of Molecular Interactions between Intercellular Adhesion Molecule-1 and Leukocyte Function-Associated Antigen-1.” In: *Journal of Immunology* (1996).

[207] M. Shimaoka et al. “Structures of the Alpha L I Domain and Its Complex with ICAM-1 Reveal a Shape-shifting Pathway for Integrin Regulation.” In: *Cell* (2003). DOI: 10.1016/s0092-8674(02)01257-6.

[208] N. Hogg, I. Patzak, and F. Willenbrock. “The Insider’s Guide to Leukocyte Integrin Signalling and Function.” In: *Nat Rev Immunol* (2011). DOI: 10.1038/nri2986.

[209] R. Shamri et al. “Lymphocyte Arrest Requires Instantaneous Induction of an Extended LFA-1 Conformation Mediated by Endothelium-bound Chemokines.” In: *Nature Immunology* (2005). DOI: 10.1038/ni1194.

[210] W. Chen, J. Lou, and C. Zhu. “Forcing Switch from Short- to Intermediate- and Long-lived States of the Alphaa Domain Generates LFA-1/icam-1 Catch Bonds.” In: *The Journal of Biological Chemistry* (2010). DOI: 10.1074/jbc.M110.155770.

[211] W. A. Comrie et al. “The Dendritic Cell Cytoskeleton Promotes T Cell Adhesion and Activation by Constraining ICAM-1 Mobility.” In: *J Cell Biol* (2015). DOI: 10.1083/jcb.201406120.

[212] R. Evans et al. “The Integrin LFA-1 Signals through Zap-70 to Regulate Expression of High-affinity LFA-1 on T Lymphocytes.” In: *Blood* (2011). DOI: 10.1182/blood-2010-06-289140.

[213] C. R. Monks et al. “Three-dimensional Segregation of Supramolecular Activation Clusters in T Cells.” In: *Nature* (1998). DOI: 10.1038/25764.

[214] A. Grakoui et al. “The Immunological Synapse: A Molecular Machine Controlling T Cell Activation.” In: *Science* (1999).

[215] T. A. Springer. “Adhesion Receptors of the Immune System.” In: *Nature* (1990). DOI: 10.1038/346425a0.

[216] A. Hashimoto-Tane et al. “Micro-adhesion Rings Surrounding TCR Microclusters Are Essential for T Cell Activation.” In: *J Exp Med* (2016). DOI: 10.1084/jem.20151088.

[217] P. T. Sage et al. “Antigen Recognition Is Facilitated by Invadosome-like Protrusions Formed by Memory/effector T Cells.” In: *J Immunol* (2012). DOI: 10.4049/jimmunol.1102594.

[218] R. Schmits et al. “LFA-1-deficient Mice Show Normal Ctl Responses to Virus but Fail to Reject Immunogenic Tumor.” In: *The Journal of Experimental Medicine* (1996). DOI: 10.1084/jem.183.4.1415.

[219] N. Parameswaran et al. “Lack of ICAM-1 on Apcs during T Cell Priming Leads to Poor Generation of Central Memory Cells.” In: *Journal of Immunology* (2005). DOI: 10.4049/jimmunol.175.4.2201.

[220] N. A. Zumwalde et al. “ICAM-1-dependent Homotypic Aggregates Regulate CD8 T Cell Effector Function and Differentiation during T Cell Activation.” In: *Journal of Immunology* (2013). DOI: 10.4049/jimmunol.1201954.

[221] Z. Cai et al. “Requirements for Peptide-induced T Cell Receptor Downregulation on Naive CD8+ T Cells.” In: *The Journal of Experimental Medicine* (1997). DOI: 10.1084/jem.185.4.641.

[222] M. F. Bachmann et al. “Distinct Roles for LFA-1 and CD28 during Activation of Naive T Cells: Adhesion Versus Costimulation.” In: *Immunity* (1997).

[223] Y. Wang et al. “LFA-1 Decreases the Antigen Dose for T Cell Activation in Vivo.” In: *International Immunology* (2008). DOI: 10.1093/intimm/dxn070.

[224] Y. R. Carrasco et al. “LFA-1/ICAM-1 Interaction Lowers the Threshold of B Cell Activation by Facilitating B Cell Adhesion and Synapse Formation.” In: *Immunity* (2004). DOI: 10.1016/S1074-7613(04)00105-0.

[225] M. Marski et al. “CD18 Is Required for Optimal Development and Function of CD4+CD25+ T Regulatory Cells.” In: *Journal of Immunology* (2005). DOI: 10.4049/jimmunol.175.12.7889.

[226] J. Wohler et al. “LFA-1 Is Critical for Regulatory T Cell Homeostasis and Function.” In: *Molecular Immunology* (2009). DOI: 10.1016/j.molimm.2009.04.004.

[227] L. A. Zuckerman, L. Pullen, and J. Miller. “Functional Consequences of Costimulation by ICAM-1 on IL-2 Gene Expression and T Cell Activation.” In: *Journal of Immunology* (1998).

[228] J. L. Ragazzo et al. “Costimulation Via Lymphocyte Function-associated Antigen 1 in the Absence of CD28 Ligation Promotes Anergy of Naive CD4+ T Cells.” In: *Proc Natl Acad Sci Usa* (2001). DOI: 10.1073/pnas.011397798.

[229] P. S.-H. Park, D. T. Lodowski, and K. Palczewski. “Activation of G Protein-coupled Receptors: Beyond Two-state Models and Tertiary Conformational Changes.” In: *Annual Review of Pharmacology and Toxicology* (2008). DOI: 10.1146/annurev.pharmtox.48.113006.094630.

[230] B. Knapp et al. “MHC Binding Affects the Dynamics of Different T-cell Receptors in Different Ways.” In: *Plos Computational Biology* (2019). DOI: 10.1371/journal.pcbi.1007338.

[231] D. Depoil and M. L. Dustin. “Force and Affinity in Ligand Discrimination by the TCR.” In: *Trends in Immunology* (2014). DOI: 10.1016/j.it.2014.10.007.

[232] J.-h. Wang and E. L. Reinherz. “The Structural Basis of $\mathrm{A}\beta$ T-lineage Immune Recognition: TCR Docking Topologies, Mechanotransduction, and Co-receptor Function.” In: *Immunological Reviews* (2012). DOI: 10.1111/j.1600-065X.2012.01161.x.

[233] D. K. Das et al. “Force-dependent Transition in the T-cell Receptor $\beta$-subunit Allosterically Regulates Peptide Discrimination and pMHC Bond Lifetime.” In: *Proc Natl Acad Sci USA* (2015). DOI: 10.1073/pnas.1424829112.

[234] P. Wu et al. “Mechano-regulation of Peptide-MHC Class I Conformations Determines TCR Antigen Recognition.” In: *Mol Cell* (2019). DOI: 10.1016/j.molcel.2018.12.018.

[235] K. N. Brazin et al. “The T Cell Antigen Receptor $\alpha$ Transmembrane Domain Coordinates Triggering through Regulation of Bilayer Immersion and CD3 Subunit Associations.” In: *Immunity* (2018). DOI: 10.1016/j.immuni.2018.09.007.

[236] D. K. Das et al. “Pre-T Cell Receptors (pre-TCRs) Leverage V$\beta$ Complementarity Determining Regions (CDRs) and Hydrophobic Patch in Mechanosensing Thymic Self-ligands.” In: *J Biol Chem* (2016).

[237] S. T. Kim et al. “Distinctive CD3 Heterodimeric Ectodomain Topologies Maximize Antigen-triggered Activation of $\alpha\beta$ T Cell Receptors.” In: *The Journal of Immunology* (2010). DOI: 10.4049/jimmunol.1000732.

[238] J. Delon, K. Kaibuchi, and R. N. Germain. “Exclusion of CD43 from the Immunological Synapse Is Mediated by Phosphorylation-regulated Relocation of the Cytoskeletal Adaptor Moesin.” In: *Immunity* (2001). DOI: 10.1016/s1074-7613(01)00231-x.

[239] E. J. Allenspach et al. “Erm-dependent Movement of CD43 Defines a Novel Protein Complex Distal to the Immunological Synapse.” In: *Immunity* (2001). DOI: 10.1016/s1074-7613(01)00224-2.

[240] B. A. Freiberg et al. “Staging and Resetting T Cell Activation in Smacs.” In: *Nature Immunology* (2002). DOI: 10.1038/ni836.

[241] N. Blanchard, V. D. Bartolo, and C. Hivroz. “In the Immune Synapse, Zap-70 Controls T Cell Polarization and Recruitment of Signaling Proteins but Not Formation of the Synaptic Pattern.” In: *Immunity* (2002). DOI: 10.1016/s1074-7613(02)00421-1.

[242] E. Fischer, H. Charbonneau, and N. Tonks. “Protein Tyrosine Phosphatases: A Diverse Family of Intracellular and Transmembrane Enzymes.” In: *Science* (1991). DOI: 10.1126/science.1650499.

[243] N. J. Burroughs, Z. Lazic, and P. A. van der Merwe. “Ligand Detection and Discrimination by Spatial Relocalization: A Kinase-phosphatase Segregation Model of TCR Activation.” In: *Biophys J* (2006). DOI: 10.1529/biophysj.105.080044.

[244] Y. Razvag et al. “Nanoscale Kinetic Segregation of TCR and CD45 in Engaged Microvilli Facilitates Early T Cell Activation.” In: *Nat Commun* (2018). DOI: 10.1038/s41467-018-03127-w.

[245] R. A. Fernandes et al. “A Cell Topography-based Mechanism for Ligand Discrimination by the T Cell Receptor.” In: *Proc Natl Acad Sci USA* (2019). DOI: 10.1073/pnas.1817255116.

[246] O. Dushek, J. Goyette, and P. A. van der Merwe. “Non-catalytic Tyrosine-phosphorylated Receptors.” In: *Immunol Rev* (2012). DOI: 10.1111/imr.12008.

[247] M. H. Bakalar et al. “Size-dependent Segregation Controls Macrophage Phagocytosis of Antibody-opsonized Targets.” In: *Cell* (2018). DOI: 10.1016/j.cell.2018.05.059.

[248] V. Junghans et al. “Hydrodynamic Trapping Measures the Interaction between Membrane-associated Molecules.” In: *Sci Rep* (2018). DOI: 10.1038/s41598-018-30285-0.

[249] G. I. Bell. “Models for the Specific Adhesion of Cells to Cells.” In: *Science* (1978).

[250] C. B. Carbone et al. “In Vitro Reconstitution of T Cell Receptor-mediated Segregation of the CD45 Phosphatase.” In: *Proc Natl Acad Sci USA* (2017). DOI: 10.1073/pnas.1710358114.

[251] E. M. Schmid et al. “Size-dependent Protein Segregation at Membrane Interfaces.” In: *Nat Phys* (2016). DOI: 10.1038/nphys3678.

[252] T. W. McKeithan. “Kinetic Proofreading in T-cell Receptor Signal Transduction.” In: *Proc Natl Acad Sci USA* (1995). DOI: 10.1073/pnas.92.11.5042.

[253] M. Lever et al. “Phenotypic Models of T Cell Activation.” In: *Nat Rev Immunol* (2014). DOI: 10.1038/nri3728.

[254] J. J. Hopfield. “Kinetic Proofreading: A New Mechanism for Reducing Errors in Biosynthetic Processes Requiring High Specificity.” In: *Proc Natl Acad Sci USA* (1974). DOI: 10/fmhbd9.

[255] J. Ninio. “Kinetic Amplification of Enzyme Discrimination.” In: *Biochimie* (1975). DOI: 10/cj2s9r.

[256] W. Cui and P. Mehta. “Identifying Feasible Operating Regimes for Early T-cell Recognition: The Speed, Energy, Accuracy Trade-off in Kinetic Proofreading and Adaptive Sorting.” In: *Plos One* (2018). DOI: 10.1371/journal.pone.0202331.

[257] W.-L. Lo et al. “Slow Phosphorylation of a Tyrosine Residue in Lat Optimizes T Cell Ligand Discrimination.” In: *Nature Immunology* (2019). DOI: 10.1038/s41590-019-0502-2.

[258] J.-B. Lalanne and P. François. “Principles of Adaptive Sorting Revealed by in Silico Evolution.” In: *Physical Review Letters* (2013). DOI: 10.1103/PhysRevLett.110.218102.

[259] P. Francois et al. “Phenotypic Model for Early T-cell Activation Displaying Sensitivity, Specificity, and Antagonism.” In: *Proc Natl Acad Sci USA* (2013). DOI: 10.1073/pnas.1300752110.

[260] P. François et al. “Phenotypic Spandrel: Absolute Discrimination and Ligand Antagonism.” In: *Physical Biology* (2016). DOI: 10.1088/1478-3975/13/6/066011.

[261] B. N. Dittel et al. “Cross-antagonism of a T Cell Clone Expressing Two Distinct T Cell Receptors.” In: *Immunity* (1999). DOI: 10.1016/s1074-7613(00)80104-1.

[262] J. M. Robertson and B. D. Evavold. “Cutting Edge: Dueling TCRs: Peptide Antagonism of CD4+ T Cells with Dual Antigen Specificities.” In: *Journal of Immunology* (1999).

[263] I. Stefanová et al. “TCR Ligand Discrimination Is Enforced by Competing Erk Positive and Shp-1 Negative Feedback Pathways.” In: *Nature Immunology* (2003). DOI: 10.1038/ni895.

[264] S. H. Stotz et al. “T Cell Receptor (TCR) Antagonism without a Negative Signal: Evidence from T Cell Hybridomas Expressing Two Independent TCRs.” In: *The Journal of Experimental Medicine* (1999). DOI: 10.1084/jem.189.2.253.

[265] M. A. Daniels et al. “Cutting Edge: A Test of the Dominant Negative Signal Model for TCR Antagonism.” In: *Journal of Immunology* (1999).

[266] C. Klammt and B. F. Lillemeier. “How Membrane Structures Control T Cell Signaling.” In: *Front Immunol* (2012). DOI: 10.3389/fimmu.2012.00291.

[267] V. Gudipati et al. “Inefficient CAR-proximal Signaling Blunts Antigen Sensitivity.” In: *Nature immunology* (2020). DOI: 10.1038/s41590-020-0719-0.

[268] J. Goyette et al. “Regulated Unbinding of Zap70 at the T Cell Receptor by Kinetic Avidity.” In: (2020). DOI: 10.1101/2020.02.12.945170.

[269] B. Liu et al. “Accumulation of Dynamic Catch Bonds between TCR and Agonist Peptide-MHC Triggers T Cell Signaling.” In: *Cell* (2014). DOI: 10.1016/j.cell.2014.02.053.

[270] V. I. Zarnitsyna et al. “Memory in Receptor–ligand-mediated Cell Adhesion.” In: *Proc Natl Acad Sci* (2007). DOI: 10.1073/pnas.0704811104.

[271] L. Limozin et al. “TCR-pMHC kinetics under force in a cell-free system show no intrinsic catch bond, but a minimal encounter duration before binding.” In: *Proc Natl Acad Sci USA* (2019). DOI: 10.1073/pnas.1902141116.

[272] J. Hong et al. “A TCR Mechanotransduction Signaling Loop Induces Negative Selection in the Thymus.” In: *Nature immunology* (2018). DOI: 10.1038/s41590-018-0259-z.

[273] E. Klotzsch and G. J. Schütz. “Improved Ligand Discrimination by Force-induced Unbinding of the T Cell Receptor from Peptide-MHC.” In: *Biophysical Journal* (2013). DOI: 10.1016/j.bpj.2013.03.023.

[274] P. A. van der Merwe. “A Subtle Role for CD2 in T Cell Antigen Recognition.” In: *The Journal of Experimental Medicine* (1999).

[275] B. L. Walling and M. Kim. “LFA-1 in T Cell Migration and Differentiation.” In: *Frontiers in immunology* (2018). DOI: 10.3389/fimmu.2018.00952.

[276] E. Jäger et al. “Simultaneous Humoral and Cellular Immune Response against Cancer-testis Antigen NY-ESO-1: Definition of Human Histocompatibility Leukocyte Antigen (HLA)-A2-binding Peptide Epitopes.” In: *The Journal of Experimental Medicine* (1998). DOI: 10.1084/jem.187.2.265.

[277] N. Trendel et al. “Perfect Adaptation of CD8 T Cell Responses to Constant Antigen Input Over a Wide Range of Affinity Is Overcome by Costimulation.” In: (2019). DOI: 10.1101/535385.

[278] A. Viola and A. Lanzavecchia. “T Cell Activation Determined by T Cell Receptor Number and Tunable Thresholds.” In: *Science* (1996). DOI: 10.1126/science.273.5271.104.

[279] E. M. Denham et al. “A Generic Cell Surface Ligand System for Studying Cell-cell Recognition.” In: *Plos Biology* (2019). DOI: 10.1371/journal.pbio.3000549.

[280] Z. Liu, B. Guo, and R. D. Lopez. “Expression of Intercellular Adhesion Molecule (ICAM)-1 or ICAM-2 Is Critical in Determining Sensitivity of Pancreatic Cancer Cells to Cytolysis by Human Gammadelta-T Cells: Implications in the Design of $\gamma\delta$-T-cell-based Immunotherapies for Pancreatic Cancer.” In: *Journal of Gastroenterology and Hepatology* (2009). DOI: 10.1111/j.1440-1746.2008.05668.x.

[281] C. E. Griffiths et al. “The ICAM-3/LFA-1 Interaction Is Critical for Epidermal Langerhans Cell Alloantigen Presentation to CD4 T Cells.” In: *The British Journal of Dermatology* (1995). DOI: 10.1111/j.1365-2133.1995.tb06911.x.

[282] K. H. Biswas et al. “E-cadherin Junction Formation Involves an Active Kinetic Nucleation Process.” In: *Proc Natl Acad Sci USA* (2015). DOI: 10.1073/pnas.1513775112.

[283] A.-S. Smith et al. “Force-induced Growth of Adhesion Domains Is Controlled by Receptor Mobility.” In: *Proc Natl Acad Sci USA* (2008). DOI: 10.1073/pnas.0801706105.

[284] R. L. Rich and D. G. Myszka. “Advances in Surface Plasmon Resonance Biosensor Analysis.” In: *Current Opinion in Biotechnology* (2000). DOI: 10.1016/s0958-1669(99)00054-3.

[285] D. G. Myszka. “Improving Biosensor Analysis.” In: *J Mol Recognit* (1999). DOI: 10.1002/(SICI)1099-1352(199909/10)12:5<279::AID-JMR473>3.0.CO;2-3.

[286] Y. H. Ding et al. “Two Human T Cell Receptors Bind in a Similar Diagonal Mode to the HLA-A2/Tax Peptide Complex Using Different TCR Amino Acids.” In: *Immunity* (1998). DOI: 10.1016/s1074-7613(00)80546-4.

[287] O. Y. Borbulevych et al. “T Cell Receptor Cross-reactivity Directed by Antigen-dependent Tuning of Peptide-MHC Molecular Flexibility.” In: *Immunity* (2009). DOI: 10.1016/j.immuni.2009.11.003.

[288] O. Y. Borbulevych, K. H. Piepenbrink, and B. M. Baker. “Conformational Melding Permits a Conserved Binding Geometry in TCR Recognition of Foreign and Self Molecular Mimics.” In: *J Immunol* (2011). DOI: 10.4049/jimmunol.1003150.

[289] H. Zhang et al. “The Contribution of Major Histocompatibility Complex Contacts to the Affinity and Kinetics of T Cell Receptor Binding.” In: *Sci Rep* (2016). DOI: 10.1038/srep35326.

[290] M. G. Rudolph, R. L. Stanfield, and I. A. Wilson. “How TCRs Bind MHCs, Peptides, and Coreceptors.” In: *Annu Rev Immunol* (2006). DOI: 10.1146/annurev.immunol.23.021704.115658.

[291] B. J. Cameron et al. “Identification of a Titin-derived HLA-A1-presented Peptide As a Cross-reactive Target for Engineered Mage A3-directed T Cells.” In: *Science Translational Medicine* (2013). DOI: 10.1126/scitranslmed.3006034.

[292] O. Dushek, R. Das, and D. Coombs. “A Role for Rebinding in Rapid and Reliable T Cell Responses to Antigen.” In: *Plos Comput Biol* (2009). DOI: 10.1371/journal.pcbi.1000578.

[293] M. A. Purbhoo et al. “Quantifying and Imaging NY-ESO-1/Lage-1-derived Epitopes on Tumor Cells Using High Affinity T Cell Receptors.” In: *Journal of Immunology* (2006). DOI: 10.4049/jimmunol.176.12.7308.

[294] D. K. Cole et al. “Hotspot Autoimmune T Cell Receptor Binding Underlies Pathogen and Insulin Peptide Cross-reactivity.” In: *The Journal of clinical investigation* (2016). DOI: 10.1172/JCI85679.

[295] B. Liu et al. “The Cellular Environment Regulates in Situ Kinetics of T-cell Receptor Interaction with Peptide Major Histocompatibility Complex.” In: *European Journal of Immunology* (2015). DOI: 10.1002/eji.201445358.

[296] J. Hong et al. “Contractile Actomyosin Arcs Promote the Activation of Primary Mouse T Cells in a Ligand-dependent Manner.” In: *PLoS One* (2017). DOI: 10.1371/journal.pone.0183174.

[297] Y. Feng et al. “Mechanosensing Drives Acuity of Alphabeta T-cell Recognition.” In: *Proc Natl Acad Sci USA* (2017). DOI: 10.1073/pnas.1703559114.

[298] A. P. Rapoport et al. “NY-ESO-1-specific TCR-engineered T Cells Mediate Sustained Antigen-specific Antitumor Effects in Myeloma.” In: *Nature medicine* (2015). DOI: 10.1038/nm.3910.

[299] S. Z. Josefowicz, L.-F. Lu, and A. Y. Rudensky. “Regulatory T Cells: Mechanisms of Differentiation and Function.” In: *Annual Review of Immunology* (2012). DOI: 10.1146/annurev.immunol.25.022106.141623.

[300] L. Chen and D. B. Flies. “Molecular Mechanisms of T Cell Co-stimulation and Co-inhibition.” In: *Nat Rev Immunol* (2013). DOI: 10.1038/nri3405.

[301] C. Paluch et al. “Immune Checkpoints As Therapeutic Targets in Autoimmunity.” In: *Frontiers in Immunology* (2018). DOI: 10.3389/fimmu.2018.02306.

[302] Y. Korem Kohanim et al. “Endocrine Autoimmune Disease As a Fragility of Immune Surveillance against Hypersecreting Mutants.” In: *Immunity* (2020). DOI: 10.1016/j.immuni.2020.04.022.

[303] D. Mason. “A Very High Level of Crossreactivity Is an Essential Feature of the T-cell Receptor.” In: *Immunol Today* (1998). DOI: 10.1016/s0167-5699(98)01299-7.

[304] L. Wooldridge et al. “A Single Autoimmune T Cell Receptor Recognizes More Than a Million Different Peptides.” In: *The Journal of Biological Chemistry* (2012). DOI: 10.1074/jbc.M111.289488.

[305] Y. Zhao et al. “High-affinity TCRs Generated by Phage Display Provide CD4+ T Cells with the Ability to Recognize and Kill Tumor Cell Lines.” In: *Journal of Immunology* (2007).

[306] M. Irving et al. “Interplay between T Cell Receptor Binding Kinetics and the Level of Cognate Peptide Presented by Major Histocompatibility Complexes Governs CD8+ T Cell Responsiveness.” In: *The Journal of Biological Chemistry* (2012).

[307] A. Tarakhovsky et al. “A Role for CD5 in TCR-mediated Signal Transduction and Thymocyte Selection.” In: *Science* (1995). DOI: 10.1126/science.7542801.

[308] H. S. Azzam et al. “CD5 Expression Is Developmentally Regulated by T Cell Receptor (TCR) Signals and TCR Avidity.” In: *Journal of Experimental Medicine* (1998). DOI: 10.1084/jem.188.12.2301.

[309] C. Peña-Rossi et al. “Negative Regulation of CD4 Lineage Development and Responses by CD5.” In: *Journal of Immunology* (1999).

[310] H. S. Azzam et al. “Fine Tuning of TCR Signaling by CD5.” In: *The Journal of Immunology* (2001). DOI: 10.4049/jimmunol.166.9.5464.

[311] P. Wong et al. “Dynamic Tuning of T Cell Reactivity by Self-peptide–major Histocompatibility Complex Ligands.” In: *Journal of Experimental Medicine* (2001). DOI: 10.1084/jem.193.10.1179.

[312] D. K. Tischer and O. D. Weiner. "Light-based Tuning of Ligand Half-life Supports Kinetic Proofreading Model of T Cell Signaling." In: *Elife* (2019). DOI: 10.7554/elife.42498.

[313] H. Mukhopadhyay et al. "Multisite Phosphorylation Modulates the T Cell Receptor Zeta-chain Potency but Not the Switchlike Response." In: *Biophys J* (2016). DOI: 10.1016/j.bpj.2016.03.024.

[314] O. S. Yousefi et al. "Optogenetic Control Shows That Kinetic Proofreading Regulates the Activity of the T Cell Receptor." In: *Elife* (2019). DOI: 10.7554/eLife.42475.

[315] J. Göhring et al. "Temporal Analysis of T-cell Receptor-imposed Forces Via Quantitative Single Molecule Fret Measurements." In: *bioRxiv* (2020). DOI: 10.1101/2020.04.03.024299.

[316] J. R. Schoenborn et al. "Feedback Circuits Monitor and Adjust Basal Lck-dependent Events in T Cell Receptor Signaling." In: *Science Signaling* (2011). DOI: 10.1126/scisignal.2001893.

[317] Y. X. Tan et al. "Inhibition of the Kinase Csk in Thymocytes Reveals a Requirement for Actin Remodeling in the Initiation of Full TCR Signaling." In: *Nature Immunology* (2014). DOI: 10.1038/ni.2772.

[318] N. S. van Oers et al. "Constitutive Tyrosine Phosphorylation of the T-cell Receptor (TCR) Zeta Subunit: Regulation of TCR-associated Protein Tyrosine Kinase Activity by TCR Zeta." In: *Molecular and Cellular Biology* (1993). DOI: 10.1128/mcb.13.9.5771.

[319] N. S. van Oers, N. Killeen, and A. Weiss. "Zap-70 Is Constitutively Associated with Tyrosine-phosphorylated TCR Zeta in Murine Thymocytes and Lymph Node T Cells." In: *Immunity* (1994). DOI: 10.1016/1074-7613(94)90038-8.

[320] P. Bruhns et al. "Specificity and Affinity of Human Fc$\gamma$ Receptors and Their Polymorphic Variants for Human Igg Subclasses." In: *Blood* (2009). DOI: 10.1182/blood-2008-09-179754.

[321] N. E. Harwood and F. D. Batista. "Early Events in B Cell Activation." In: *Annual Review of Immunology* (2010). DOI: 10.1146/annurev-immunol-030409-101216.

[322] Y. Liu et al. "Chimeric Star Receptors Using TCR Machinery Mediate Robust Responses against Solid Tumors." In: *Science Translational Medicine* (2021). DOI: 10.1126/scitranslmed.abb5191.

[323] K. M. Bushell et al. "Large-scale Screening for Novel Low-affinity Extracellular Protein Interactions." In: *Genome Res* (2008). DOI: 10.1101/gr.7187808.

[324] C. J. Cohen et al. "Enhanced Antitumor Activity of T Cells Engineered to Express T-cell Receptors with a Second Disulfide Bond." In: *Cancer Research* (2007). DOI: 10.1158/0008-5472.can-06-3986.

[325] S. J. Gagnon et al. "T Cell Receptor Recognition Via Cooperative Conformational Plasticity." In: *J Mol Biol* (2006). DOI: 10.1016/j.jmb.2006.08.045.

[326] U. Utz et al. "Analysis of the T-cell Receptor Repertoire of Human T-cell Leukemia Virus Type 1 (HTLV-1) Tax-specific CD8+ Cytotoxic T Lymphocytes from Patients with HTLV-1-associated Disease: Evidence for Oligoclonal Expansion." In: *J Virol* (1996). DOI: 10.1128/jvi.70.2.843-851.1996.

[327] J. Ruppert et al. “Prominent Role of Secondary Anchor Residues in Peptide Binding to HLA-A2.1 Molecules.” In: *Cell* (1993). DOI: 10.1016/0092-8674(93)90472-3.

[328] A. Achour et al. “Murine Class I Major Histocompatibility Complex H-2dd: Expression, Refolding and Crystallization.” In: *Acta Crystallogr D Biol Crystallogr* (1999). DOI: 10.1107/s0907444998005265.

[329] M. B. Parrott and M. A. Barry. “Metabolic Biotinylation of Secreted and Cell Surface Proteins from Mammalian Cells.” In: *Biochem Biophys Res Commun* (2001). DOI: 10.1006/bbrc.2001.4437.

# Chapter A

# Supplementary information

**Table S1: Fitted $K_D$ with the indicated method for the 1G4 TCR in SPR at 37°C.**
N/A: Not applicable. The geo. SD refers to the geometric SD factor (fold change; 1.0 equals no variance). minA: Minimal alanine peptide. Code for peptide library: 1) S, T, A, V, G 2) L, I, M 3) Y, F, W, T, L, I, M, A, P, G, Q, N 4) as 3 + D, E 5) V, L. See also Table 6.9.

| Name | Sequence | $K_D$ (Bmax fitted) | | | $K_D$ (Bmax const.) | | |
|---|---|---|---|---|---|---|---|
| | | Geo. mean (µM) | Geo. SD | n | Geo. mean (µM) | Geo. SD | n |
| NYE 9V | SLLMWITQV | 7.6 | 1.37 | 10 | 4.8 | 1.27 | 7 |
| NYE 3A | SLAMWITQV | 6.9 | 1.24 | 5 | 6.0 | 1.34 | 5 |
| NYE 6V | SLLMWVTQV | 17 | 1.29 | 6 | 21 | 1.56 | 6 |
| NYE 3Y | SLYMWITQV | 37 | 1.32 | 7 | 55 | 1.30 | 5 |
| NYE 4D | SLLDWITQV | 80 | 1.90 | 4 | 139 | 1.14 | 4 |
| NYE 6T | SLLMWTTQV | 79 | 1.56 | 4 | 161 | 1.19 | 4 |
| NYE 4A | SLLAWITQV | 130 | 2.31 | 4 | 296 | 1.20 | 4 |
| NYE 5Y | SLLMYITQV | 163 | 2.11 | 3 | 425 | 1.25 | 3 |
| NYE 5F | SLLMFITQV | 249 | 7.83 | 8 | 1431 | 1.24 | 8 |
| NYE 8K | SLLMWITKV | 236 | 4.27 | 3 | 1611 | 1.26 | 3 |
| NYE 4A8K | SLLAWITKV | 583 | 5.17 | 7 | 1683 | 1.24 | 7 |
| Tax 5F | LLFGFPVYV | 66 | N/A | 1 | 1369 | N/A | 1 |
| Tax 4A8A | LLFAYPVAV | 177 | N/A | 1 | 2342 | N/A | 1 |
| Tax WT | LLFGYPVYV | 6987 | 1.31 | 3 | 2462 | 1.48 | 3 |
| Tax 5H8A | LLFGHPVAV | 8584 | N/A | 1 | 2935 | N/A | 1 |
| Tax 8W | LLFGYPVWV | 21 | N/A | 1 | 3498 | N/A | 1 |
| Pep. lib. | 123114115 | 492 | 1.76 | 3 | 1483 | 1.33 | 3 |
| minA | ALAAAAAAV | 188 | 18.52 | 3 | 2036 | 1.53 | 3 |

**Table S2: Fitted $K_D$ with the indicated method for the A6 TCR in SPR at 37°C.**
N/A: Not applicable. The geo. SD refers to the geometric SD factor (fold change; 1.0 equals no variance). minA: Minimal alanine peptide. Code for peptide library: 1) S, T, A, V, G 2) L, I, M 3) Y, F, W, T, L, I, M, A, P, G, Q, N 4) as 3 + D, E 5) V, L. See also Table 6.9.

| Name | Sequence | $K_D$ (Bmax fitted) | | | $K_D$ (Bmax const.) | | |
|---|---|---|---|---|---|---|---|
| | | Geo. mean (µM) | Geo. SD | n | Geo. mean (µM) | Geo. SD | n |
| Tax WT | LLFGYPVYV | 2.0 | 1.28 | 6 | 1.6 | 1.20 | 5 |
| Tax 5F | LLFGFPVYV | 3.0 | 1.97 | 2 | 2.2 | 2.40 | 2 |
| Tax 7T | LLFGYPTYV | 3.4 | N/A | 1 | 2.8 | N/A | 1 |
| Tax 5W | LLFGWPVYV | 6.1 | N/A | 1 | 5.0 | N/A | 1 |
| Tax 1M | MLFGYPVYV | 6.1 | N/A | 1 | 6.1 | N/A | 1 |
| Tax 1A | ALFGYPVYV | 4.2 | 1.15 | 4 | 6.5 | 1.14 | 4 |
| Tax 1V | VLFGYPVYV | 6.8 | 1.25 | 3 | 7.8 | 1.24 | 3 |
| Tax 7R | LLFGYPRYV | 11 | 1.18 | 3 | 21 | 1.28 | 3 |
| Tax 6V | LLFGYVVYV | 14 | N/A | 1 | 21 | N/A | 1 |
| Tax 7N | LLFGYPNYV | 21 | N/A | 1 | 22 | N/A | 1 |
| Tax 7M | LLFGYPMYV | 21 | N/A | 1 | 34 | N/A | 1 |
| Tax 7Q | LLFGYPQYV | 22 | N/A | 1 | 37 | N/A | 1 |
| Tax 6L | LLFGYLVYV | 31 | N/A | 1 | 52 | N/A | 1 |
| Tax 5A | LLFGAPVYV | 27 | 1.54 | 3 | 55 | 1.13 | 3 |
| Tax 5H | LLFGHPVYV | 35 | 1.47 | 3 | 56 | 1.16 | 3 |
| Tax 7H | LLFGYPHYV | 42 | 1.70 | 4 | 62 | 1.73 | 4 |
| Tax 8F | LLFGYPVFV | 39 | 1.38 | 4 | 65 | 1.41 | 4 |
| HuD2L9V | LLYGFVNYV | 32 | 1.11 | 2 | 75 | 1.18 | 2 |
| Tax 8W | LLFGYPVWV | 62 | 1.51 | 3 | 85 | 1.60 | 3 |
| Tax 4A | LLFAYPVYV | 72 | 1.07 | 3 | 117 | 1.17 | 3 |
| Tel1p | MLWGYLQYV | 95 | 1.11 | 2 | 253 | 1.04 | 2 |
| Tax 8A | LLFGYPVAV | 342 | 3.95 | 3 | 562 | 1.13 | 3 |
| Tax 7H8A | LLFGYPHAV | 216 | 1.96 | 2 | 1728 | 1.07 | 2 |
| Tax 4A8A | LLFAYPVAV | 122 | 3.45 | 3 | 1817 | 1.33 | 3 |
| Tax 5H8A | LLFGHPVAV | 1603 | 6.99 | 4 | 2459 | 1.26 | 4 |
| NYE 9V | SLLMWITQV | 2176 | 3.55 | 2 | 1458 | 1.22 | 2 |
| NYE 4A8K | SLLAWITKV | 586 | 4.46 | 6 | 1609 | 1.29 | 6 |
| NYE 5F | SLLMFITQV | 1019 | 18.36 | 5 | 2555 | 1.12 | 5 |
| NYE 3Y | SLYMWITQV | 119 | N/A | 1 | 2822 | N/A | 1 |
| Pep. lib. | 123114115 | 817 | 6.53 | 3 | 1316 | 1.37 | 3 |
| minA | ALAAAAAAV | 618 | 19.23 | 4 | 2602 | 1.54 | 4 |